THE AMERICAN MINERALOGIST
JOURNAL OF THE MINERALOGICAL SOCIETY OF AMERICA

Vol. 32 JULY–AUGUST, 1947 Nos. 7 and 8

LIQUID INCLUSIONS IN GEOLOGIC THERMOMETRY

EARL INGERSON, *Geophysical Laboratory,*
Washington, D. C.

ABSTRACT

A satisfactory method of determining temperatures of crystallization from the liquid inclusions in minerals would aid in the solution of many problems of geologic thermometry. Recently published data on the specific volume of water at high temperatures and pressures allow much more accurate determination of the effect of original pressure than has been possible before. Data on the critical temperature of aqueous solutions of alkali halides provide the basis for better evaluation of the effect of concentration.

Curves have been prepared showing the relation of degree of filling of inclusions and temperature of disappearance of the vapor phase, both for pure water and for a 10 per cent solution of NaCl and KCl. Two sets of curves show the relation between temperature of disappearance of the vapor phase, pressure at the time of formation, and temperature of formation.

Measurements on quartz from pegmatites indicate temperatures below 250° C. Pressure corrections where depth can be estimated range from 54° to 73° C. for specimens studied thus far by the author.

INTRODUCTION

The classic work on liquid inclusions in minerals, especially quartz, was done by Sorby (1858) almost ninety years ago. The method of estimating temperature of formation of minerals from such inclusions has been used in a desultory fashion since that time, but few contributions to theory or technique have been made since Sorby's paper appeared.

The unsatisfactory status of the subject is indicated by the fact that a leading textbook of petrology merely indicates that a small vapor bubble is likely to mean relatively low temperature of formation and a large bubble higher temperature. Also, a summary of geologic thermometry remarks that the problem becomes insoluble above the critical temperature. However, recent work on the specific volume of water at high temperatures and pressures makes possible much more accurate approximations of temperature than the diagram in the above-mentioned textbook would lead one to believe, and estimates above the critical temperature of the depositing solutions can sometimes be made if the pressure can be estimated from the geologic data.

The fundamental assumption has not changed since Sorby's time,—that a liquid inclusion cavity was just filled with fluid at the temperature and pressure under which it was formed. These conditions, and the composition of the solution, determine the degree of filling of the cavity as it is observed at room temperature. If a crystal containing such inclusions is heated, the liquid will expand and fill the cavities at the temperature of formation if the original pressure did not exceed significantly the vapor pressure of the solution. If the pressure was considerably greater, then more fluid would have been compressed into each inclusion; consequently, on re-heating, the liquid would fill the cavity at a lower temperature than that of crystallization of the mineral.

Other assumptions. It must also be assumed that the change of volume of the mineral itself is not significant and that changes in volume and concentration brought about by deposition of material from the solution as it cools are such as not to affect the result. Relative compressibilities of water and quartz are shown in Table 1. Data on water are from Dorsey (1940), pp. 240 and 243 and on quartz are from Sosman (1927), p. 427. The compressibility of water is more than 13 times that of quartz even at 2000 atmospheres pressure. At higher temperatures the differences are even greater.

TABLE 1. COMPRESSIBILITIES OF WATER AND QUARTZ
(All values $\times 10^{-6}$)

T	P=V.P. H_2O	P=1 atm.	P=2000 atm.	
	Water	Quartz	Water	Quartz
30	45.2	2.76	34.9	2.65
75	48.4	2.78	34.3	2.67
150	67.9			
225	136.5			

In most liquid inclusions any material deposited during cooling must be the same as the including mineral, since no foreign material can be observed on the walls of the cavities. Water at 200° dissolves about 0.1 per cent of silica. If the liquid in inclusions in quartz contained 10 times that much silica and deposited all of it during cooling, the total change in composition would be only 1 per cent and the volume change would be only about 1 part in 300.

These are, therefore, second order factors whose total effects are less than the probable errors in estimating the effect of pressure, so the assumption that they can be neglected appears to be justified.

Secondary inclusions. It is necessary to distinguish carefully between primary and secondary liquid inclusions in a mineral. Only the primary ones record the temperature at which the mineral crystallized; secondary inclusions may give an indication of prevailing temperature during a later reworking.

Crystals in vugs and other open spaces in veins almost certainly have not been crushed and cemented together by later solutions; nor is it likely that they have been dissolved and recrystallized. Therefore, the assumption that the inclusions in such crystals are primary and can be used for estimates of temperature is probably warranted.

In interlocking crystalline aggregates in the massive parts of veins, and in metamorphic and igneous rocks, however, the relations are much more complex. The crystals of such aggregates may have been partially or entirely recrystallized after the formation of the vein or rock. Therefore, some or all of the inclusions may indicate the temperature of the recrystallization rather than that of the original formation.

If planes of liquid inclusions cross grain boundaries without offset or change of orientation, the inclusions are almost certainly secondary. If planes of inclusions have more or less constant orientation(s) over an entire thin section, regardless of the orientation of the individual grains, the chances are good that the inclusions are secondary, even in planes not observed to cross grain boundaries.

Where planes of inclusions are confined to individual mineral grains or where arrangement in planes is not evident, the chances are better that the inclusions are primary. Control of orientation by the crystal lattice of grains can be evidence that inclusions are primary, but it is also possible for secondary inclusions to be so controlled.

In each case all available evidence should be marshalled in deciding the origin of inclusions,—paragenesis, alteration, replacement, etc.

TECHNIQUE

If a heating stage is available, polished plates can be observed as they are heated and the actual temperature at which the inclusions become full of liquid determined directly. If no heating stage is available, it is possible to calculate the temperature of disappearance of the vapor phase from the degree of filling of the inclusions. However, it is rarely possible to estimate degree of filling with a satisfactory degree of precision. Only when an inclusion has a very regular form is there a chance to make a reasonably accurate estimate. Such forms include negative crystals, elongate prismatic or tubular inclusions of uniform diameter and flat oval-shaped inclusions where the vapor bubble is appressed so that the relative areas are proportional to the relative volumes. Figure 1 gives the relation between degree of filling and the temperature at which the inclusions are just filled with fluid for pure water and for a 10 per cent chloride solution. For example, if the ratio of vapor to total volume at room temperature is 0.2, the vapor would disappear at 250° C. if the liquid is pure water, at 274° C. if it is a 10 per cent solution of alkali halides.

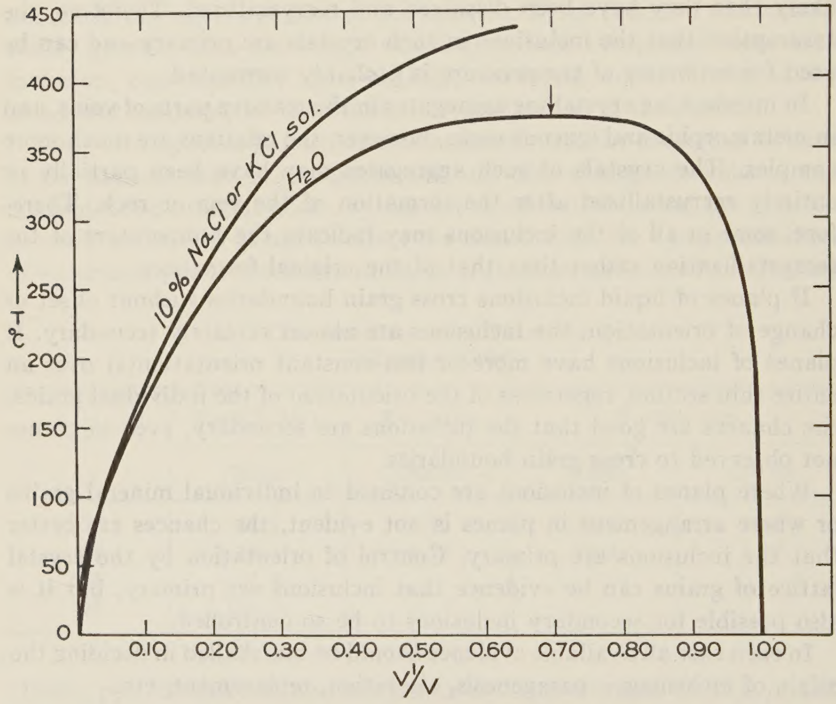

FIG. 1. Graph showing relation between degree of filling of inclusions and temperature at which they become filled with a homogeneous phase. For ratios less than about 0.70 of vapor to total volume (left side of dome) this phase is liquid; for higher ratios the phase is vapor. The curve marked "10 per cent NaCl or KCl solution" is probably usable for any solution with approximately 10 per cent of any combination of alkali halides with minor amounts of carbonates, silica, and other compounds.

EFFECT OF CONCENTRATION

The value of 10 per cent has been chosen because the few available data indicate that the solutions in liquid inclusions (at least in quartz) are likely to have concentrations of that order of magnitude.[1]

---

[1] See, for example, Königsberger and Müller (1906). D. W. J. Grey, of the St. John del Rey Mining Company, writes that samples of solution taken from vugs in quartz veins well

Sorby (1858, pp. 461–462) studied the expansion of a 10 per cent solution of KCl up to 200° C. and derived a formula for calculating temperature of disappearance of the vapor phase at higher temperatures for known degrees of filling. Schröer (1927) determined the critical tempera-

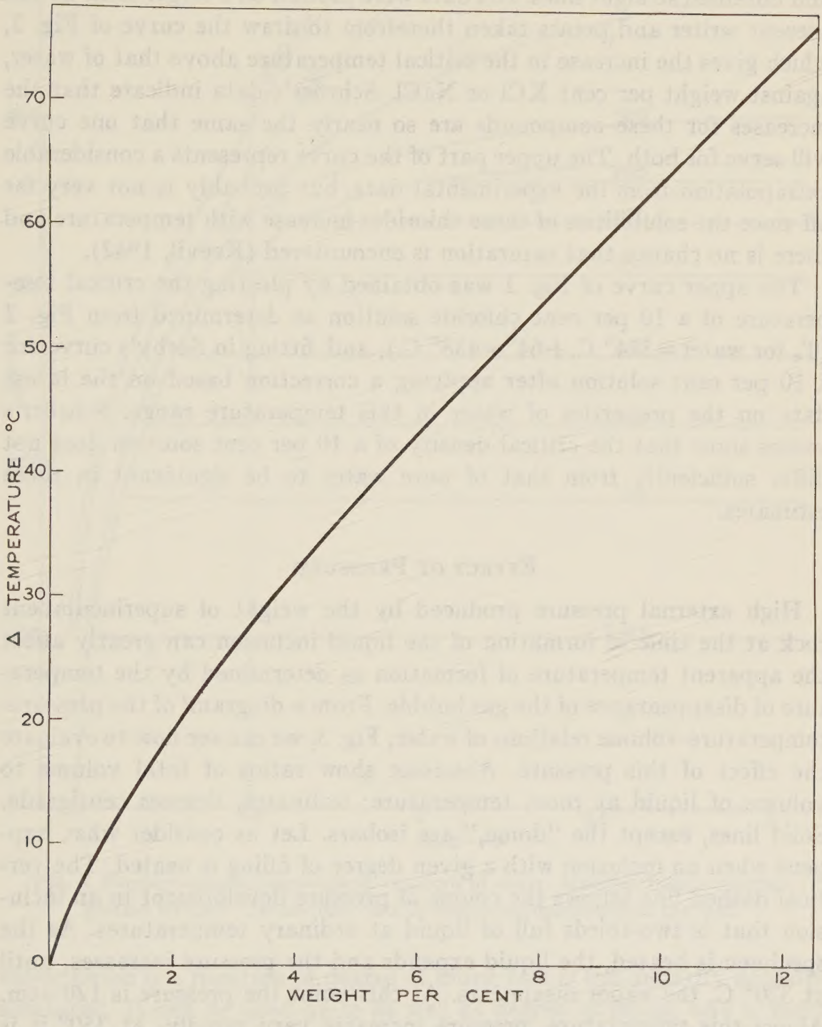

FIG. 2. Critical temperatures of solutions of NaCl or KCl. ΔT to be added to the critical temperature of water, 374° C. Calculated from data of Schröer (1927).

---

below the zone of ground water circulation show concentrations up to 12 per cent NaCl, with minor amounts of other compounds. The mine waters are high in sulfate, but no sulfate was found in the vugs.

tures of solutions of several alkali halides, including solutions of NaCl and KCl up to 5 per cent by weight. He plotted ln 100x against ln ΔT and obtained straight lines. His data were plotted on a larger scale by the present writer and points taken therefrom to draw the curve of Fig. 2, which gives the increase in the critical temperature above that of water, against weight per cent KCl or NaCl. Schröer's data indicate that the increases for these compounds are so nearly the same that one curve will serve for both. The upper part of the curve represents a considerable extrapolation from the experimental data, but probably is not very far off since the solubilities of these chlorides increase with temperature and there is no chance that saturation is encountered (Keevil, 1942).

The upper curve of Fig. 1 was obtained by plotting the critical temperature of a 10 per cent chloride solution as determined from Fig. 2 (T_c for water = 374° C. + 64° = 438° C.), and fitting in Sorby's curve for a 10 per cent solution after applying a correction based on the latest data on the properties of water in this temperature range. Schröer's values show that the critical density of a 10 per cent solution does not differ sufficiently from that of pure water to be significant in these estimates.

EFFECT OF PRESSURE

High external pressure produced by the weight of superincumbent rock at the time of formation of the liquid inclusion can greatly affect the apparent temperature of formation as determined by the temperature of disappearance of the gas bubble. From a diagram[2] of the pressure-temperature-volume relations of water, Fig. 3, we can see how to evaluate the effect of this pressure. Abscissae show ratios of total volume to volume of liquid at room temperature; ordinates, degrees centigrade. Solid lines, except the "dome," are isobars. Let us consider what happens when an inclusion with a given degree of filling is heated. The vertical dashed line follows the course of pressure development in an inclusion that is two-thirds full of liquid at ordinary temperatures. As the specimen is heated, the liquid expands and the pressure increases, until at 320° C. the vapor disappears. At this point the pressure is 120 atm. Above this temperature, pressure increases very rapidly; at 350° it is 500 atm.; at 400°, 2500 atm.

It is apparent that degree of filling and temperature determine the pressure. Conversely, if degree of filling and original pressure are known the temperature can be found. Temperature of disappearance of the

---

[2] Compiled from the following sources: Birch (1942), Dorsey (1940), Smith and Keyes (1934), and Van Nieuwenburg and Blumendal (1932).

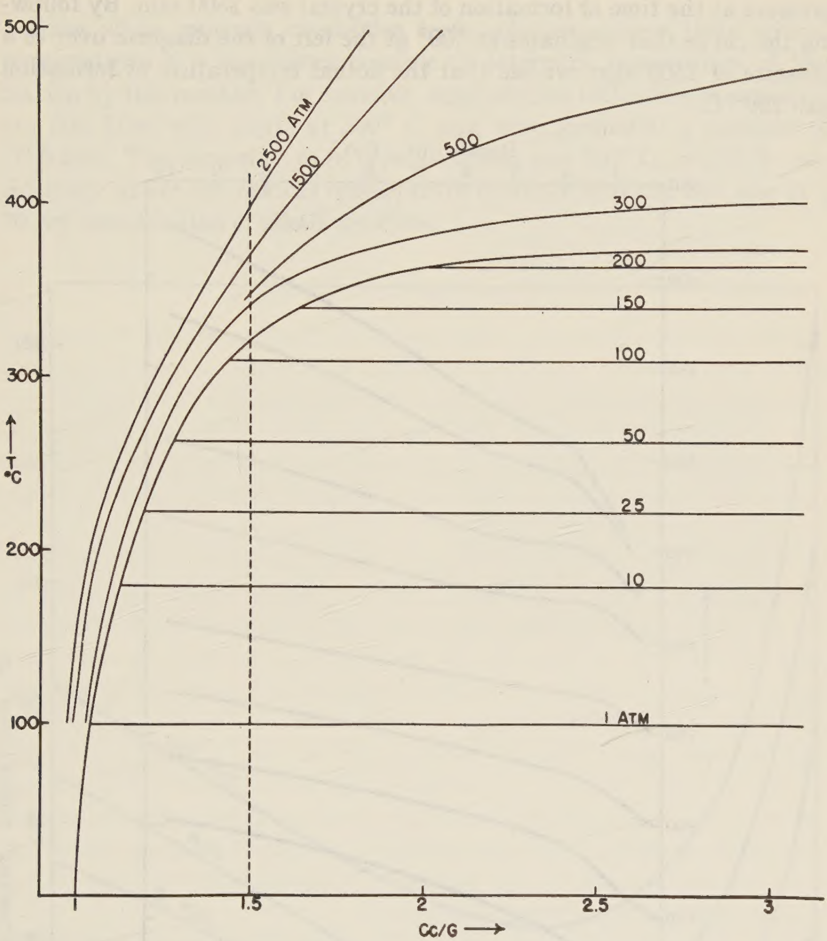

FIG. 3. Pressure-temperature-volume relations of water. Modified from a diagram plotted by O. F. Tuttle from data in references mentioned in the text.

vapor phase is a function of degree of filling and is the quantity actually measured. It can be used quite as well as degree of filling, and is more convenient. A diagram[3] prepared with this in mind, Fig. 4, gives temperature of formation when original pressure can be estimated and the temperature of disappearance of the vapor phase is known. Suppose, for example, that in a given crystal the inclusions are filled with liquid at 100° C. From the geologic occurrence it can be estimated that rock pressure at the time of formation of the crystal was 2500 atm. By following the curve that originates at 100° at the left of the diagram over to a pressure of 2500 atm. we see that the actual temperature of formation was 200° C.

---

[3] Data from same sources as Fig. 3. Overlapping data from different sources always gave the same correction within 5° C. and usually within 2° C.

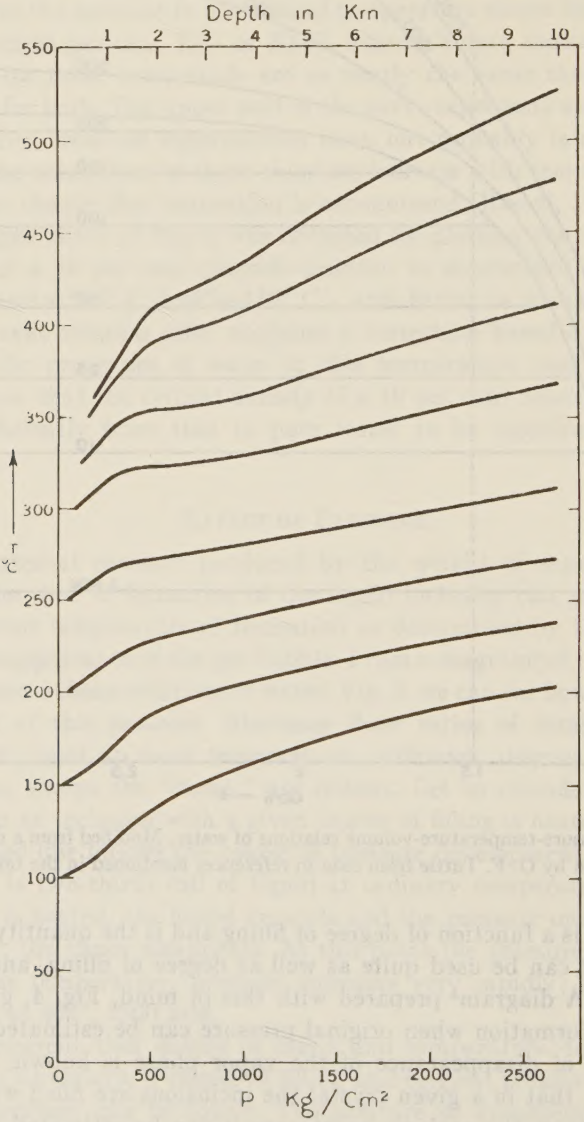

FIG. 4. Curves showing relations between temperature of disappearance of vapor phase, pressure (or depth) at the time of formation of the inclusion, and temperature of formation of the inclusion. Observed temperatures of disappearance are given by points at left end of curves; then each curve shows increasing temperature of formation corresponding to higher pressures.

Even when minerals crystallize from solutions above their critical temperatures it is sometimes possible to determine temperature of formation by this method. For example, suppose that inclusions in a mineral are just filled with liquid at 360° C. and were formed at a pressure of 2100 atm. The temperature of crystallization was 500° C., which is considerably above the critical temperature not only of water but also of a 10 per cent solution of alkali chlorides.

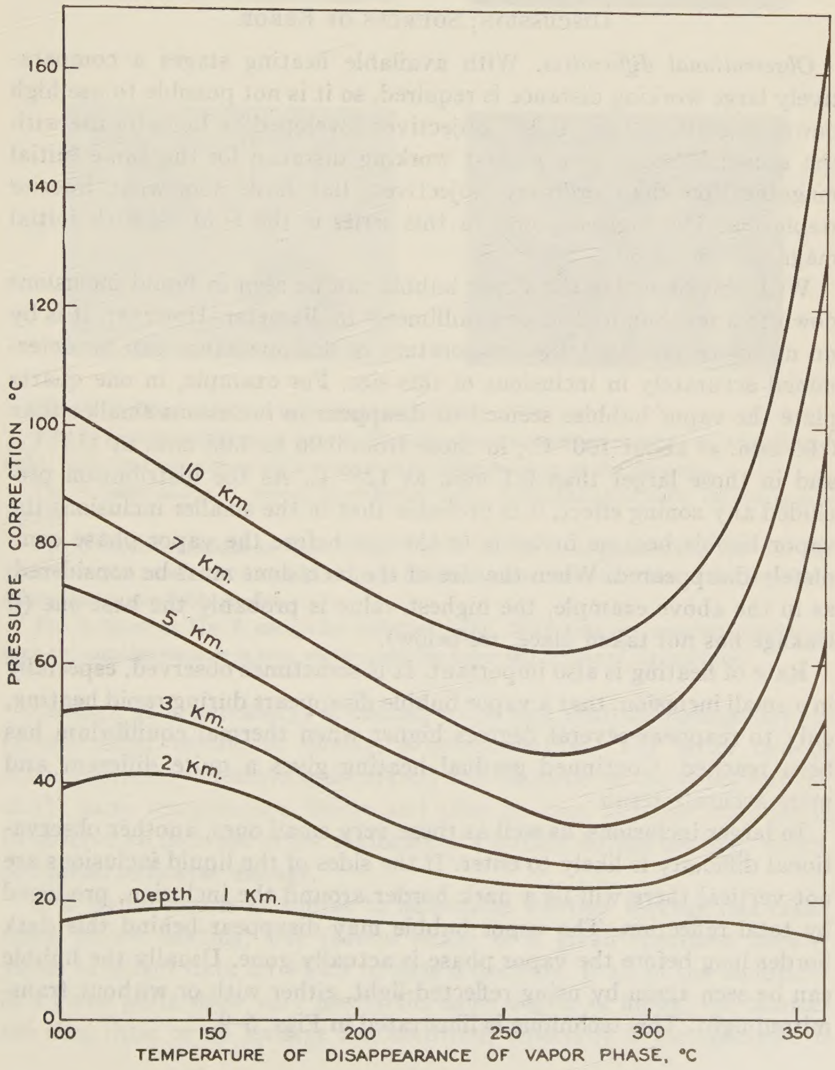

FIG. 5. Data of Fig. 4 plotted for use of temperature of disappearance of the vapor phase without interpolation.

Figure 4 has its curves for even temperatures of disappearance of the vapor phase. Since a bubble rarely disappears at just 100° or 250° C., interpolation is almost always necessary. In Fig. 5 temperature correction is plotted against temperature of disappearance of the vapor phase and the curves are for kilometers of depth. Since it is rarely possible to be sure of depth of cover nearer than a kilometer or so, at the time of formation of a crystal, necessity for interpolation is much less frequent with the data in this form.

Discussion; Sources of Error

Observational difficulties. With available heating stages a comparatively large working distance is required, so it is not possible to use high power objectives. The "U.M." objectives developed by Leitz for use with the universal stage give greater working distance for the same initial magnification than ordinary objectives, but have somewhat inferior resolution. The highest power in this series is the U.M. 4, with initial magnification of 30×.

With this objective the vapor bubble can be seen in liquid inclusions down to a few hundredths of a millimeter in diameter. However, it is by no means certain that the temperature of disappearance can be determined accurately in inclusions of this size. For example, in one quartz plate the vapor bubbles seemed to disappear in inclusions smaller than 0.05 mm. at about 100° C.; in those from 0.06 to 0.08 mm. at 115° C.; and in those larger than 0.1 mm. at 125° C. As the distribution precluded any zoning effect, it is probable that in the smaller inclusions the vapor bubble became invisible to the eye before the vapor phase completely disappeared. When the size of the inclusions must be considered, as in the above example, the highest value is probably the best one (if leakage has not taken place, *see* below).

Rate of heating is also important. It is sometimes observed, especially in a small inclusion, that a vapor bubble disappears during rapid heating, only to reappear several degrees higher when thermal equilibrium has been reached. Continued gradual heating gives a quite different and more accurate result.

In larger inclusions, as well as these very small ones, another observational difficulty is likely to enter. If the sides of the liquid inclusions are not vertical there will be a dark border around the inclusion, produced by total reflection. The vapor bubble may disappear behind this dark border long before the vapor phase is actually gone. Usually the bubble can be seen again by using reflected light, either with or without transmitted light. This technique is illustrated in Figs. 6–9.

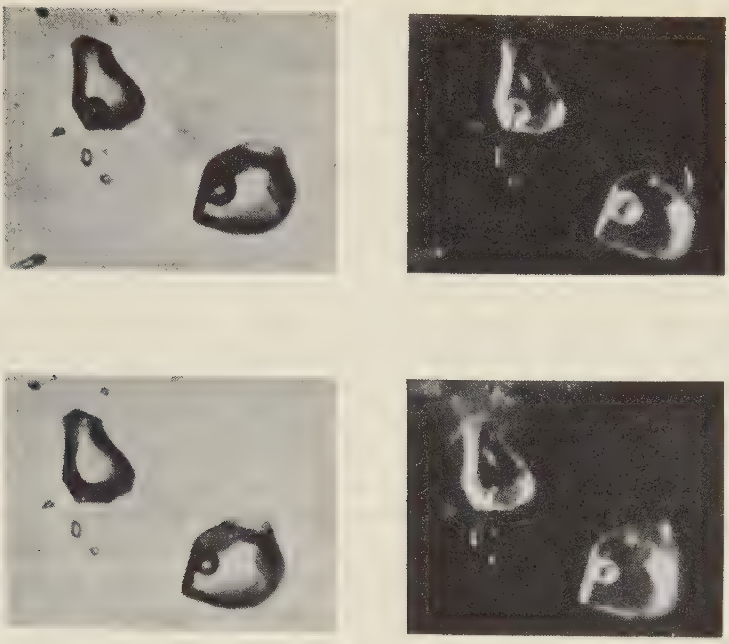

Figs. 6–9. Observation of vapor bubbles (×200).

Fig. 6. Liquid inclusions in quartz. Picture taken at room temperature by transmitted light. Note that one side of each vacuole is invisible because of the dark rim.

Fig. 7. Same as Fig. 6, except by reflected light. Note that all of each vacuole is now visible.

Fig. 8. Same inclusions as Figs. 6 and 7 after heating to approximately 160° C. The vacuole in the smaller inclusion is entirely hidden by the dark rim; that in the larger has diminished appreciably in size.

Fig. 9. Same as Fig. 8, except by reflected light. Note that the complete outline of even the smaller vacuole is now visible near the lower left corner of its inclusion.

Leakage. It is necessary, of course, to be sure that no leakage has occurred either before, or during, a determination. The latter can be accomplished by measuring accurately the diameter of the vapor bubble, at the same temperature, before and after heating. It is not uncommon to observe an increase in the diameter of a bubble during heating, which, of course, indicates leakage.

It is by no means as simple to determine whether leakage has taken place before heating, but careful study of a given specimen usually yields sufficient data on which to base a decision. If all of the inclusions in a given plate show very nearly the same degree of filling, the chances are that little or no leakage has occurred, especially if the specimen is free of fractures. If, however, the degree of filling is highly variable, and changes in an irregular manner throughout the specimen, leakage has probably occurred. In many specimens leakage can be definitely established by relating lines of inclusions with large vapor bubbles (or entirely filled with vapor or gas) to fractures in the specimen.

Where part of the liquid has escaped, the first effect is to raise the temperature at which the contents of the inclusion become homogeneous. After enough has escaped so that the inclusion contains just the critical volume of liquid, the effect reverses and the loss of more liquid (or vapor) lowers the temperature at which homogeneity is reached. In the first case (more than critical volume of liquid) the vapor bubble decreases in size and vanishes so that the cavity is completely filled with liquid; in the second, the bubble expands until the cavity is filled with vapor.

If some of the inclusions of a given specimen have lost part of their contents, but they all still become homogeneous by disappearance of the vapor phase, then the lowest temperature found is probably a maximum for the crystallization of the specimen. If many of the inclusions show the same temperature of disappearance of the vapor phase, with the others showing erratic higher values, then the lower temperature, at which the many disappear, may be taken as the estimated temperature of formation of the crystal.

Estimates of pressure. There is always some uncertainty as to the exact depth of cover at the time when a mineral was crystallizing. Errors will vary from negligibly small to a factor of several-fold.

Even when depth of cover can be estimated accurately, it cannot be established that the solutions were under a pressure equal to that produced by the weight of the overlying rocks. If there was not enough fluid to fill the available pore space at the pressure produced by the overburden, the pressure could have been lower than that calculated. On the other hand, strength of the crust might have allowed pressure considerably greater than that calculated from depth of cover.

Holden (1925) outlines a method for estimating pressure from the inclusions themselves, independent of any figure for depth of burial. The method involves finding inclusions both with and without CO_2 in the same specimen, so it is of limited applicability. It is possible that other methods that are more generally useful can be found. Holden neglected the effect of pressure in estimating temperature, so for most cases his technique would have to be modified.

RESULTS

Most of the actual determinations thus far have been on quartz. The results from pegmatite quartz, a few of which are shown in Table 2, are interesting because they give temperatures much lower than the commonly accepted value of approximately 575° C. for this type of quartz-bearing deposit. Of the several specimens studied, from widely scattered deposits in Brazil, North Carolina, and Connecticut, none have been found with temperatures of formation greater than 250° C., even with pressure corrections added. It is of interest to note that in one specimen in which beryl crystals occurred with the quartz, the vapor phase in a liquid inclusion in one of these disappeared at 175° C. as against 155° C. for those in the quartz. Most vein minerals in which liquid inclusions have been looked for do contain them. Liquid inclusions are also found in many minerals in metamorphic and igneous rocks. It is therefore apparent that this method, with the indicated refinements, is useful, not only in making isolated estimates of temperature, but may also aid in the revision of considerable parts of the scale of geologic thermometry.

Table 2

Locality	Range of Temperature	Probable Best Value	Remarks
Parahyba	150°	156°	Rose; P. cor. = +62°
Parahyba	101°	101°	Smoky; P. cor. = +73°
Brazil	67–157°	100°	Topaz included; P. cor. = +73°
Brazil	167–245°	180°	Milky; P. cor. = +54°
Connecticut	153–165°	155°	Inclusion in beryl, 175°
Connecticut	156–158°	157°	
North Carolina	160°	160°	Near a small vug
North Carolina	182°	182°	Same specimen, away from vug

References

Birch, Francis, et al. (editors) (1942), Handbook of Physical Constants: *Geol. Soc. Am.*, Special Paper **36,** 208–211.

Dorsey, N. Ernest (1940), The properties of ordinary water-substance: *Am. Chem. Soc.*, Monograph **81,** esp. pp. 591–594.

Holden, Edward F. (1925), The cause of color in smoky quartz and amethyst: *Am. Mineral.*, **10,** 203–252.

Keevil, N. B. (1942), Vapor pressures of aqueous solutions at high temperatures: *Jour. Am. Chem. Soc.*, **64,** 841–850.

Königsberger, J., and Müller, W. J. (1906), Ueber die Flüssigkeitseinschlüsse in Quartz alpiner Mineralklüfte: *Centralblatt für Mineralogie*, 72–76.

Schröer, Erich (1927), Untersuchungen über den kritischen Zustand. I. Beitrag zur Kenntnis des kritischen Zustandes des Wassers und wässriger Lösungen: *Zeit. Phys. Chem.*, **129,** 79–110.

Smith, Leighton B., and Keyes, Frederick G. (1934), The volumes of unit mass of liquid water and their correlation as a function of pressure and temperature: *Proc. Am. Acad. Arts and Sci.*, **69,** 285–312.

Sorby, H. C. (1858), On the microscopical structure of crystals: *Quart. Jour. Geol. Soc. London,* **14,** 453–500.

Sosman, R. B. (1927), The Properties of Silica; *Am. Chem. Soc.*, Monograph **37.**

Van Nieuwenburg, C. J., and Blumendal, H. B. (1932), The isotherms of water from 350°–480° C. and for pressures up to 600 kg/cm^2: *Rec. Trav. Chim. Pays Bas*, **51,** 707–714.

DETERMINATION OF PLAGIOCLASE WITH THE FOUR-AXIS UNIVERSAL STAGE

FRANCIS J. TURNER, *University of California, Berkeley, California.*

ABSTRACT

The paper outlines a procedure for measuring optical and crystallographic directions in twinned plagioclase with a four-axis universal stage. Identification of twinning laws and determination of anorthite content are discussed, with special reference to ambiguous cases at the sodic and calcic ends of the plagioclase series. The standard data of Duparc and Reinhard and Nikitin, regarding variation in the crystallographic orientation of the indicatrix with composition (conventionally shown by migration curves in stereographic projection), are presented as a series of curves based on rectangular coordinates. Special cases where one of the directions X, Y or Z coincides with, or is normal to, a twinning axis are reviewed. Finally, attention is drawn to a general tendency, commented upon by a number of writers, for discrepancy between points plotted from data measured on a universal stage, and the standard curves.

INTRODUCTION

The only comprehensive account of universal-stage technique in English—that of R. C. Emmons (1943)—is written for users of the Emmons stage (Bausch and Lomb) with five rotation axes. Some American and British laboratories are equipped only with four-axis stages, such as that formerly manufactured by the firm of Leitz; and moreover there are petrographers (of whom the writer is one) who prefer the four-axis stage for most measurements, and particularly for petrofabric analysis. This paper is written for those who use a four-axis stage for optical determination of feldspars.* It is assumed that the reader is familiar with such elementary procedures as location of X Y and Z, and measurement of optic axial angle.

The objects of the paper are:

(1) To stage concisely by means of illustrative examples the procedure of W. Nikitin (1936) for determining composition of plagioclase.

(2) To make available for routine laboratory use the optical data given by Nikitin in his comprehensive colored plate (Nikitin, 1936, pl. vii). (This may then be preserved from the inevitable damage resulting from constant handling.)

(3) To state, with appropriate diagrams, additional crystallographic data necessary for unambiguous identification of the twinning axes.

(4) To discuss the numerous cases where the measured data may lead to ambiguous determinations of twinning law or of anorthite content.

(5) To draw attention to various anomalies discussed in detail in the

---

* Since only the innermost rotation axis and the N–S and E–W tilting axes of the stage are used, the procedures described in this paper could equally well be carried out with a three-axis stage.

important but hitherto neglected paper of C. T. Barber (1936*a*).

Use of symbols for crystallographic and optical planes and directions throughout this paper is illustrated by the following examples:

CP_{1-2} = composition plane common to subindividuals (1) and (2) in a twinned grain.
$\perp CP_{1-2}$ = pole of CP_{1-2}, or normal to CP_{1-2}.
Cl_1 = cleavage plane in subindividual (1).
$\perp Cl_1$ = pole of Cl_1, or normal to Cl_1.
${}^2CP_1$ = second set of twin lamellae (transverse to CP_{1-2}) cutting across subindividual (1).
$\perp(001)$ = pole of (001), or normal to (001).
[100], [010], [001] = *a*, *b* and *c* crystal axes, respectively.
$\dfrac{\perp[001]}{(010)}$ = normal to the *c* axis within the plane (010).
A_{2-3} = twinning axis for two twinned subindividuals (2) and (3).
a_1 = optic axis in subindividual (1).

MEASUREMENT PROCEDURE

If, as is usually the case, the crystal to be measured shows obvious twinning, it is first roughly sketched, and the various subindividuals appropriately numbered. For each subindividual, the three principal directions X, Y and Z are located with reference to the plane of the microsection. This is done by bringing at least two of these directions in turn to coincide with the E–W axis of the stage, by alternate rotation to extinction on the innermost vertical axis and tilting to extinction on the N–S axis (for different degrees of tilt on E–W).

Example:—In subindividual (1), one of the principal optical directions is brought to coincide with E–W when the reading on the scale of the innermost vertical rotation axis is 79°, and the tilt on N–S is 30° downward to the observer's left. The direction parallel to E–W is identified (by rotating the whole stage through 45° and testing with a gypsum plate) as Z. The result is recorded thus:

$Z_1 \quad 79 \leftarrow 30$

A corresponding record for readings when Y of the same subindividual is brought parallel to E–W, is

$Y_1 \quad 355 \rightarrow 9$

X_1 is located later by plotting on a projection.

In each subindividual, cleavage and composition planes are sought and brought into coincidence with the plane which contains the E–W tilting axis and the main vertical axis of the microscope. This involves setting the N–S axis at zero, rotating the section on the innermost vertical axis till the trace of the plane to be measured coincides with E–W, and then tilting on E–W to give the sharpest definition possible. Great accuracy of measurement is difficult to attain, but is unnecessary in cases where twin axes are used in determining composition.

Example:—Composition planes for all three pairs of subindividuals (1), (2) and (3), coincide with the vertical plane parallel to E–W, when the scale reading for the innermost rotation axis is 18°, and the tilt on E–W is 22° toward the observer. The record is

CP_{1-2-3} 18 − 22 ↓

Fine transverse twin lamellae and accompanying cleavage locally developed in subindividual (3) are similarly brought parallel to the E–W vertical plane when the scale for the innermost vertical rotation axis reads 104° and the tilt on E–W is 16° away from the observer. This is recorded thus,

${}^2CP_3(={}^2Cl_3)$ 104 − 16 ↑

The complete data for a phenocryst of plagioclase showing three sets of subindividuals large enough to be measured, and local additional fine transverse lamellae in one of these, were recorded thus (cf. Fig. 1):

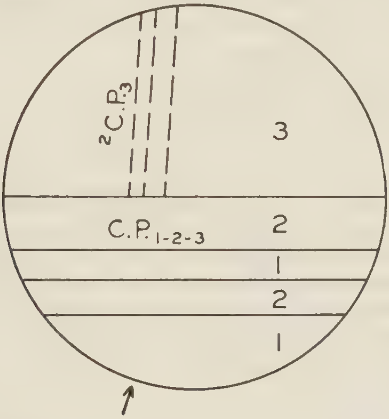

FIG. 1. Plagioclase twinned on ablite (1–2) and Carlsbad (2–3) laws, with second set of twinning and cleavage showing in one subindividual (3).

Y_1	355 → 9, $a_1$20 ↑
Z_1	79 ← 30
Y_2	44 ← 9, $a_2$41 ↑
Z_2	316 → 10
X_3	11 → 9
Y_3	290 ← 42
CP_{1-2-3}	18 − 22 ↓
${}^2CP_3(={}^2Cl_3)$	104 − 16 ↑

The expression "a_1 20" after Y_1, indicates the position of an optic axis which is brought to coincide with the vertical axis of the microscope by tilting on E–W through 20° away from the observer, when Y_1 has first been brought parallel to E–W.

PROJECTION PROCEDURE

Points of emergence of the measured directions Y_1, Z_1, Y_2, Z_2, X_3, Y_3, and poles of the measured composition and cleavage planes are now plotted on a suitable projection. Either a stereographic net (Wulff net) or an equal-area net (Schmidt net) will serve for this purpose. The writer somewhat prefers the latter, since the linear scale for a given angular distance (e.g. 10°) is more nearly uniform in a Schmidt net, and rapid plotting in the central part of the projection is thereby somewhat facilitated. In any case the numbering of the divisions on the circumference of the net must correspond with that of the scale for the innermost rotation axis of the stage—usually a clockwise sequence from 0° to 360°, with the zero point at the south pole. The net is covered with transparent paper which can be rotated freely about the center of the net. In the examples given below the *lower* hemisphere is projected, since this conforms to the standard procedure of petrofabric analysis, and at the same time simplifies the process of plotting.

Examples: (1) To plot X_1, Y_1 and Z_1, given

Y_1	$355 \rightarrow 9$, a_1 $20\uparrow$;
Z_1	$79 \leftarrow 30$.

Rotate the tracing sheet until the marginal index arrow (arbitrarily drawn) stands at 79° on the net. On the E–W diameter of the net plot Z_1, 30° in from the E end. Rotate the sheet till the index stands at 355° on the net, and plot Y_1, 9° in from the W end of the E–W diameter of the net. Z_1 should now lie on or close to the great circle at 90° from Y_1. On this circle plot X_1, 90° from Z_1. The axial point A_1 may also be plotted 20° upward from the E–W diameter on the great circle containing X_1 and Z_1. Note that on projections of the lower hemisphere, the direction in which any point is plotted is the same as that of the arrow in the corresponding recorded data.

(2) To plot CP_{1-2-3} $18-22\downarrow$: Rotate the tracing sheet till the index stands at 18° on the net, and plot the pole of CP_{1-2-3} (i.e. $\perp CP_{1-2-3}$) on the N–S diameter of the net, 22° down from the N end. In the case of feldspars it is convenient also to plot the trace of the main composition plane upon the projection, i.e., to draw the great circle at 90° from the pole of the plane in question (full arc in Fig. 2).

DETERMINATION OF TWINNING LAW AND COMPOSITION OF FELDSPAR FROM THE PLOTTED DATA

The completed projection shows X, Y and Z for each subindividual, together with poles of all measured composition and cleavage planes, projected upon the plane of the thin section. It is possible now to estimate the composition of the feldspar by measuring on the projection the mean angles between each of X, Y and Z, and the poles of observed composition and cleavage planes, using the curves of Fig. 5. Since direct measurement of these crystallographic planes may be attended by considerable error, the writer prefers, wherever possible, to use twinning axes as axes of reference with which to compare the relative positions of X, Y and Z in each subindividual (cf. Nikitin, 1936, p. 103). To do this it is first necessary to identify the twinning law in question before referring to the curves of Figs. 5 to 7. The types of twinning commonly encountered in feldspars are summarized below:

Type	*Name*	*Composition plane*	*Twinning axis*	*Comments*
Normal	Albite	(010)	⊥(010)	Usually multiple
Normal	Manebach	(001)	⊥(001)	Usually simple
Normal	Baveno	(021) or $(0\bar{2}1)$	⊥(021) or ⊥$(0\bar{2}1)$	Usually simple; rare in plagioclase
Parallel	Carlsbad	(010)	[001]	Simple
Parallel	Ala B	(010)	[100]	Usually multiple
Complex	Albite-Carlsbad	(010)	$\frac{\perp[001]}{(010)}$	Usually multiple
Complex	Albite-Ala	(010)	$\frac{\perp[100]}{(010)}$	Usually multiple
Parallel	Acline	(001)	[010]	Usually multiple
Parallel	Ala A	(001)	[100]	Usually multiple
Complex	Manebach-Acline	(001)	$\frac{\perp[010]}{(001)}$	Optically indistinguishable from Ala A
Complex	Manebach-Ala	(001)	$\frac{\perp[100]}{(001)}$	Optically indistinguishable from Acline
Parallel	Pericline	Rhombic Section	[010]	Optically indistinguishable from Acline in plagioclase of medium composition

The following routine procedure is recommended for determining first the twinning law by which two subindividuals are related, and second their mean composition.

(1) If the directions X_1, X_2, etc. have been accurately located in subindividuals (1) and (2), and if the composition of the measured subindividuals is uniform, the point of emergence of the twinning axis A_{1-2} upon the projection is the point of intersection of the three great circles respectively containing X_1 and X_2, Y_1 and Y_2, Z_1 and Z_2. Usually these arcs do not intersect at a point, but form the boundaries of a triangle of error, the center of which gives the approximate location of the twinning axis. Even when this triangle is fairly large—especially when the angle of intersection of two great circles is small—the results need not be discarded, since exact location of the twinning axis is not essential for approximate determination of composition. Two general cases may at once be distinguished:

(a) The twinning axis coincides with, or approximates to, the plotted pole of the composition plane (as the case of A_{1-2}, Fig. 2). The twin is of the normal type, and the twinning axis (excluding the remote possibility of a Baveno twin) is either ⊥(010) or ⊥(001).

(b) The twinning axis lies within or close to the arc representing the projection cf the composition plane (as in the case of A_{1-3} and A_{2-3}, Fig. 2). The twin is then of either the parallel or the complex type.

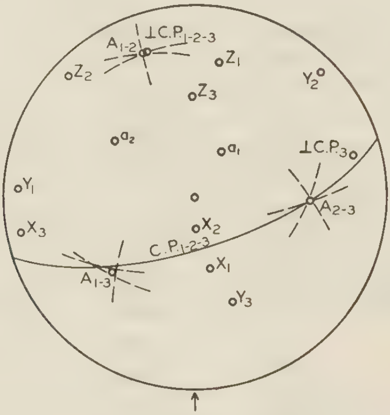

Fig. 2. Equal-area projection (lower hemisphere) of optical and crystallographic data for plagioclase crystal of Fig. (1), twinned on albite and Carlsbad laws.

(2) In either case the mean values are now obtained for the three angles between the twinning axis and each of X, Y and Z, respectively. Rotate the sheet until X_1 and X_2 lie on a great circle of the projection net, and measure the angular distance between them across the arc within which the twinning axis emerges. Half this measured angle $X_1 \wedge X_2$ is the mean value for $X \wedge A_{1-2}$. Similarly measure and halve the appropriate angles $Y_1 \wedge Y_2$ and $Z_1 \wedge Z_2$.

(3) For parallel and complex twins, now measure the angle between the twinning axis and the pole of the second set of twin lamellae or cleavage planes crossing one or other of the two subindividuals in question (e.g. $\perp^2 CP_3$ or $\perp^2 Cl_3$). The angle so obtained can be used to identify the twinning axis. Since neither of the measured points is accurately located on the projection, the angle between them cannot in some cases be determined with greater accuracy than ±5°. Except in the case of very sodic or very calcic plagioclase where the transverse lamellae are of the pericline type, this error is immaterial in identifying the twin axis.

(4) The following illustration shows how the data obtained above may be utilized in the final determination. The angles measured on the projection, Fig. 2, are:

Twin 1–2. Normal twin

$A_{1-2} \wedge X$	81°
$\wedge Y$	64°
$\wedge Z$	27°

Twin 2–3. Parallel or complex twin

$A_{2-3} \wedge X$	51°
$\wedge Y$	51°
$\wedge Z$	62°
$A_{2-3} \wedge \perp^2 CP_3$	28° ±

Twin 1–3. Parallel or complex twin

$A_{1-3} \wedge X$	41°
$\wedge Y$	51°
$\wedge Z$	$80\frac{1}{2}$°
$A_{1-3} \wedge \perp^2 CP_3$	63° ±

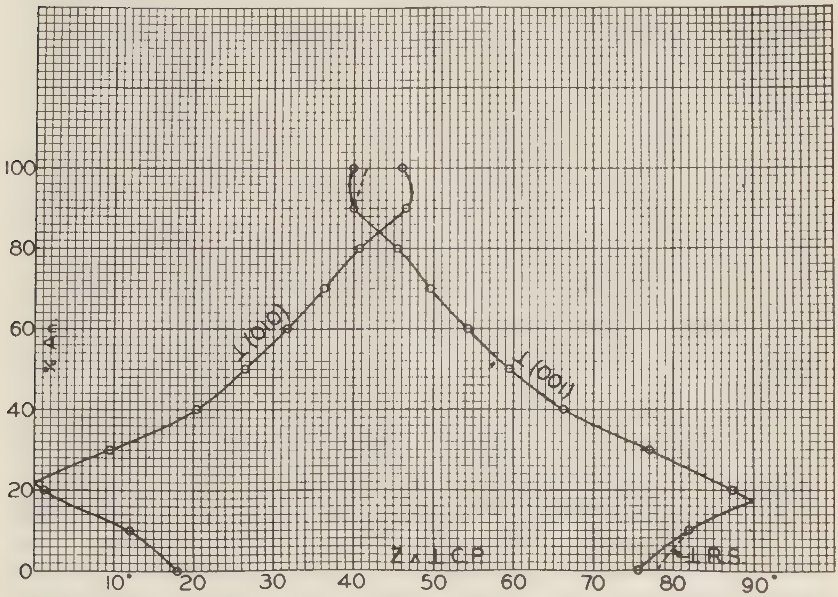

FIG. 3. Relation of angle between Z and the normal to the composition plane (Z∧⊥C.P.), and anorthite content in plagioclase. Broken curve refers to normal to rhombic section.

(a) *Twin 1–2.* Since this is a normal twin, reference is made to Fig. 5. The respective angles between the twinning axis and each of X and Y are plotted one against the other to give a point *P* close to the curve for ⊥(010). This establishes the twinning axis as ⊥(010) and composition plane as (010) (albite law). The composition is given as An_{49} by the point where the normal drawn from *P* intersects the curve. (The numbers 0–10 on this and all other curves of Figs. 5–7 correspond to anorthite percentages 0–100.)

(b) *Twin 2–3.* It has just been shown that the common composition plane for all three measured subindividuals is (010). If this had not previously been done it would be necessary to measure separately the angle $Z\wedge \perp CP_{2-3}$ (29°), which identifies the composition plane CP_{2-3} as (010) (cf. Figs. 3 or 4). To determine the twinning axis* plot on Fig. 4 the angles $A_{2-3}\wedge \perp^2 CP_3 = 28° \pm$, and $Z\wedge \perp CP_{2-3} = 29°$; then the twinning axis must be [001] (Carlsbad law). Now referring to the corresponding curve of Fig. 6 plot the angles $A_{2-3}\wedge X$ and $A_{2-3}\wedge Y$, to give *P* which indicates a mean composition An_{47}.

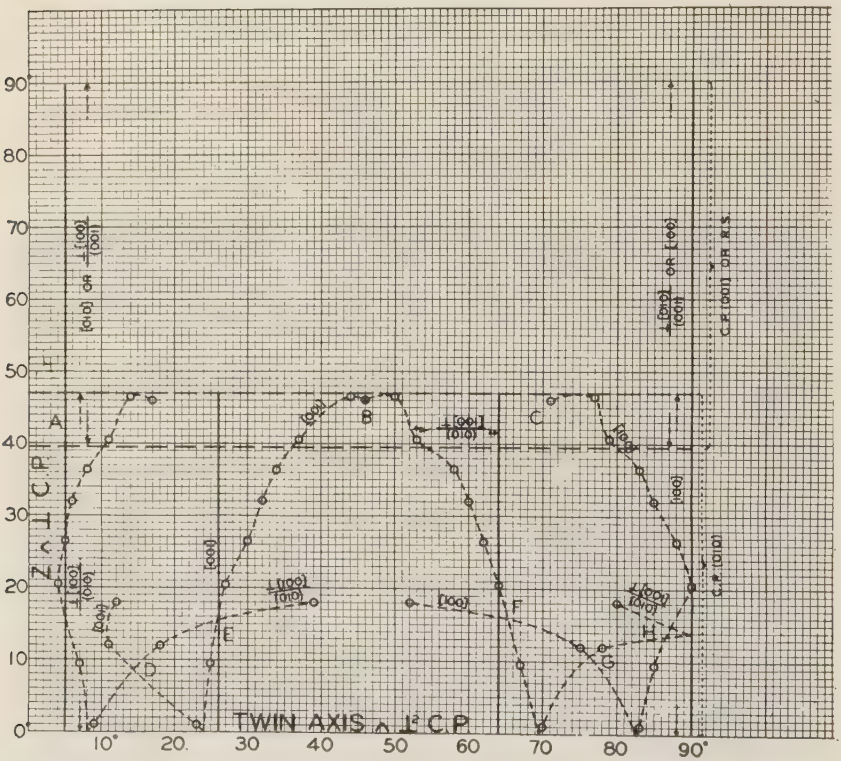

Fig. 4. Angle between twinning axis and normal to second composition plane or cleavage plane, plotted against Z∧⊥C.P. Broken curve applies where the second composition plane is the rhombic section.

---

* Nikitin (1936, p. 102), Emmons (1943, p. 156) and others identify the twinning axis of a parallel or complex twin merely by noting to which of the standard migration curves (equivalent to those of Figs. 6 and 7 in this paper) the plotted point representing the positions of X, Y and Z lies closest. The writer has found this unsatisfactory since the curves in question often lie close together, and the plotted point may be as much as 5° or 10° from the curve to which it actually belongs. It is therefore recommended that as far as possible the twinning axis should be identified before the optical data are plotted on Figs. 6 and 7.

(c) *Twin 1–3.* From the above, it follows that subindividuals (1) and (3) must be related by twinning on the Carlsbad-albite law with ⊥[001]/(010) as twinning axis. This is confirmed (Fig. 4) by the angle $A_{1-3} \wedge \perp^2 CP_3 = 63° \pm$. Plotting the corresponding X and Y angles on Fig. 7 gives a point *P* indicating a composition An_{45}.

A discrepancy between the values for composition as determined in different pairs of subindividuals belonging to a single crystal (in the above case An_{49}, An_{47}, An_{45}) is by no means uncommon. It shows that even with a universal stage the An content of plagioclase cannot be determined more closely than ±3%.

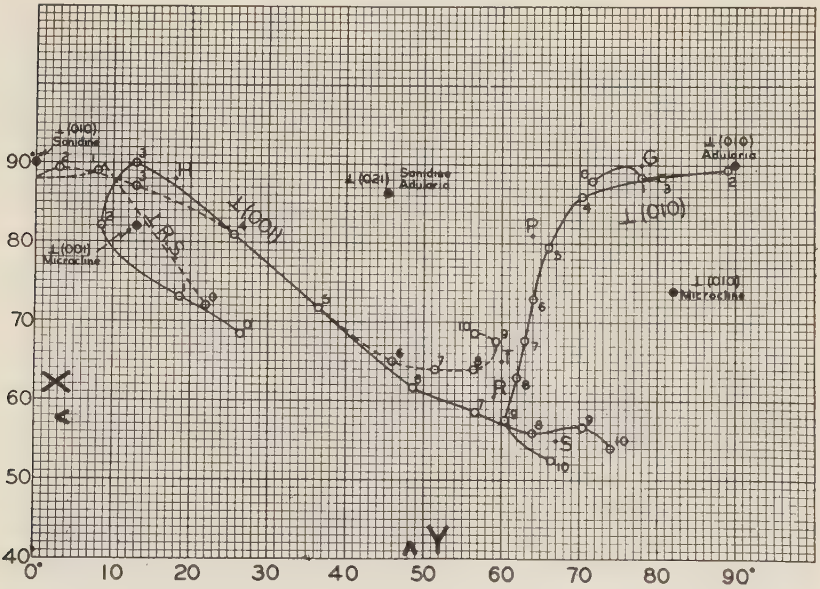

FIG. 5. Angles between X and Y and normals to composition planes in plagioclase. Numbers 0–10 on each curve indicate anorthite contents 0–100%.

The above case has been described fully so that the reader may check the method by carrying out each step in turn. Contrary to widely prevalent belief the procedure is neither complex nor unduly lengthy. Optical measurements, projection of the measured data, and subsequent identification of twin laws and determination of composition in this particular case took about 30 minutes. Ten to fifteen minutes should suffice for a crystal in which only two subindividuals are completely measured; while a determination based on measurement of X, Y and Z and one set of cleavages in an untwinned grain (using Fig. 5) takes less than ten minutes.

AMBIGUOUS CASES

If observations are confined to two subindividuals, a number of cases involving some degree of ambiguity commonly arise. Most of these may be solved satisfactorily if additional data are obtained from other subindividuals of the same crystal.

(a) *Ambiguous cases with normal twinning*

(1) In Fig. 5 (cf. also Figs. 3 and 4), identification of the twinning axis of normal twins for the range An_{70} to An_{100} is usually uncertain. Direct measurement of the second (transverse) set of cleavage planes or twin lamellae in one of the principal subindividuals, and determination of the angles between X and Y respectively and the pole of this second plane usually leads to an unambiguous solution.

Example:

$$\begin{aligned} A_{1-2} \wedge X &= 60\tfrac{1}{2}^\circ \\ \wedge Y &= 59^\circ \end{aligned}$$

The corresponding point *R* in Fig. 5 could represent either

(a) Albite twinning with $\perp(010)$ as twinning axis; composition An_{86}; or (b) Manebach twinning with $\perp(001)$ as twinning axis; composition An_{72}. The former is more likely if the twin is of the lamellar type. Further measurement gives

$$\begin{aligned} \perp{}^2CP_1 \wedge X_1 &= 55^\circ \\ \wedge Y_1 &= 67^\circ \end{aligned}$$

The corresponding point *S* in Fig. 5, taken in conjunction with the previous alternative, confirms alternative (a).

Ambiguity is possible in some cases even after additional measurements have been made. Suppose, for example, that in the instance just described the point given by the second set of measurements were $T(\perp{}^2CP_1 \wedge X = 65^\circ;\ \perp{}^2CP_1 \wedge Y = 60^\circ)$. There are still two alternatives, of which the first is more likely to be the correct solution:

(a) Albite twinning, with transverse ($^2CP_1$) pericline lamellae; composition An_{86}.

(b) Manebach twinning, with transverse ($^2CP_1$) albite lamellae; composition An_{72}. Measurement of a Carlsbad twin in the same crystal removes all doubt.

(2) The curve for albite twinning—$\perp(010)$ in Fig. 5—is ambiguous over the range An_0 to An_{40}. That for $\perp(001)$ in Fig. 5 is also liable to ambiguity over the same range, if the plotted point falls inside and some distance from the ideal curve. Doubt is usually removed by plotting data for other subindividuals in the same crystal.

Example:

$$\begin{array}{rl} & \left.\begin{array}{r}\perp(010)\wedge X\ 90^\circ\\ \perp(010)\wedge Y\ 78^\circ\end{array}\right\}\begin{array}{l}G \text{ in Fig. 5;}\\ An_{9} \text{ or } An_{32}.\end{array}\\ \text{In the same crystal} & \left.\begin{array}{r}\perp(001)\wedge X\ 88^\circ\\ \perp(001)\wedge Y\ 18^\circ\end{array}\right\}\begin{array}{l}H \text{ in Fig. 5;}\\ An_{33}.\end{array}\end{array}$$

The composition must be $An_{32}\pm$.

Axial angle and refractive index may also be used to solve certain cases, e.g. to distinguish An_{10} ($2V=82°$, sign $+$; $\beta<\mu$ Canada balsam) from An_{32} ($2V=83°$, sign $-$; $\alpha>\mu$ Canada balsam).

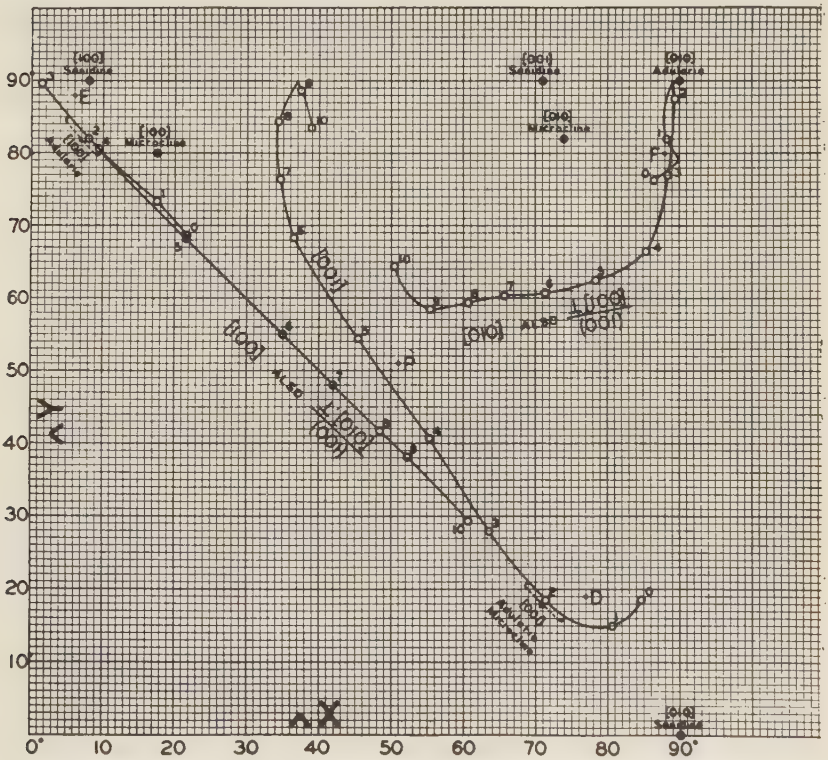

FIG. 6. Angles between X and Y and twinning axes of parallel and complex twins in plagioclase. Numbers 0–10 on each curve indicate anorthite contents 0–100%.

(b) *Ambiguous identity of the twinning axis in parallel and complex twins*

(1) It is impossible to distinguish optically between the twinning axes [100] and ⊥[010]/(001), or again between [010] and ⊥[100]/(001). In neither case would such a distinction have any practical importance, since the two axes of each pair are mutually inclined at very small angles. Each pair is therefore represented (within limits of experimental error) by a single curve in Fig. 6.

(2) When $Z \wedge \perp CP$ (the pole of the main composition plane) is less than about 20°—i.e. when $CP = (010)$ and the composition of the plagioclase is between An_0 and An_{40}—ambiguity arises if the second (transverse) set of planes measured in one of the main subindividuals is a set of twin lamellae. These are most likely to be pericline lamellae, the position of which in relation to the axes of the crystal lattice changes rapidly with variation in anorthite content in the more sodic plagioclases. This accounts for the irregular form of the broken curve of Fig. 4. Identification of the twinning axis is ambiguous in the case of points falling near *D*, *E*, *F*, *G* or *H* in Fig. 4. Nor is this ambiguity removed when appropriate data for X and Y are plotted alternatively on Figs. 6 and 7; for the very twinning axes that are liable to be confused in Fig. 4 have curves that lie close together in Figs. 6 and 7.

Example:

$$Z \wedge \perp CP_{1-2} = 8°$$
$$A_{1-2} \wedge \perp^2 CP_1 = 15°$$

Plotted on Fig. 4, these figs. give a point close to *D*. Alternative interpretations.

(a) $A_{1-2} = [001]$; composition $= An_{15} \pm$.

(b) $A_{1-2} = \frac{\perp[100]}{(010)}$; composition $An_{15} \pm$.

Additional data from the same crystal are:

$$A_{1-2} \wedge X = 77°$$
$$A_{1-2} \wedge Y = 19°$$

Alternative interpretations:

(a) Figure 6, point *D*.
$A_{1-2} = [001]$; composition $= An_{15}$.

(b) Figure 7, point *D*.
$A_{1-2} = \frac{\perp[100]}{(010)}$; composition $= An_{13}$.

Although the composition has been determined as An_{13-15}, the identity of the twinning axis still remains uncertain. The only sure way to avoid ambiguity where plagioclase is a sodic variety, is to measure and plot a second set of cleavage planes ($^2Cl_1$ or $^2Cl_2$) instead of twin lamellae.

(3) Where the anorthite content of plagioclase is high (i.e. $Z \wedge \perp CP_{1-2} = 39°\text{–}47°$) the case in which $A_{1-2} \wedge \perp^2 CP_{1-2} = 5° \pm$ is insolubly ambiguous. Thus points in the vicinity of *A* in Fig. 4 are open to any of the following alternative interpretations:

(i) $CP_{1-2} = (010)$, $A_{1-2} = \frac{\perp[100]}{(010)}$; albite—ala twin.

(ii) $CP_{1-2} = (001)$, $A_{1-2} = [010]$; acline twin.

(iii) $CP_{1-2}=(001)$, $A_{1-2}=\frac{\perp[100]}{(001)}$; Manebach—ala twin, indistinguishable from acline twin by optical means.

(iv) CP_{1-2}=rhombic section, $A_{1-2}=[010]$; pericline twin.

The same ambiguity holds if a cleavage $^2Cl_1$ is measured instead of twin lamellae $^2CP_1$.

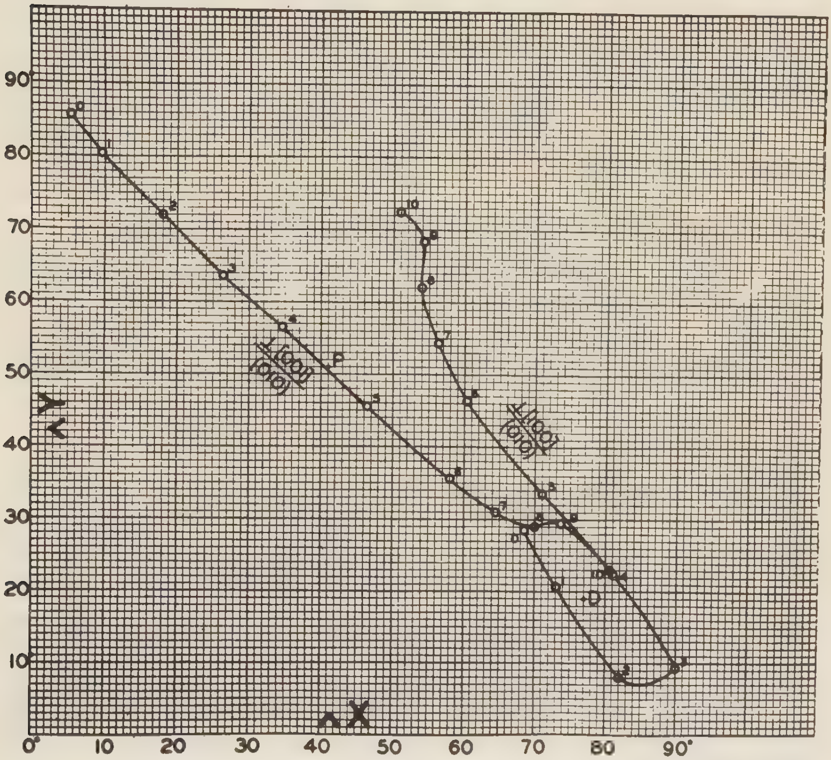

Fig. 7. Angles between X and Y and twinning axes of parallel and complex twins in plagioclase. Numbers 0–10 on each curve indicate anorthtite contents 0–100%.

(4) From Fig. 4 there would appear to be ambiguity for points in the vicinity of *B* and *C*. These correspond to calcic plagioclase with $Z\wedge\perp CP_{1-2}=42°–47°$, in which the second set of measured lamellae ($^2CP_1$ or $^2CP_2$) proves to be due to pericline twinning. Such cases are solved when the angles $A_{1-2}\wedge X$ and $A_{1-2}\wedge Y$ are plotted on Figs. 6 and 7. The anorthite ends of the curves for [001] and ⊥[001]/(001) are sufficiently divergent over the range An_{80} to An_{100} to dispel any such ambiguity as may be apparent in the vicinity of *B* on Fig. 4.

(c) *Ambiguity as to composition in parallel and complex twins*

Any point falling on the curves for [100] or [010] or $\perp[100]/(010)$ in Figs. 6 and 7, within the range An_0 to about An_{40} is ambiguous with regard to anorthite content of the grain in question. The difficulty may usually be overcome by plotting data for other subindividuals of the same crystal.

Example:

$$\left.\begin{array}{l}[100] \wedge \text{X} = 6^\circ\\ [100] \wedge \text{Y} = 88^\circ\end{array}\right\} \begin{array}{l} E \text{ in Fig. 6;}\\ \text{An}_{26} \text{ or An}_{33}\end{array}$$

In the same crystal

$$\left.\begin{array}{l}[010] \wedge \text{X} = 88^\circ\\ [010] \wedge \text{Y} = 80^\circ\end{array}\right\} \begin{array}{l} F \text{ in Fig. 6;}\\ \text{An}_{27} \text{ or An}_{8}\end{array}$$

Composition must be $\text{An}_{26}\pm$.

General recommendations for avoiding ambiguity

The following recommendations are made with a view to obtaining results free of all ambiguity:

(1) When working with calcic plagioclase, An_{75} to An_{100}, use as far as possible parallel or complex twins with any of the following as twinning axes:

[001]; Carlsbad twin; Fig. 6.

$\dfrac{\perp[001]}{(010)}$; Carlsbad-albite twin; Fig. 7.

[100] or $\dfrac{\perp[010]}{(001)}$; Ala or Manebach-acline twin respectively; Fig. 6.

(2) For plagioclase of medium composition, An_{40} to An_{75}, any kind of twinning may be used without ambiguity.

(3) Determination of composition in sodic plagioclase, An_0 to An_{40}, is particularly liable to lead to ambiguous results. These may be avoided in three ways:

(a) Use twins where the composition plane $\text{CP}_{1-2} = (010)$; i.e. where $\text{Z} \wedge \perp\text{CP}_{1-2} < 20^\circ$. Identify the twin axis A_{1-2} by measuring a second set of cleavages (e.g. $^2\text{Cl}_1$) rather than twin lamellae (e.g. $^2\text{CP}_1$). Use especially crystals showing Carlsbad twinning ($\text{A}_{1-2} = [001]$) or Carlsbad-albite twinning ($\text{A}_{1-2} = \perp[001]/(010)$).

(b) Use twins where the composition plane $\text{CP}_{1-2} = (001)$ or the rhombic section, i.e., where $\text{Z} \wedge \perp\text{CP}_{1-2} > 65^\circ$. Measure fully at least three subindividuals so that points on two or three curves may be interpreted simultaneously.

(c) Highly sodic plagioclase An_0 to An_{10} can be distinguished from more calcic plagioclase An_{25} to An_{40} (with which it is liable to be confused on curves for the common twins whose axes are $\perp(010)$ and [010]) by determining the optic axial angle and sign. For An_0 to An_{10} the sign is positive and the axial angle ranges from 71°–83°; for An_{25} to An_{40} the sign is negative and the axial angle 80°–90°.

SPECIAL CASES WHERE X, Y OR Z IS PARALLEL TO A TWINNING AXIS

If X is parallel to the twinning axis, then Y_1 coincides with Y_2 and Z_1 coincides with Z_2, and consequently there is no optical indication of twinning. A like condition holds good if either Y or Z is parallel to an axis of twinning. Inspection of the standard curves shows that this condition, although not precisely realized, is very closely approached in several instances of parallel and complex twinning in plagioclase:

(1) An_{17}; twinning axis [010]; $Z\wedge[010]=1°$;

(2) An_{17}; twinning axis $\frac{\perp[100]}{(001)}$; $Z\wedge\frac{\perp[100]}{(001)}=2°$.

(3) An_{30}; twinning axis [100]; $X\wedge[100]=1\frac{1}{2}°$.

(4) An_{30}; twinning axis $\frac{\perp[010]}{(001)}$; $X\wedge\frac{\perp[010]}{(001)}=1\frac{1}{2}°$.

SPECIAL CASES WHERE X, Y OR Z IS PERPENDICULAR TO A TWINNING AXIS

Consider the special case where one of the three directions X, Y or Z is perpendicular to the twinning axis (e.g., Y in Fig. 10). Then this particular direction is the same in the two twinned subindividuals; and the other two pairs of directions, X_1, Z_1, X_2, Z_2 in Fig. 10, all lie in one plane, i.e., their poles lie on a single great circle of the projection. There may thus be a choice between two possible twinning axes—A and A′, the bisectors of the axis Z_1 Z_2 and X_1 X_2 in Fig. 10. Where, as in Fig. 10 the plane of X_1, Z_1, X_2 and Z_2 is oblique to the composition plane, graphic determination of the twinning axis still leads to a unique solution; since only one direction (in this case A) satisfies the second requirement of a twinning axis, viz., that it must lie normal to or within the composition plane.

There are three particular cases, however, where special conditions lead to solutions involving a choice of twinning axes, or to some other ambiguity. Each case is represented in the plagioclase series.

Case I Oligoclase, An_{22}, twinned with (010) *as composition plane.* The special condition for oligoclase, An_{22} is that Z is normal to the composition plane (010) (cf. Fig. 3), i.e., to any twinning axis lying within that plane. This leads to the following conditions peculiar to oligoclase of this particular composition:

(1) In any instance of parallel or complex twinning with (010) as composition plane graphic determination of the twinning axis leads to two alternative solutions. In the example shown in Fig. 8, twinning on either [001] (A) or ⊥[001]/(010) (A′) would account equally well for the relative orientation of the two subindividuals concerned. In other cases there is a similar choice between [100] and ⊥[100]/(010). If the data for X and Y are plotted on the two appropriate curves of Figs. 6 and 7, the compositions so determined are identical, as shown in the following example projected in Fig. 8:

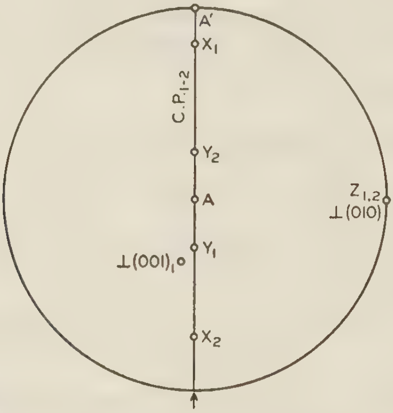

FIG. 8. Equal-area projection for oligoclase An_{22} twinned with $[001]=A$ or $\dfrac{\perp[001]}{(010)}=A'$ as alternative twinning axes. C.P. = composition plane, (010).

$A \wedge \perp^2 Cl_1 = 26°$; therefore $A = [001]$

$A' \wedge \perp^2 Cl_1 = 64°$; therefore $A' = \dfrac{\perp[001]}{(010)}$

$\left.\begin{array}{l} A \wedge X = 70° \\ A \wedge Y = 20° \end{array}\right\}$ From [001] curve, Fig. 6, composition $= An_{22}$.

$\left.\begin{array}{l} A' \wedge X = 20° \\ A' \wedge Y = 70° \end{array}\right\}$ From $\dfrac{\perp[001]}{(010)}$ curve, Fig. 7, composition $= An_{22}$.

In actual practice a similar choice of twinning axes exists for oligoclase ranging from An_{20} to An_{25}; for Z_1 and Z_2 so nearly coincide that slight errors in location of either lead to great elongation of the triangle of error along the obliquely intersecting arcs X_1, X_2 and Y_1, Y_2.

(2) If two subindividuals of composition An_{22} are twinned on the albite law, i.e., by reflection across (010), their optic orientations are

identical; i.e., for this precise composition albite twinning cannot be detected optically.

(3) The optic orientation of oligoclase, An$_{22}$ is almost identical with that of low-temperature orthoclase (adularia), such as occurs in plutonic and metamorphic rocks. When feldspar occurs in scattered untwinned grains, as in many metamorphic rocks, or in small simply twinned laths in the groundmass of lavas, oligoclase may readily be confused with orthoclase unless refractive index tests can be made.

A similar condition is closely approached in oligoclase, An$_{17}$ to An$_{20}$, twinned on the pericline law. In this case Y makes an angle of 87°–89° with the rhombic section, cf. Fig. 5.

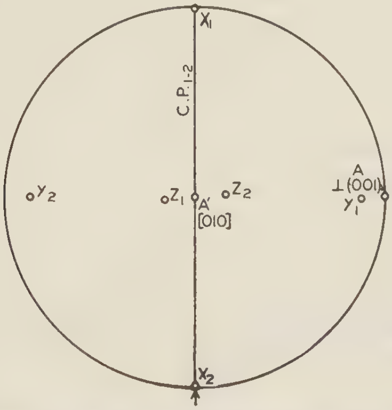

FIG. 9. Equal-area projection for oligoclase-andesine An$_{30}$ twinned with ⊥(001)=A or [010]=A′ as alternative twinning axes. CP$_{1-2}$=composition plane (001).

Case II. Sodic plagioclase with X or Z normal to twinning axis and parallel to composition plane. If one of the directions X, Y or Z is normal to a twinning axis and also lies in the composition plane, graphic determination of the twinning axis again leads to two solutions. Here there is a choice between an axis of normal twinning, and one of parallel or complex twinning. Within limits of experimental error, this condition is fulfilled for plagioclase of various compositions within the range of oligoclase.

(a) Oligoclase-andesine, An$_{30}$; X lies in (001); X is almost normal to ⊥[100]/(001), which coincides with, and cannot be distinguished optically from [010]. Graphic determination of the twinning axis (Fig. 9) leads to two alternatives, either ⊥(001) (A), or [010]= ⊥[100]/(001) (A′).

(b) Oligoclase, An$_{18}$; Z lies in (001); Z is nearly normal to [100] = ⊥[010]/(001). Within the limits of experimental error there is a choice between ⊥(001), and [100]= ⊥[010]/(001) as twinning axes.

(c) Albite and oligoclase, An_3 to An_{30}; X is very nearly parallel to (010); X is very nearly perpendicular to [010].

Case III. Simulation of normal twinning (Bytownite An_{85}). An essential part of the Emmons procedure for determining feldspars with a five-axis stage, and a useful check in the zone method of Rittmann, is the direct microscopic distinction between normal twins and twins of the parallel or complex type (Emmons and Gates, 1939, p. 579; Emmons, 1943, pp. 104, 129). The composition plane of the twinned crystal is brought parallel to the vertical N–S plane, and the crystal is now tilted through any angle about the E–W axis of the stage, i.e., about the normal to the composition plane. If the change in interference color is identical in the two subindividuals, i.e., if they remain exactly matched in color throughout tilting, the twin is diagnosed as a normal twin; if the color change is unequal, the twin is parallel or complex.

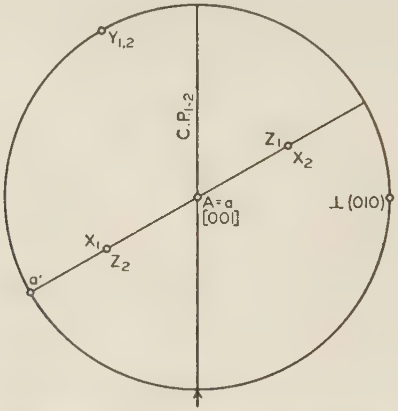

FIG. 10. Ideal case of Carlsbad twinning—[001] = twinning axis—to give coincidence of optic axes (a, a′) in both subindividuals (cf. An_{85}).

In his intensive study of feldspars in some Indian basalts, Barber (1936*a*, pp. 258–262) noted five separate instances where bytownite, An_{85}, twinned on the Carlsbad law gave the optical reaction of a normal twin, when treated as just described. He concluded that "in feldspars of this composition (85 per cent. An.) the birefringence of two hemitropes twinned according to the Carlsbad law is equal in all positions in the zone perpendicular to (010)" (Barber, 1936*a*, p. 262). No further explanation was offered. It was pointed out that this phenomenon had been observed only in bytownite (An_{85}) but that it nevertheless illustrates "the danger of relying on curtailed procedure for the recognition of the twinning law."

It would seem that the phenomenon recorded by Barber could occur in any feldspar in which the following three conditions, illustrated in projection in Fig. 10, were simultaneously fulfilled:

(a) Y is perpendicular to the twinning axis [001], A, but is inclined at any angle to the composition plane (010).

(b) 2V=90°

(c) The twinning axis, [001], makes angles of 45° with X and Z respectively. Under these conditions (and in no other circumstances) both optic axes of the two twinned subindividuals coincide; one pair also coincides with twinning axis, A.

The interference color shown by any section of plagioclase depends upon the relative retardation of the emergent rays; and this, for a given thickness of section and a given angle of tilt on E–W, depends upon the angles between the emergent ray and each of the optic axes.* These same angles also determine the vibration directions of the emergent rays,† and so in turn the intensity of illumination of a section as seen between crossed nicols. Now, for any degree of tilt on E–W, the two subindividuals of the ideal twin of Fig. 10 have in common the two optic axes (a and a') and the direction of the emergent ray (which must lie in the composition plane). Consequently both subindividuals show exactly the same interference tint and equal intensity of illumination.

Bytownite, An_{85}, does not exactly conform to the ideal conditions depicted in Fig. 10: but it approximates sufficiently closely to account for the phenomenon recorded by Barber. The angle $Y \wedge [001]$, as indicated in Fig. 6, is 88°; 2 V, according to data recorded by Barber (1936*a*, p. 277) is close to 85°; the angles $X \wedge [001]$ and $Z \wedge [001]$, measured from Barber's (1936*a*, p. 261) stereographic projection are 35° and 55°, respectively. This appears to be the only case in the plagioclase series, in which all three conditions specified above approach fulfillment.

There are two additional general cases, however, in which it may be difficult or impossible to distinguish between normal and parallel twins by the optical means described by Emmons:

(a) If X or Y or Z is normal to the composition plane, then both subindividuals remain in extinction when the crystal is rotated about the normal after the latter has been brought to coincide with the E–W axis of the stage. This is true for oligoclase An_{22} twinned on any law with (010) as composition plane; and it is very nearly true for oligoclase, An_{17} to An_{20}, twinned on the pericline law.

---

* Johannsen (1918, pp. 351–355) derives the equation

$$\gamma' - \alpha' = (\gamma - \alpha) \sin\theta \sin\theta'$$

where $\gamma' - \alpha'$ = relative retardation of a random section, and θ and θ' are respective angles between the emergent ray (the normal to the section) and the two optic axes.

† The vibration directions bisect the angles of intersection of the traces of the two planes each of which contains the direction of the emergent ray and one optic axis.

(b) Where X, Y or Z is nearly parallel to a twinning axis for medium and calcic oligoclase, the optic axes of one subindividual very nearly coincide with those of the other. The optical behavior of the two subindividuals should therefore be almost identical when the crystal is rotated about the normal to the composition plane.

DETERMINATIONS ON ZONED CRYSTALS AND MICROLITES

When plagioclase crystals are strongly zoned, where adjoining lamellae are notably different in composition, or when the crystals to be measured are small laths or microlites in which X, Y and Z can be measured in only one subindividual, it is obviously impossible or undesirable to use a twinning axis as the crystallographic direction of reference with which to compare the positions of X, Y, and Z in the lattice. In such cases a cleavage or composition plane is measured as accurately as possible and its pole plotted directly on the projection and used as the reference point. The directions X, Y and Z are measured in such lamellae and zones as are large enough for this, and plotted on the projection. Appropriate angles can now be measured and the anorthite content determined from the curves of Fig. 5.

This method, though quick, is somewhat inaccurate. It is difficult to locate cleavage or composition planes precisely by microscopic means, especially if they are inclined at less than 75° to the plane of the section. Composition planes are usually more sharply defined and more continuous than cleavage planes; but they are liable to be determined by vicinal faces (cf. Barber, 1936*a*, pp. 233, 236), whereas cleavage faces must always be rational.

An alternative method is that of Rittmann (1929) generally referred to as the "zone method." This has been described fully by various writers (e.g. Barber, 1936*a*, pp. 278–281; Emmons, 1943, pp. 115–134) and need not be considered further here, beyond noting that some experienced workers (e.g. Barber, 1936*a*, p. 281) consider it unsatisfactory and inaccurate. It is, however, the only practicable method for determining composition of very narrow zones of microlites (usually elongated parallel to *a*) so small that X, Y, and Z cannot be located accurately.

DEPARTURES FROM STANDARD CURVES

A number of writers have commented upon the commonly observed discrepancy between points plotted from data measured by the universal stage, and the ideal curves given by Duparc and Reinhard (1924), Nikitin (1936) and others. The same applies to the equivalent curves of Figs. 5, 6 and 7.

The most comprehensive discussion of this topic in English, illustrated by abundant experimental data, is that of Barber (1936*a*, pp. 230–258) who concluded that the physical conditions, especially temperature, prevailing at the time of crystallization are probably responsible for the observed variation. Barber dismissed variation in potash content, as having minor influence only, and discounted inaccuracies in measurement, inaccuracies in the standard curves, and errors due to vicinal faces as composition planes, as possible causes of the discrepancies noted. The problem is still not satisfactorily solved. In a subsequent paper Barber (1936*b*) recorded some experimental results which failed to confirm his hypothesis of temperature control; but several European workers, notably Köhler (1942*a*, 1942*b*), Scholler (1942), Tertsch (1942), and Oftedahl (1944) have since brought forward additional experimental evidence pointing to the existence of appreciable optical differences between high- and low-temperature plagioclases of corresponding compositions. The latest account, accompanied by a full list of European references, is that of E. Wenk (1945, pp. 368–371).

The writer records his own experience that optical data for andesine and labradorite in basic and semibasic lavas and sills in eastern Otago, New Zealand, consistently depart appreciably, sometimes by as much as 10°, from the standard curves (cf. Benson and Turner, 1940, pp. 196, 198; Benson, 1944, pp. 74, 75). This might well be attributed to the high temperatures and low pressures typical of volcanic conditions; but there is also the possibility of a chemical influence, for many of the rocks in question are notably alkaline.

ACKNOWLEDGMENTS

The writer wishes to acknowledge his gratitude to Mr. Theo. H. Crook who very kindly prepared all diagrams accompanying this paper. His thanks are also due to Professor A. Pabst for helpful discussion on a number of points relating to optics of twinned plagioclase.

REFERENCES

BARBER, C. T. (1936*a*), The Tertiary igneous rocks of the Pakokku District and the Salingyi Township of the Lower Chindwin District, Burma, with special reference to the determination of the feldspars by the Fedoroff Method: *Mem., Geol. Sur. India*, **68,** pt. 2.

——— (1936*b*), The effect of heat on the optical orientation of plagioclase feldspars: *Mineral. Mag.*, **24,** 343–352.

BENSON, W. N. (1944), The basic igneous rocks of Eastern Otago and their tectonic environment, Part IV: *Trans. Roy. Soc. New Zealand*, **74,** pt. 1, 71–123.

——— AND TURNER, F. J. (1940), Mugearites in the Dunedin district: *Trans. Roy. Soc. New Zealand*, **70,** pt. 3, 188–199.

DUPARC, L., AND REINHARD, M. (1924), La Détermination des Plagioclases dans les Coupes Minces: *Mem. Soc. Phys. and Hist. Nat. Genève*, **40,** fasc. 1.

Emmons, R. C. (1943), The Universal Stage: *Mem. Geol. Soc. Am.*, no. **8.**

———, and Gates, R. M. (1939), New method for the determination of feldspar twins: *Am. Mineral.*, **24,** 577–589.

Johannsen, A. (1918), *Manual of Petrographic Methods*, McGraw-Hill, New York.

Köhler, A. (1942a), Die Abhängigkeit der Plagioklasoptik von vergangenen Wärmeverhalten: *Min. Petr. Mitt.*, **53,** 24–49.

——— (1942*b*), Drehtischmessungen an Plagioklaszwillingen von Tief- und Hochtemperaturoptik: *Min. Petr. Mitt.*, **53,** 159–179

Nikitin, W. (1936), *Die Fedorow-Methode*, Borntraeger, Berlin.

Oftedahl, C. (1944), High temperature optics in plagioclases of the Oslo region: *Norsk Geol. Tidssk.*, **24,** 75–78.

Scholler, H. (1942), Versuche zur Temperaturabhängigkeit der Plagioklasoptik: *Min. Petr. Mitt.*, **53,** 180–221.

Tertsch, H. (1942), Zur Hochtemperaturoptik basischer Plagioklase: *Min. Petr. Mitt.*, **54,** 193–217.

Wenk, E. (1945), Kritischer Vergleich von Anorthitbestimmungen an Plagioklasen: *Schweiz. Min. Petr. Mitt.*, **25,** 349–382.

THE CELL AND SYMMETRY OF PYRRHOTITE

M. J. Buerger, *Massachusetts Institute of Technology, Cambridge, Massachusetts.*

Abstract

According to the literature, ferromagnetic pyrrhotite exists in the composition range $Fe_{.48}S_{.52}$ to $Fe_{.466}S_{.534}$ and has the nickel arsenide type structure with cell dimensions $a=3.43$ Å, $c=5.68$ Å; paramagnetic "troilite" is confined to the composition range $Fe_{.50}S_{.50}$ to $Fe_{.48}S_{.52}$, and has two kinds of structures: nickel arsenide type in the high sulfur half of the field, and a superstructure type in the region near the ideal composition FeS.

New results are reported here which are at variance with this information. Single crystals of ferromagnetic pyrrhotite from Schneeberg, Saxony, and from Morro Velho, Brazil, were investigated by the precession method. The photographs show a hexagonal cell much larger than any hitherto proposed for either troilite or pyrrhotite. Its dimensions are $a=6.87$ Å, $c=22.7$ Å. This cell has sixteen times the volume of a nickel arsenide type cell. The diffraction symbol of pyrrhotite is $6/mmm\ C\ 6_3/---$. If this effect arises from a single crystal the space group is $C6_32$, but there is a possibility that the diffraction effect may arise from a twin. This supercell is not the same as the one hitherto reported in the literature for troilite, and it belongs to a type of pyrrhotite outside of the troilite range where no superstructure is supposed to occur.

Status of "Pyrrhotite"

The arrangement of atoms in pyrrhotite was deduced by Alsén[1] from data derived from rotating-crystal, Laue and powder photographs of crystals from Kongsberg, Sweden, as well as from powder photographs of other material. Alsén assigned to pyrrhotite the structure now known as the nickel arsenide arrangement, with the following cell dimensions:

$$a = 3.43 \text{ Å}$$
$$c = 5.68 \text{ Å}$$

Subsequently Hägg and Sucksdorf[2] investigated artificial preparations of varied iron:sulfur ratio, using the powder method. They demonstrated that the variation of composition was due to omission of iron atoms from the structure. They also discovered that, while the powder photographs showed the nickel arsenide pattern found by Alsén, provided that the sulfur content was above about $51\frac{1}{2}$ atomic per cent, preparations with less sulfur gave powder photographs with superstructure lines. They were able to index these photographs on the basis of hexagonal or trigonal symmetry for a hexagonal cell having the following dimensions:

---

[1] Alsén, Nils, Röntgenographische Untersuchung der Kristallstruckturen von Magnetkies, Breithauptite, Pentlandite, Millerite und verwandten Verbindungen: *Geol. Fören. Förhandl. Stockholm,* **47,** 19–72 (1925).

[2] Hägg, Gunnar, and Sucksdorff, Ingrid, Die Kristallstruktur von Troilit und Magnetkies: *Zeit. physik. Chem.,* **B22,** 444–452 (1933).

$$a = 6.946 \text{ Å } (\approx \sqrt{3} \times 3.43\text{Å})$$
$$c = 11.720 \text{ Å } (\approx 2 \times 5.68\text{Å}).$$

The *a* axis of this supercell is the long diagonal of Alsén's cell, the *c* axis is twice that of the Alsén's cell, and its volume is six times that of Alsén's cell. This supercell occurs only in the neighborhood of the ideal formula FeS.

Sidhu and Hicks[3] studied ferromagnetic crystals from Minas Geraes, Brazil, and paramagnetic crystals from Maggiadone, Italy, by the rotating-crystal and Laue methods. In these materials they found no evidences of a superstructure. On the other hand, powder photographs of natural material from Kisbanya, Roumania, and Rossland, B. C., as well as synthetic material supplied by Roberts[4] showed the superstructure lines of Hägg and Sucksdorf. (In a later abstract, Sidhu and Hicks[5] report a superlattice in magnetic pyrrhotite, having the same characteristics as Hägg and Sucksdorf's superlattice.)

More recently, a very thorough magnetic investigation has been made of artificial Fe-S preparations by Haraldsen,[6,7,8,9,10] whose study was accompanied by powder photograph identification of phases. As a result of his investigation, Haraldsen presented a rather complicated phase diagram.[10] For the purposes of the present paper, Haraldsen's findings can be summarized as follows: There are two different kinds of ferrous sulfide, α and β. The α form occurs from $Fe_{.50}S_{.50}$ to approximately $Fe_{.48}S_{.52}$ while β occurs beyond $Fe_{.48}S_{.52}$. These ranges correspond to paramagnetic and ferromagnetic ferrous sulfide. The boundary between these two does not, however, correspond with the boundary between superstructure and simple structure. This occurs at $Fe_{.49}S_{.51}$. In other words, the α magnetic type has a superstructure near ideal composition FeS, but is without it from $Fe_{.49}S_{.51}$ to approximately $Fe_{.48}S_{.52}$. At this point the α magnetic type gives way to the β magnetic type, but without sharp structural change. Furthermore, the superstructure which occurs near ideal composition FeS vanishes on heating above a critical temperature of 138° C. This inversion is a first order one, characterized by a sudden change of about one per cent in the length of the c axis. Thus the superstructure is confined to a small, nearly rectangular, field on the phase diagram whose upper temperature limit is about 138° C. and whose composition limit is $Fe_{.49}S_{.51}$.

---

[3] Sidhu, Surian S., and Hicks, Victor, The space lattice and "superlattice" of pyrrhotite: *Phys. Rev.*, **52,** 667 (1937).

[4] Roberts, Howard S., Polymorphism of FeS-S solid solutions: *Jour. Am. Chem. Soc.*, **57,** 1034–1038 (1935).

[5] Sidhu, S. S., and Hicks, Victor, On the superstructure and magnetism of pyrrhotite (Abstract): *Phys. Rev.*, **53,** 207 (1938).

[6] Haraldsen, Haakon, Eine thermomagnetische Untersuchung der Umwandlungen im Troilit-Pyrrhotin-Gebiet des Eisen-Schwefel-Systems: *Zeit. anorg. allgem. Chem.*, **231,** 78–96 (1937).

[7] Haraldsen, Haakon, Die Umwandlungen des Eisen (II)-Sulfids: *Zeit. Elektrochem.*, **45,** 370–372 (1939).

[8] Haraldsen, Haakon, Omvandlingene i Troilit-Blandkrystallområdet: *Tidsskrift for Kjemi og Bergvesen*, Nr. **9** (1939).

[9] Haraldsen, Haakon, Über die Eisen (II)-Sulfidmischkristalle: *Zeit. anorg. allgem. Chem.*, **246,** 169–194 (1941).

[10] Haraldsen, Haakon, Über die Hochtemperaturumwandlungen der Eisen (II)-Sulfidmischkristalle: *Zeit. anorg. allgem. Chem.*, **246,** 195–226 (1941).

[11] Buerger, M. J., The photography of the reciprocal lattice: *ASXRED Monograph*, No. **1** (1942).

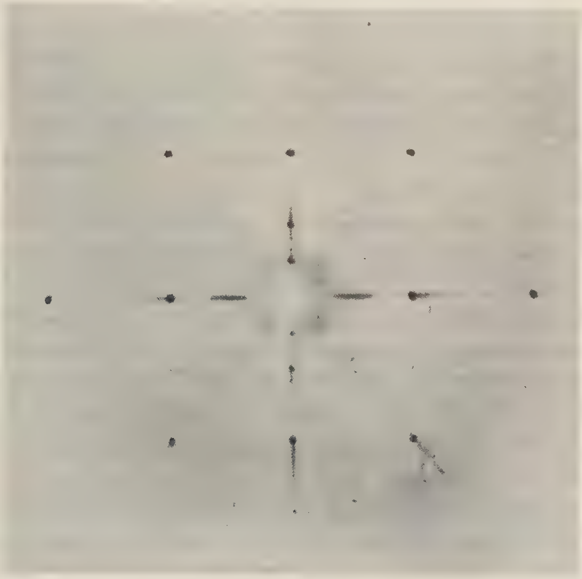

FIG. 1. Zero level, "b" axis precession photograph of pyrrhotite from Morro Velho, Brazil; MoKα radiation. (c^* vertical, a^* horizontal).

NEW X-RAY STUDY OF PYRRHOTITE

The writer examined single crystals of pyrrhotite by the precession[11] method. This method offers a very rapid and convenient way of determining the cell dimensions and diffraction symmetries of single crystals, for the photographs are undistorted enlargements of the reciprocal lattice.

Pyrrhotite crystals are notoriously imperfect; they are usually curved and display exaggerated lineage[12] structure. Fragments for the precession study were detached from comparatively good crystals from Schneeberg, Saxony, and Morro Velho, Brazil. Crystals from both of these localities are ferromagnetic. Their precession photographs are essentially identical. Both displayed the diffraction symmetry $6/mmm$ and both immediately revealed superstructure characteristics. The following cell dimensions were computed for the Schneeberg material:

---

[12] Buerger, M. J., The lineage structure of crystals: *Zeits. Krist.* (A), **89**, 195–220 (1934).

$$a = 6.87\text{Å} \qquad (= 2 \times 3.43\text{Å})$$
$$c = 22.7\text{Å} \qquad (= 4 \times 5.68\text{Å}).$$

It will be noted that this cell has twice the *a* axis, four times the *c* axis, and sixteen times the volume of the nickel arsenide-like cell assigned to pyrrhotite by Alsén. However, this cell does not have the dimensions of the superstructure cell first found by Hägg and Sucksdorf[2] and confirmed by Haraldsen for the small region near ideal FeS. Furthermore, it occurs, not in the paramagnetic troilite region, but in the ferromagnetic pyrrhotite region.

The diffraction record contains no systematic extinctions of space group type, except $00l$ absent when l is odd. (There are other systematic absences but they are not of space group type.) The diffraction symbol is therefore apparently $6/mmm\ C6_3/---$. If this is an accurate representation of the space group symmetry, the space group is $C6_32$. It is possible that the missing $00l$ spectra are due to a fortuitous circumstance and that the diffraction symbol is actually $6/mmm\ C-/---$. If this is the case, the space group might be one of the following: $C\bar{6}2m$, $C\bar{6}m2$, $C6mm$, $C62$, $C6/mmm$.

Diffraction effects lacking extinctions due to glide planes, as those of pyrrhotite do, are open to the suspicion that they may arise from twinned aggregates.[13] It is, therefore, not unlikely that pyrrhotite belongs either to a lower hexagonal symmetry or to an orthorhombic or monoclinic symmetry.

CONCLUSIONS

As a consequence of the new cell data for pyrrhotite, it is evident that this crystal cannot have the nickel arsenide arrangement, at least in ideal form. It is possible, however, that it may have a structure related to the nickel-arsenide structure by some distortion of it to a superstructure. On the other hand, the metal atoms in the nickel arsenide structure do not have an environment similar to the environment of iron atoms in the only other ferromagnetic sulfide, cubanite.[14] For this reason it is desirable to withhold judgment on the nature of the structure of pyrrhotite until it is critically investigated.

---

[13] Buerger, M. J., The symmetry and crystal structure of the minerals of the arsenopyrite group: *Zeits. Krist.* **95(A)**, 99–102 (1936).

[14] Buerger, M. J., The structure of cubanite, $CuFe_2S_3$, and the coordination of ferromagnetic iron: *Jour. Am. Chem. Soc.*, **67**, 2056 (1945).

THE CRYSTAL STRUCTURE OF CUBANITE

M. J. Buerger, *Massachusetts Institute of Technology, Cambridge, Massachusetts.*

Abstract

The structure of cubanite has been uniquely determined with the aid of intensity data derived from Weissenberg photographs. The space group is *Pcmn* and the cell has the following dimensions: $a=6.45$, $b=11.095$, $c=6.221$ *kX*. This cell contains 4 $CuFe_2S_3$. The copper atoms and one-third of the sulfur atoms each occupy the equipoint 4*c* (reflection planes), while the iron atoms and the remaining two-thirds of the sulfur atoms are in the general position, 8*d*. The structure is defined by the following parameters (origin at inversion center):

	x	y	z
Cu	$\frac{7}{12}$	$(\frac{1}{4})$	.122
S_1	$\frac{11}{12}$	$(\frac{1}{4})$	.270
Fe	$\frac{1}{12}$	.083	.135
S_2	$\frac{5}{12}$	.083	.265

The x and z parameters are subject to some further slight refinement by three-dimensional Fourier synthesis.

The structure is based upon almost ideal, hexagonal close-packing of sulfur atoms. The metal atoms are each surrounded by four sulfur atoms in almost ideal tetrahedral coordination. The structure may be regarded as made up of slices of the wurtzite structure parallel to (010), joined to identical but inverted slices by means of the sharing of one of the edges of each iron coordination tetrahedron. This curious sharing of a tetrahedral edge is correlated with the ferromagnetic properties of cubanite.

Introduction

The structure of cubanite is of more than ordinary interest. In the first place cubanite shares with the native iron, magnetite, and pyrrhotite the distinction of being ferromagnetic. While the structures of iron and magnetite are known, it is doubtful whether the structure assigned to pyrrhotite is correct, at least in detail, for the true cell of pyrrhotite is a multiple of the cell of the assigned structure.[1] Thus a knowledge of the structure of cubanite might be expected to cast light on the nature of the weak ferromagnetism in iron-bearing sulfides.

In the second place cubanite is known to unmix from chalcopyrite,[2] giving rise to oriented[3] plates in the chalcopyrite matrix. It is known that the segregation must arise from ordering of the atoms in a disordered high-temperature form of chalcopyrite,[4] but the character of the ordering mechanism cannot be known until the structure of cubanite is known.

---

[1] Buerger, M. J., The cell and symmetry of pyrrhotite: *Am. Mineral.*, **32,** 411–414 (1947).

[2] Schwartz, G. M., Intergrowths of chalcopyrite and cubanite; experimental proof of the origin of the intergrowths and their bearing on the geological thermometer: *Ec. Geol.*, **22,** 44–61 (1927).

[3] Buerger, N. W., and Buerger, M. J., Crystallographic relations between cubanite segregation plates, chalcopyrite matrix, and secondary chalcopyrite twins: *Am. Mineral.*, **19,** 289–303 (1934).

In this paper an account is given of the determination of the structure of cubanite. While all the coordinates of all the atoms have not been highly refined, they have been determined closely enough to permit a contribution to an understanding of the problems mentioned above.

CELL AND SYMMETRY

In an earlier contribution,[5] the diffraction symbol of cubanite was shown to be *mmmPc-n*. This embraces the two space groups *Pcmn* and $Pc2_1n$. The cell dimensions were also reported. More accurate cell dimensions for cubanite from the Frood Mine, Sudbury, Ontario are as follows:

$$a = 6.45kX$$
$$b = 11.095$$
$$c = 6.221$$

These new values were obtained with the aid of a precision, back-reflection Weissenberg apparatus[6] but utilizing one radiation only. Unfortunately with this radiation the *h*00 reflections were too poorly disposed on the photographs to permit refining the *a* axis dimension.

The cubanite cell contains 4 $CuFe_2S_3$.

STRUCTURE DETERMINATION

Introduction.—The structure of cubanite was determined from intensity considerations, except that rough geometrical packing considerations guided the search for *z* parameters. As the structure became revealed it became evident that the only kind of Fourier method which would aid in the parameter determination was the method of sections. Since this required more quantitative intensity data than were at hand and could be obtained in a reasonable time, the refinement of the structure by Fourier methods was deferred until such data were at hand.

The intensities required for the determination of the structure as given in this paper were derived from zero-level Weissenberg photographs made with filtered Mo$K\alpha$ radiation. This provided the relative intensities of the *hk*0, *h*0*l*, and 0*kl* spectra.

---

[4] Buerger, M. J., The temperature-structure-composition behavior of certain crystals: *Proc. Nat. Acad. Sci.*, **20**, 444–453 (1934).

[5] Buerger, M. J., The unit cell and space group of cubanite: *Am. Mineral.*, **22**, 1117–1120 (1937).

[6] Buerger, M. J., The precision determination of the linear and angular lattice constants of single crystals: *Zeits. Krist.*, (A) **97**, 433–468 (1937).

Equipoint Possibilities.—The cubanite cell contains 4 $CuFe_2S_3$. This necessitates finding equipoint combinations adding to 4, 8, and 12. Space group $Pc2_1n$ contains only the general equipoint, 4*a*. Space group *Pcmn* contains the general equipoint 8*d* as well as the special positions on sets of inversion centers, 4*a* and 4*b*, and on reflection planes, 4*c*. The correct equipoint combination for cubanite is determined by the following intensity analysis:

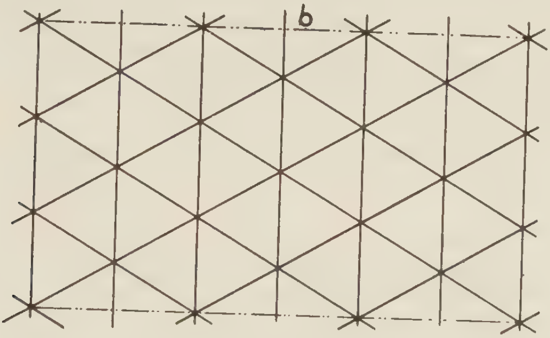

FIG. 1

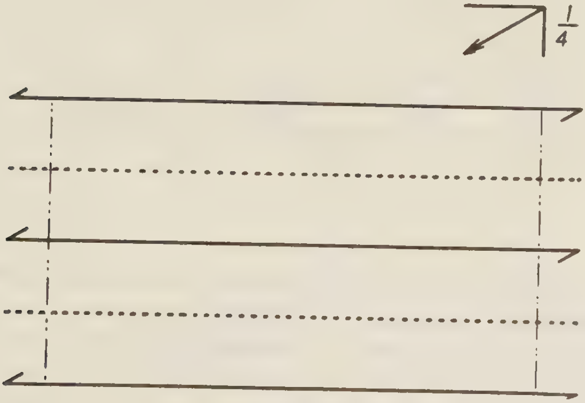

FIG. 2

Preliminary Intensity Considerations.—A conspicuous feature of the intensity distribution is the special intensity pattern of the *hk*0 reflections. Of the possible *hk*0 reflections permitted by both space groups, only a limited number appear (in a pattern to be discussed shortly), the rest being missing or very weak. This pattern of strong reflections is characterized by a regular decline of the orders of 060, and a regular decline of the orders of 330. The significance of this is that all atoms must be located on (010) sheets spaced $b/6$ apart and also on (110) sheets which divide a and b into thirds.

In Fig. 1 these two sets of intersecting sheets are shown projected on (001). In projection they constitute a net. The net must, of course, be made conformable with the symmetry elements of the space group. The symmetry elements of the two space groups, $Pc2_1n$ and $Pcmn$, which come up for consideration, are shown projected on (001) in Fig. 2. The net of Fig. 1 can be located in the symmetry common to the two space groups only in the one way shown in Fig. 3.

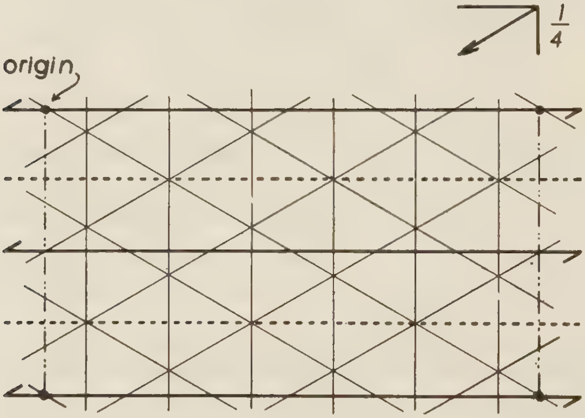

FIG. 3

Since, as pointed out above, all atoms must be confined to lines of the net in order to satisfy intensity requirements, each atom must be located on some node of the net. Very approximately, iron and copper have the same scattering power, so that the two kinds of metal atoms in cubanite are indistinguishable. There are only two ways of distributing the metals in the net of Fig. 3 so as to satisfy symmetry and also place the correct number in the cell. One is to place the metals on the nodes in the vertical glide planes, the other is to place them on the nodes next nearest to these glide planes. These schemes result in the metal distributions shown in Figs. 4 and 5, respectively. These possible locations have the x and y parameters given in Table 1.

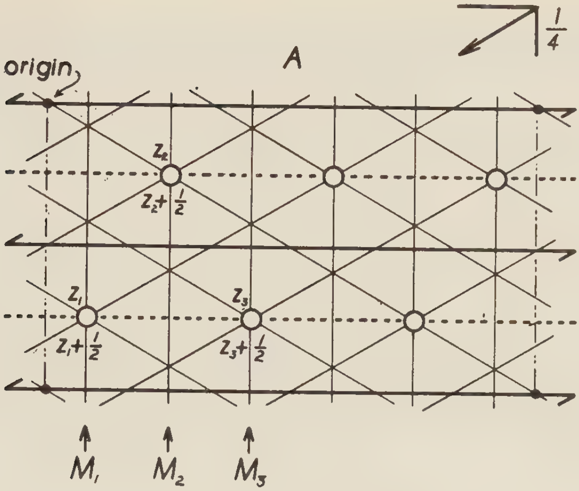

FIG. 4

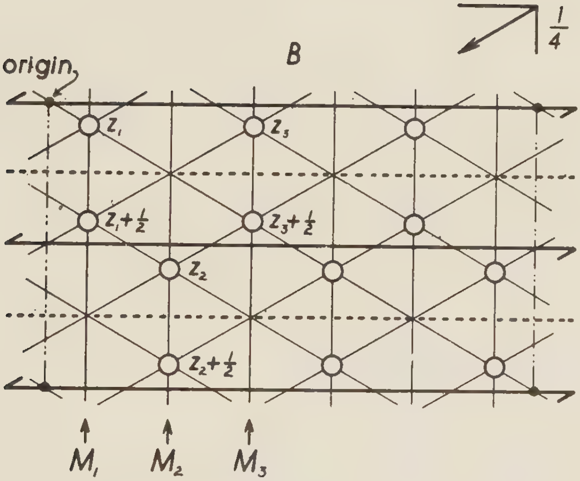

FIG. 5

TABLE 1. PERMISSIBLE x AND y COORDINATES OF ATOMS IN CUBANITE
(Origin is on a two-fold screw of $Pc2_1n$, or on an inversion center of *Pcmn*.)

Possibility *A*, Fig. 4.			Possibility *B*, Fig. 5.		
	x	y		x	y
M_1 (or S_1)	$\frac{3}{4}$	$\frac{1}{12}$	M_1 (or S_1)	$\frac{1}{12}$	$\frac{1}{12}$
M_2 (or S_2)	$\frac{1}{4}$	$\frac{1}{4}$	M_2 (or S_2)	$\frac{7}{12}$	$\frac{1}{4}$
M_3 (or S_3)	$\frac{3}{4}$	$\frac{5}{12}$	M_3 (or S_3)	$\frac{1}{12}$	$\frac{5}{12}$

Note: Coordinates are given for the less symmetrical space group $Pc2_1n$. For space

Following the same argument, the sulfur atoms, which are equal in number to the metal atoms, must be distributed in one of the two ways shown in Figs. 4 and 5. This limits the structure to four possible projections. Using the abbreviations M for metal, S for sulfur, *A* for the distribution shown in Fig. 4 and *B* for the one shown in Fig. 5, these possible structures are M_AS_A, M_AS_B, M_BS_A, and M_BS_B.

Structure possibility M_AS_A projects on (010) as a simple plane lattice array. Hence, it would be characterized by regular declines of intensity in orders of all *hk*0 reflections. This is contrary to the observed intensity sequences, which are not regular declines for all order series. Thus combination M_AS_A can be eliminated from further consideration.

Combination M_BS_A can be eliminated on similar grounds: As a rather good approximation either of the metals Cu or Fe has twice the scattering power of S. Now arrangement *A* has two atoms (sulfur in this case) projected on each point, and arrangement *B* (metals in this case) has one atom projected on each point. The sum of both arrays is a lattice array of points. Furthermore the points have equal scattering powers, since a sulfur point has two sulfur atoms, each with half the scattering power of a metal point. Thus the composite array should scatter very approximately as a simple lattice array of points, which is characterized by a regular decline of intensity of the orders of all *hk*0 reflections. Since this is contrary to the observed intensity sequences, combination M_BS_A can be eliminated from further consideration.

This reasoning eliminates any structure containing sulfur atoms in S_A. The remaining combinations, M_AS_B and M_BS_B are of structural interest because S_B is also the projection of hexagonal close-packed sulfur atoms in which the remaining, z, parameter of sulfur is $\frac{1}{4}$. Close packing of the sulfur atoms is also consistent with the axial ratio of the cubanite cell, as shown by the following comparison:

AXIAL RATIOS

	Cubanite	Hexagonal close packing
a	.581	.577
b	1	1
c	.560	.549

The suggestion that the sulfur atoms are in close packing in cubanite is strong enough to serve as a useful guide in the subsequent exploration of parameters.

Relation between Remaining Structure Combinations.—An attempt is now called for to decide between arrangements M_AS_B and M_BS_B. For preliminary exploration, the following approximations are possible. If sulfur is assigned a scattering power of unity, then iron and copper each have scattering powers of approximately 2. Furthermore, because of the symmetry of the projections, amplitudes can be computed for *hk*0 spectra by means of the structure factor of space group *Pcmn* (see subsequent section).

Arrangement M_BS_B gives rise to a simple pattern of amplitudes (uncorrected for Lorentz, polarization, or *f* factors). This is shown in Table 2. Arrangement M_AS_B gives rise to the same absolute amplitudes, but with different signs for certain of the spectra for which *h* is odd. Since these phase differences cannot be distinguished, it follows that structure M_AS_B cannot be distinguished from structure M_BS_B by any criterion based upon the reflections *hk*0.

TABLE 2

	6	9		0		0		9		0		0		9
	5		0		3		0		0		3		0	
	4	3		0		0		3		0		0		3
h	3		0		9		0		0		9		0	
	2	3		0		0		3		0		0		3
	1		0		3		0		0		3		0	
	0	9		0		0		9		0		0		9
		0	1	2	3	4	5	6	7	8	9	10	11	12
								k						

The observed intensities of diffraction by cubanite follows the pattern of amplitudes shown in Table 2. This confirms that the structure of cubanite is indeed one of the combinations M_AS_B or M_BS_B. From the point of view of packing, the combination M_AS_B corresponds to a pyrrhotite type of packing. In this case, the copper atoms would merely substitute for certain iron atoms in the pyrrhotite structure, thus causing it to display superstructure characteristics. The combination M_BS_B is based upon a complication of the wurtzite packing and represents a structural type not previously observed.

Both structures suggested above have the same distribution of equipoints, but with different parameters. Their properties, so far as known to this point, are summarized in Table 3. (In this table, the initial sulfur atoms are differently chosen from those in Table 1 in order to give them *z* parameters nearer zero.)

TABLE 3. APPROXIMATE COORDINATES OF ATOMS IN POSSIBLE CUBANITE STRUCTURES
(z parameters based upon assumption that sulfur atoms are close packed and that metal atoms are in interstices.)

Space Group	Atoms	Equipoint	M_AS_B, Pyrrhotite-Like Structure			M_BS_B, Wurtzite-Like Structure		
			x	y	z	x	y	z
$Pc2_1n$	$M_1=Fe_1$	$4a$	$\frac{3}{4}$	$\frac{1}{12}$	0	$\frac{1}{12}$	$\frac{1}{12}$	$\frac{1}{8}$
	$M_2=Cu$	$4a$	$\frac{1}{4}$	$\frac{1}{4}$	0	$\frac{7}{12}$	$\frac{1}{4}$	$\frac{1}{8}$
	$M_3=Fe_2$	$4a$	$\frac{3}{4}$	$\frac{5}{12}$	0	$\frac{1}{12}$	$\frac{5}{12}$	$\frac{1}{8}$
	S_1	$4a$	$\frac{5}{12}$	$\frac{1}{12}$	$\frac{1}{4}$	$\frac{5}{12}$	$\frac{1}{12}$	$\frac{1}{4}$
	S_2	$4a$	$\frac{11}{12}$	$\frac{1}{4}$	$\frac{1}{4}$	$\frac{11}{12}$	$\frac{1}{4}$	$\frac{1}{4}$
	S_3	$4a$	$\frac{5}{12}$	$\frac{5}{12}$	$\frac{1}{4}$	$\frac{5}{12}$	$\frac{5}{12}$	$\frac{1}{4}$
$Pcmn$	$M_1=Fe$	$8d$	$\frac{3}{4}$	$\frac{1}{12}$	0	$\frac{1}{12}$	$\frac{1}{12}$	$\frac{1}{8}$
	$M_2=Cu$	$4c$	$\frac{1}{4}$	$\frac{1}{4}$	0	$\frac{7}{12}$	$\frac{1}{4}$	$\frac{1}{8}$
	S_1	$8d$	$\frac{5}{12}$	$\frac{1}{12}$	$\frac{1}{4}$	$\frac{5}{12}$	$\frac{1}{12}$	$\frac{1}{4}$
	S_2	$4c$	$\frac{11}{12}$	$\frac{1}{4}$	$\frac{1}{4}$	$\frac{11}{12}$	$\frac{1}{4}$	$\frac{1}{4}$

In passing, it should be noted that the more natural space group of cubanite is $Pcmn$ because the general position is just filled by the most abundant atom. Space group $Pc2_1n$ requires the same atomic species to be of two symmetrically unrelated varieties. This is equivalent to saying that if $Pc2_1n$ is the space group, the structure is identical with a corresponding structure in $Pcmn$ except for a distortion, and there appears to be no obvious reason for such a distortion.

Structure Factors.—The structure factors for the reflections from the several prism zones of $Pcmn$ and from the [010] zone of $Pc2_1n$ are listed in Table 4. It should be observed that the forms of the structure factor for the reflections $h0l$ (including $h00$ and $00l$) are identical for the two possible space groups. Thus the undetermined z parameters of the atoms may be explored in a single search by the utilization of these spectra.

TABLE 4. STRUCTURE FACTORS FOR PRISM-ZONE REFLECTIONS

Reflection	Class	Space Group $Pcmn$	Space Group $Pc2_1n$
$hk0$	h even, k even	$8\cos 2\pi hx \cos 2\pi ky$	
	h odd, k odd	$-8\sin 2\pi hx \sin 2\pi ky$	
$h0l$	$h+l$ even	$8\cos 2\pi hx \cos 2\pi lz$	$4\cos 2\pi hx \cos 2\pi lz$
	$h+l$ odd	$-8\sin 2\pi hx \sin 2\pi lz$	$-4\sin 2\pi hx \sin 2\pi lz$
$0kl$	k even, l even	$8\cos 2\pi ky \cos 2\pi lz$	
	k odd, l even	$-8\sin 2\pi ky \sin 2\pi lz$	

For the purposes of further parameter study the intensities have been computed according to a plan discussed elsewhere.[7]

Preliminary Search for Parameters of Metal Atoms.—In the preliminary search for parameters satisfying the intensity requirements, it is useful to assume that the sulfur atoms are close packed, as suggested by the z parameters in Table 3. The only question is then, in which set of interstices do the metals lie? If the metals are assumed to have the parameters given by the M_AS_B structure of Table 3, the computed $h0l$ intensities bear no relation to the observed intensities, even with reasonable variations from the ideal parameters. On the other hand, when the metals are assumed to have the parameters given by the M_BS_B structure of Table 3, there is a noteworthy correspondence between computed and observed intensities. The correspondence is considerably improved by increasing the z parameter of Fe to .135. The parameter values then reasonably explain the $00l$ and $h0l$ spectra.

Computations of the intensities of $0kl$ spectra using the structure factor for *Pcmn* then yield a set of intensities in good preliminary agreement with the observed intensities. These considerations thus confirm structure M_BS_B as based upon space group *Pcmn*. The space group $Pc2_1n$ thus comes up for consideration only as a possibly slightly generalized equivalent of *Pcmn*. Since further parameter refinement based upon *Pcmn* reproduces the spectra rather exactly, this may be regarded as the correct space group.

Refinement of y Parameters.—With the structure type, approximate parameters, and space group fixed, the number of variable y parameters reduce to two: one for Fe and one for S_2. These parameters can be fixed by studying the $0l0$ spectra, 14 even orders of which can be recorded by MoKα radiation. Only the higher orders not divisible by 6 are useful in this study, for those divisible by 6 form a series of very strong spectra of gradually declining intensity, and their intensities are insensitive to small variations in the y parameters from the neighborhood of the ideal $\frac{1}{12}$. The amplitudes of sensitive orders for the ideal parameters are as follows:

0·10·0	−2.2
0·14·0	−2.9
0·16·0	1.5
0·20·0	2.9
0·22·0	−1.9
0·26·0	−0.9
0·28·0	1.0

This series is already in good agreement with the observed intensities and it turns out that any variation of the two y parameters away from the ideal values spoils the correspondence. From this it may be concluded that the y parameters of both Fe and S_2 are very close to $\frac{1}{12}$.

---

[7] Buerger, M. J., Numerical structure factor tables: *G. S. A. Special Publication No.* **33** (1941).

Refinement of z and x Parameters.—Any further trial and error refinement of parameters is fraught with great difficulties. Furthermore, refinement of parameters by Fourier synthesis of the electron density projected on (100), (010), or (001) is useless. Both of these situations are primarily due to the fact that the structure presents such regularities that non-equivalent atoms project to very nearly the same points when the structure is projected on any pinacoid. The greatest resolution occurs in projection on the (100) plane, but even here the resolution is not very good, yet because there is some resolution, an intensity fit can be found for the $0kl$ reflections by varying the z parameters. A rather good fit occurs for

	y	z
Fe	.083	.135
Cu	.250	.122
S_1	.083	.270
S_2	.250	.265

The only possible way to refine the x and z parameters is to prepare, by Fourier synthesis, sections of the three-dimensional electron density distribution at y levels of $\frac{1}{12}$ and $\frac{1}{4}$, thus locating the Fe and S_2 in the first section and the Cu and S_1 in the second section. These syntheses require quantitative intensities for all reflections hkl. Since these intensities are not yet available on a quantitative basis, this project is temporarily deferred.

THE STRUCTURE

As a result of the foregoing analysis, it is evident that the space group of cubanite is *Pcmn*. The best coordinates found by a trial and error search are as follows:

	x	y	z
Cu in 4c	$\sim\frac{7}{12}$	$(\frac{1}{4})$	.122
S_1 in 4c	$\sim\frac{11}{12}$	$(\frac{1}{4})$	.270
Fe in 8d	$\sim\frac{1}{12}$	.083	.135
S_2 in 8d	$\sim\frac{5}{12}$	.083	.265

The x and z parameters should not be regarded as final, but merely as rather close. More precise values await a three-dimensional Fourier study.

The structure is based upon an almost ideal, hexagonal close-packed array of sulfur atoms. Each metal atom occurs in an interstitial space between sulfur atoms in such a way that the metal has an almost ideal tetrahedral sulfur coordination.

The structure, however, is not one which has hitherto been described.

Its unusual characteristics can be appreciated with the aid of Fig. 6. This diagrammatically shows a region of the structure with ideal parameters in the neighborhood of $z=0$, specifically $-\frac{1}{4}<z<\frac{1}{4}$. The structure can be seen to be composed of slabs of the wurtzite arrangement parallel to (010) and averaging $b/2$ wide. Since the wurtzite arrangement is polar, the metal coordination tetrahedra all point up, or else they all point down. In the cubanite structure, the wurtzite-like slabs are joined to one another by inversion centers so that neighboring slabs have their tetrahedral apex directions reversed. The central section of each slab is composed of copper tetrahedra and the sides of the slab are composed of iron tetrahedra. Since an inversion center occurs at the midpoint of an edge of the iron tetrahedron, it has the effect of joining all iron tetrahedra in pairs which share this edge.

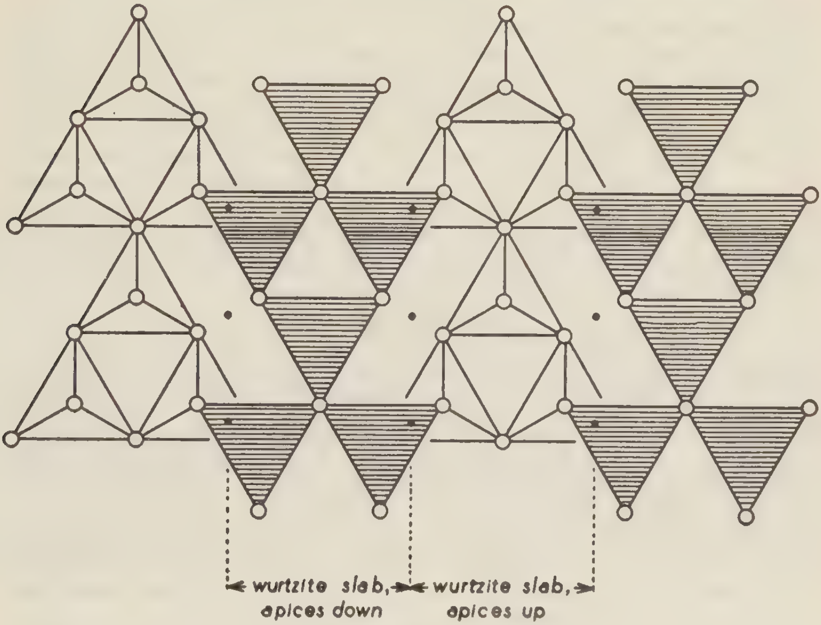

FIG. 6

The sharing of tetrahedral edges is most unorthodox, even in nonionic crystals. Since the sharing occurs for iron tetrahedra only, it is difficult to avoid the correlation of this curious feature with the unusual characteristic of ferromagnetism. The only other ferromagnetic sulfide is pyrrhotite, and there is a reasonable doubt about the correctness of the structure assigned to it, since pyrrhotite does not have the translation periods of the assigned structure.[1]

With the structure of cubanite known, the mechanism of the unmixing of cubanite from chalcopyrite can be studied. This is discussed in a subsequent contribution.

MINERALOGICAL ASPECTS OF THE SYSTEM $Fe_3O_4—Mn_3O_4—ZnMn_2O_4—ZnFe_2O_4$

BRIAN MASON, *Canterbury University College,*
Christchurch, New Zealand.

ABSTRACT

The phase relations in the system $Fe_3O_4—Mn_3O_4—ZnMn_2O_4—ZnFe_2O_4$ have been determined at temperatures up to 1300° C. by the study of synthetic preparations and natural minerals. The equilibrium diagram shows complete mutual miscibility of the components at temperatures above 1000° and a considerable field of incomplete miscibility at ordinary temperatures. Mix-crystals rich in iron have a cubic lattice, those rich in manganese a tetragonal lattice. Diagrams are given showing the variation with composition in dimensions and volume of the unit cell, and in the axial ratio for tetragonal phases. Analyses of magnetite, jacobsite, franklinite, vredenburgite, hetaerolite and hausmannite are plotted on a composition diagram, and composition limits for these mineral species are proposed. The use of vredenburgite as a geologic thermometer is suggested.

INTRODUCTION

This paper presents the results of an experimental study of the system $Fe_3O_4—Mn_3O_4—ZnMn_2O_4—ZnFe_2O_4$, using both synthetic preparations and natural minerals. This system is important mineralogically for the number of distinct species which have been recognized within it: magnetite, Fe_3O_4; jacobsite, $MnFe_2O_4$; franklinite $ZnFe_2O_4$; hetaerolite, $ZnMn_2O_4$; hausmannite, Mn_3O_4; and vredenburgite, which is generally an oriented intergrowth of jacobsite and hausmannite, but which has been recorded in a homogeneous state. This investigation was undertaken mainly in order to study the mutual relationships of these individual minerals, and their conditions of formation, and to define their range in composition as far as possible in relation to the physico-chemical conditions under which they occur as stable phases. Other interesting phenomena within the system are the change in crystal lattice from one with cubic symmetry for the iron-rich members to one with a tetragonal symmetry for the manganese-rich members, and the occurrence of complete mutual miscibility in the solid state of the components at high temperatures (in spite of lattice differences) and a wide field of incomplete miscibility at lower temperatures. The variation in magnetic properties, from strong ferromagnetism for Fe_3O_4 to paramagnetism for the other components, is also striking but was only partly studied.

The experimental work upon which this paper is based was carried out during 1942 and 1943 at the University of Stockholm. It was abruptly terminated by my departure from Sweden in 1943; the essential parts of the experimental work had been completed by that time, but further investigations were intended with a view to studying more closely the change from a cubic to a tetragonal lattice within the system, and making detailed measurements of variation of magnetic properties with composition. Since that time it has not been possible to continue with these experiments, and this paper does not deal as fully with these aspects as might be wished.

In this connection it is my pleasant duty to acknowledge my indebtedness to those I was associated with at the University of Stockholm, especially Professor Percy Quensel, of the Mineralogical Institute, and Professor Arne Westgren, of the Institute of Inorganic Chemistry, for the hospitality I received while working as a foreign guest in their Institutes. Their advice and encouragement, together with the many kindnesses which I received from all quarters during my enforced stay in Sweden, are gratefully remembered.

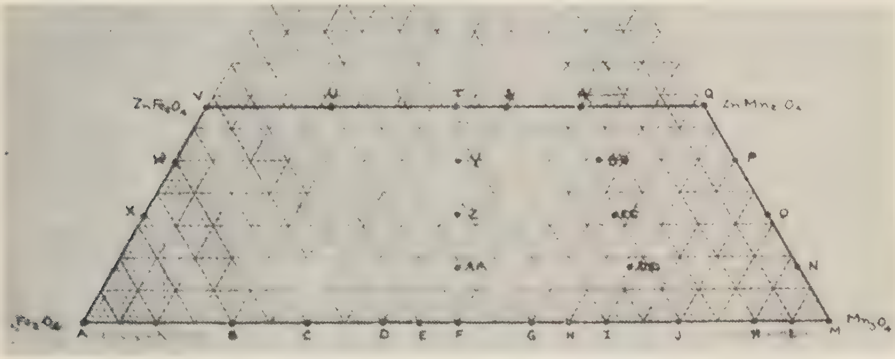

Fig. 1. Synthetic preparations within the system.

The Nature of the System

The system here studied clearly falls within the four-component system Fe—Mn—Zn—O. By plotting the components Fe_3O_4, Mn_3O_4, $ZnMn_2O_4$, $ZnFe_2O_4$ on a tetrahedron with Fe, Mn, and Zn as the corners of the base and O as the apex it can readily be seen that these components all lie in a plane parallel to the base and situated $\frac{4}{7}$ of the distance towards the apex, since the ratio of oxygen atoms to the total number of atoms in all these components is 4:7. The system Fe_3O_4—Mn_3O_4—$ZnMn_2O_4$—$ZnFe_2O_4$ is thus part of the three-component system whose components are Fe_3O_4, Mn_3O_4, and a hypothetical Zn_3O_4. All compositions within this system can therefore be represented on a truncated equilateral triangle with the Fe_3O_4—Mn_3O_4 join forming the base and the $ZnFe_2O_4$—$ZnMn_2O_4$ join truncating the triangle one-third of the distance towards the apex (Fig. 1). Such a truncated triangle is used throughout this paper for representing compositions within this system, compositions being plotted as atom percentages of Fe, Mn, and Zn.

TABLE 1

Prep.	Composition				Phases	Cubic	Tetragonal			Remarks
	Fe	Mn	Zn	T		*a*	*a*	*c*	*c/a*	
A					C	8.381				Natural magnetite, analyzing 99.2% Fe_3O_4
B	80	20		1170	$C+R_2O_3$					
				1220	$C+R_2O_3$					
				1300	C	8.444				
C	70	30		1050	$C+R_2O_3$					
				1220	C	8.455				
D	60	40		1220	C	8.483				
E	55	45		1150	C	8.501				
F	50	50		1100	C	8.505				
G	40	60		1150	C	8.515				
H	35	65		1200	T		8.378	8.827	1.054	
				750	T					In vacuo, unchanged
I	30	70		1150	T		8.307	8.972	1.080	
				990	T					In vacuo, unchanged
				750	T					In vacuo, unchanged
J	20	80		1150	T		8.235	9.180	1.115	
				950	T					In vacuo, unchanged
				750	$T+T_1$		8.194 8.284	9.281 9.030	1.133 1.090	In vacuo
				650	T					In vacuo, unchanged
K	10	90		1150	T		8.190	9.310	1.137	
				750	T					In vacuo, unchanged
L	5	95		1100			8.162	9.410	1.153	
M		100		1100			8.140	9.435	1.159	
N		91.7	8.3	890	T		8.123	9.391	1.156	
O		83.3	16.7	710	$T+(Mn_3O_4)$					Brackets indicate small amount
				890	T		8.107	9.341	1.152	
P		75	25	890	T		8.084	9.286	1.149	
Q		66.7	33.3				8.076	9.225	1.142	
R	16.7	50.0	33.3	890	T		8.162	8.991	1.102	
				800	$T+(T_1)$		8.120 (8.204)	9.107 8.872)	1.121 (1.081)	Brackets indicate small amount
				710	T+(C)	(8.423)	8.114	9.115	1.123	Brackets indicate small amount
				590	T+(C)	(8.422)	8.111	9.139	1.127	Brackets indicate small amount
				515						2 or 3 very faint lines only
S	26.7	40.0	33.3	920	T		8.217	8.869	1.080	
				810	T		8.214	8.861	1.079	
				700	C+T	8.424	8.125	9.099	1.120	
				600	C+T	8.422	8.117	9.121	1.124	
T	33.3	33.3	33.3	920	T		8.253	8.790	1.065	
U	50.0	16.7	33.3	890	C	8.426				
W	75		25	1000	$C+R_2O_3$					
X	83.3		16.7	1000	$C+R_2O_3$					
Y	37.5	37.5	25	1000	T		8.282	8.780	1.060	
				920	T		8.287	8.780	1.059	
Z	41.7	41.7	16.6	1000	C	8.494				
AA	45.8	45.8	8.4	1000	C	8.498				
				920	$C+R_2O_3$					
BB	18.8	56.2	25	1000	T		8.181	9.065	1.108	
				920	$T+T_1$		8.138 (8.183)	9.143 (9.025)	1.124 (1.103)	Brackets indicate small amount
				810	$T+T_1$		8.137 (8.212)	9.136 (8.953)	1.123 (1.090)	Brackets indicate small amount
				710	$T+T_1$		8.133 (8.250)	9.136 (8.934)	1.123 (1.083)	Brackets indicate small amount
				600	C+T	8.433	8.129	9.169	1.128	
CC	20.8	62.5	16.7	920	T		8.194	9.114	1.112	
				810	$T+T_1$		8.158 8.193	9.195 9.016	1.127 1.100	
				710	$T(+T_1)$		8.156	9.165	1.124	Lines of second phase hardly visible
				600	$T+R_2O_3$					
DD	22.9	68.8	8.3	890	T		8.215	9.111	1.109	
				810	$T+R_2O_3$					

EXPERIMENTAL PROCEDURE

Synthetic preparations were made covering a wide range of compositions within this system (Fig. 1 and Table 1). From Fig. 1 it would appear that the coverage was somewhat irregular, but the concentration of synthetic preparations towards the manganese side of the composition diagram is on account of the closer study of the change from a cubic to a tetragonal lattice, and the region of limited miscibility, both of which are situated on this side of the diagram.

These synthetic preparations were made in the following way. Manganous sulphate, ferrous sulphate, and zinc sulphate (analytical reagent quality) were weighed out in the desired proportions and dissolved in hot water; the solution was precipitated by a small excess of sodium hydroxide solution for those containing manganese and iron only, or sodium carbonate solution for those containing zinc also, the precipitate washed first by decantation and then on a filter until free from sulphate, and dried by heating in an oven with free access of air at 165° for 24 hours. The products thereby obtained were semi-amorphous, giving few or no lines on an *x*-ray powder photograph. In order to assure that the proportions of iron, manganese, and zinc in the products corresponded to the amounts of parent materials taken, the percentages of iron, manganese, and zinc in some of the products were confirmed by chemical analysis.

These synthetic preparations were converted into the AB_2O_4 type compounds by heating in an electric furnace at temperatures up to 1300° C. for periods varying from 12 to 24 hours. Syntheses containing more than 80% of the Fe_3O_4 component could not be prepared in this way without exceeding 1300°, beyond the capacity of the furnaces available; in this composition range at temperatures below 1300° the products contained Fe_2O_3 as well as the AB_2O_4 compound.

All these heatings were carried out with free access to the air, with the exception of some of the preparations along the Fe_3O_4—Mn_3O_4 join, which were heated in sealed evacuated tubes at temperatures between 650° and 1000°, the sealed evacuated tubes being necessary for these compositions and at these temperatures in order to prevent oxidation to the corresponding R_2O_3 type compound. With these exceptions, which are indicated in Table 1, the system was thus investigated under a partial pressure of oxygen of approximately 159 mm.

The phase relations in the products obtained by heatings at different temperatures were investigated by means of *x*-ray powder photographs. The cameras used for making the powder photographs were of the Seeman-Bohlin focussing type as designed by Phragmén. Chromium radiation was employed. The lattice dimensions of the various phases were also determined from the powder photographs, and the relationship between lattice dimensions and chemical composition in the solid solution series thereby obtained. These relationships made it then possible to determine the composition of any phase within the system from the determination of its lattice dimensions. This was extensively used for determining the composition of the separate phases for samples falling within the region of incomplete miscibility, and thereby building up the boundaries of this region at different temperatures. This technique for opaque materials corresponds with the utilization of the relations between refractive index and chemical composition so extensively employed in the elucidation of phase relationships in silicate systems.

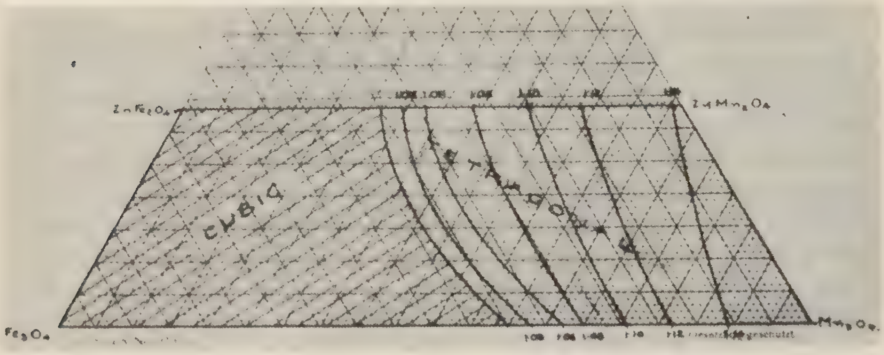

FIG. 2. Cubic and tetragonal lattices and variation of the axial ratio (c/a) with composition.

In routine work the accuracy of measurement of the lattice dimensions from powder photographs was ±0.1% or better. For determining the relationship between lattice dimensions and chemical composition special precautions were taken, and the measurements for this purpose have an accuracy of ±0.05%. All temperatures are in degrees Centigrade.

RESULTS OBTAINED

The results obtained from the experiments with synthetic preparations are set out in Table 1, and are expressed by the curves in Figs. 2, 3, 4, and 5.

Figure 2 shows the composition regions within which the cubic lattice and the tetragonal lattice are respectively stable, and also shows the change in axial ratio with composition for the tetragonal phase. The axial ratio reaches a maximum of 1.16 for pure Mn_3O_4.

It has been suggested by Eckermann (2), on the basis of earlier work on the Fe_3O_4—Mn_3O_4 system by Montoro (10) and the writer (8), that the change from a cubic to a tetragonal lattice in that system is dependent not only on composition but also on temperature. Systematic experiments to test this suggestion have not been carried out. However, it may be pointed out that preparation 1 (Fe 30, Mn 70), which according to Eckermann's tentative phase diagram should possess cubic symmetry between 700° and 1000° and tetragonal symmetry above 1000°, was uniformly tetragonal between 750° and 1150° (Table 1). Another feature of Eckermann's diagram for the change from cubic to tetragonal symmetry is that this change is shown to take place for any one composition with increasing temperature, whereas a change of this type is usually to a lattice of greater symmetry with increasing temperature—e.g., leucite, α-β quartz, low-high tridymite and cristobalite, monoclinic pyroxene—orthorhombic pyroxene; changes to a lattice of lower symmetry with increasing temperature are, however, known (e.g., α-β sulphur).

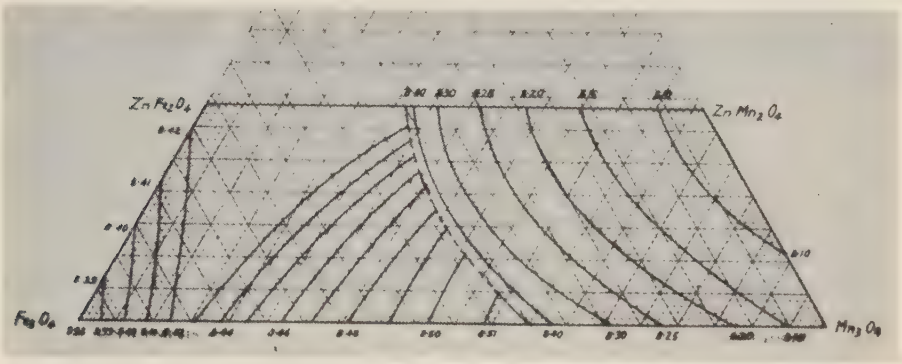

FIG. 3. Relationship between composition and a for cubic and tetragonal lattices.

Figure 3 shows the variation in a with chemical composition for both the cubic and tetragonal phases. It will be seen that a relatively large area of the cubic field is enclosed between the curves for 8.42 Å and 8.43 Å; within this area the lattice dimensions change relatively slightly with composition, and a value for a between 8.42 Å and 8.43 Å does not indicate any very precise chemical composition, particularly if zinc is present in considerable amount. For the tetragonal phase a decreases rapidly away from the boundary between the two fields, reaching a minimum of 8.076 Å for pure $ZnMn_2O_4$.

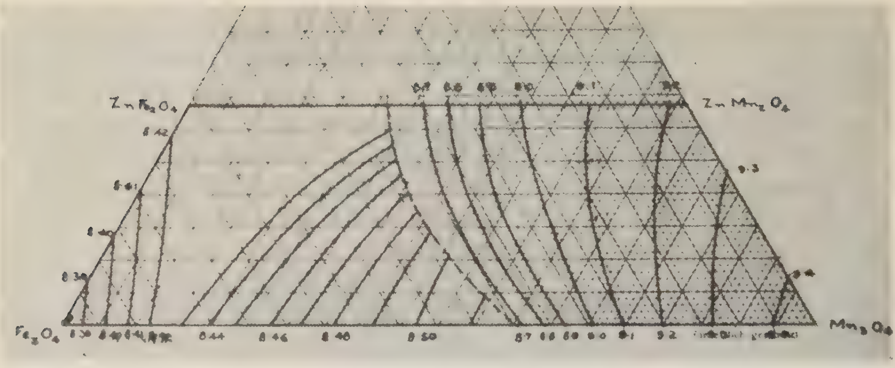

FIG. 4. Relationship between composition and *a* for cubic lattices and *c* for tetragonal lattices.

Figure 4 shows the variation with chemical composition of *a* for the cubic phase and *c* for the tetragonal phase. For the tetragonal phase, *c* increases rapidly away from the boundary between the two fields, reaching a maximum of 9.435 Å for pure Mn_3O_4.

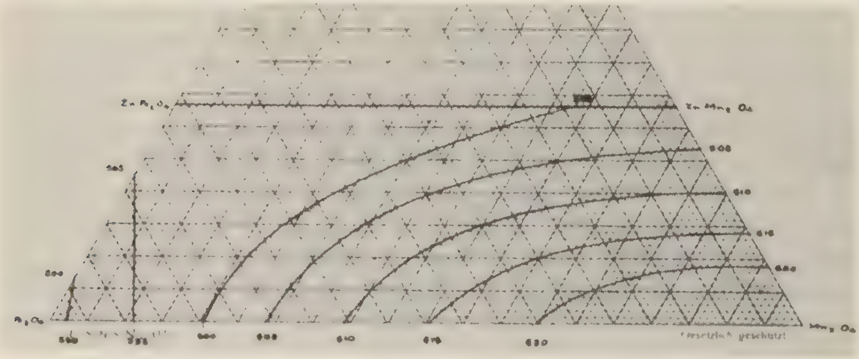

FIG. 5. Variation in unit cell volume (in Å^3) with composition.

Figure 5 shows the variation in the unit cell volume with chemical composition. The unit cell volume varies from a minimum of 588 Å^3 for pure Fe_3O_4 to a maximum of 625 Å^3 for pure Mn_3O_4. It is evident that the manganese ions are the principal determining factor in the increase of cell volume, substitution of zinc for iron having relatively little effect, whereas substitution of manganese for iron or for zinc is reflected by a relatively rapid increase in cell volume.

THE EQUILIBRIUM DIAGRAM

Figure 6 is a partial equilibrium diagram for the system, showing conditions between ordinary temperatures and the highest temperatures reached during this investigation, viz. 1000°–1300°. It has been constructed from the results of experimental work on synthetic preparations (Table 1), and from the study of mineral specimens.

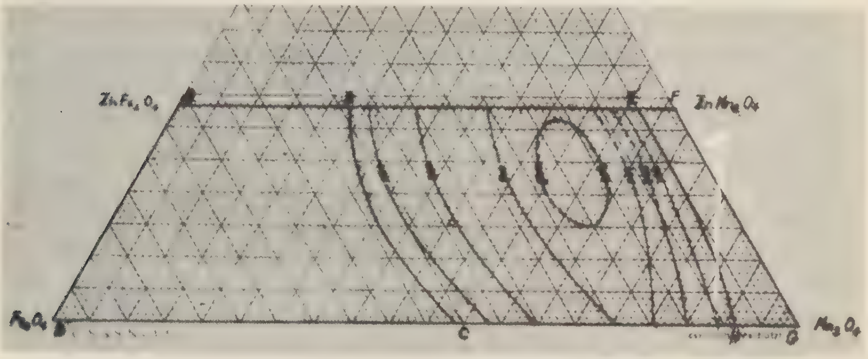

FIG. 6. Equilibrium diagram for the system. *ABCD* is the field of cubic mix-crystals. *EFGH* is the field of tetragonal mix-crystals. *CDEH* is the field of incomplete miscibility; isotherms show the boundaries of the field of incomplete miscibility at different temperatures.

In Fig. 6 the field *ABCD* is one of complete miscibility in the solid state, the single phase present being a solid solution of the respective components and having a cubic lattice. The field *EFGH* is also one of complete miscibility in the solid state, the single phase present being also a solid solution of the respective components but having a tetragonal lattice. Separating these two fields is the field *CDEF*, which is a field of incomplete miscibility in the solid state. For any composition within this field at ordinary temperatures two phases coexist in stable equilibrium. As the temperature rises the field of solid immiscibility contracts and finally disappears between 900° and 1000°. The isotherms in Fig. 6 indicate the boundaries of the field of incomplete miscibility at different temperatures.

The boundaries of the field of incomplete miscibility at temperatures between 600° and 1000° were determined by holding synthetic preparations at definite temperatures for a sufficient time for equilibrium to be attained. Under these conditions powder photographs of preparations whose composition fell within the field of incomplete miscibility for that temperature showed the presence of two phases; the composition of these two phases, which are points on the boundaries of the field of incomplete miscibility at that temperature, were determined by measuring the lattice dimension, axial ratios, and cell volumes of these phases and correlating these with the diagrams giving variation of lattice dimensions, axial ratios, and cell volumes with composition (Figs. 2, 3, 4, and 5). For tetragonal phases the variation of these properties with composition was sufficiently rapid for the compositions of unknown phases to be determined with a probably uncertainty of about ±2%; for cubic phases the uncertainty was too great for useful information concerning composition to be obtained; however, above 700° the field of limited miscibility lies almost entirely within the region of tetragonal lattices, so above this temperature the isotherms bounding the field of limited miscibility could be directly established. Below this temperature the isotherms within the region of cubic lattices were established by extrapolation and the study of mineral specimens.

For the synthetic preparations rich in zinc it was only necessary to take portions of the original preparations and heat them in air at the respective temperatures for one to two days. The stable phase in air from 590° upwards was the AB_2O_4 compound, and there was no tendency for the iron or manganese to form the R_2O_3 type oxides. Below 590° these preparations gave either blank photographs or a few very faint and diffuse lines, indicating a lack of crystallinity. As the amount of zinc in the preparations was decreased, however, there was an increasing tendency for the iron and manganese to form the R_2O_3 type oxides, and along the Fe_3O_4-Mn_3O_4 join the R_3O_4 oxides were not stable in air below 1000°, being oxidized to the sesquioxides. For preparations in this region it was therefore necessary first to heat them at a sufficiently high temperature to convert them to the R_3O_4 oxide, and then to reheat them in sealed evacuated tubes at the temperatures below 1000°. It was found, as might be expected, that equilibrium was reached much less readily than in those preparations which could be heated directly from their original semi-amorphous condition to the temperature required, the readjustment to falling temperature being much more sluggish than that to rising temperature. Thus preparation J (Fe 20, Mn 80) was converted into the R_3O_4 oxide by heating at 1150° and then heated in a sealed evacuated tube at 750° for three days, when it was found to have disintegrated into two phases; on heating at 650° under similar conditions, however, it showed no signs of any change, the rate of readjustment at this temperature evidently being practically zero.

Thus it was not possible to determine the isothermal boundaries of the region of incomplete miscibility for temperatures below 600° by laboratory experiments on synthetic preparations. The limiting curves for the region of incomplete miscibility were established from a study of natural minerals—whether homogeneous or showing intergrowths of the vredenburgite type, and in the latter case, the determination of the composition of the two phases of the intergrowth from measurements of the lattice dimensions. This was possible with a fair degree of accuracy for the Fe_3O_4—Mn_3O_4 tie-line, as a number of specimens of vredenburgite whose composition fell on this tie-line were available for study. Only one specimen of a zincian vredenburgite was available for study, so the extension of these limiting curves towards the $ZnFe_2O_4$—$ZnMn_2O_4$ tie-line is subject to some degree of extrapolation.

The results of measurements of lattice dimensions on the phases present in different specimens of vredenburgite are given in Table 2.

TABLE 2. LATTICE DIMENSIONS OF THE PHASES PRESENT IN DIFFERENT SPECIMENS OF VREDENBURGITE

Locality	a_{cubic}	$a_{\text{tetr.}}$	$c_{\text{tetr.}}$
Långban 1	8.504	8.167	9.345
Långban 2	8.502		
Jakobsberg 1	8.496	8.158	9.342
Jakobsberg 2	8.487	8.152	9.339
Jakobsberg 3	8.503	8.165	9.349
Kodur 1	8.483	8.162	9.369
Kodur 2	8.480	8.157	9.371
Kodur 3	8.478	8.171	9.333
Franklin (zincian)	8.422	8.115	9.190

Analyses of the vredenburgites from Långban, Jakobsberg, and Kodur show no zinc. The variation in lattice dimensions of the respective phases for the different specimens, while not great, is beyond the margin of error of the measurements, and is probably largely due to the presence of small and variable amounts of magnesium substituting iron and manganese. Analyses of vredenburgite from Jakobsberg show up to 1.25% MgO (7). The presence of magnesium in solid solution will have the effect of reducing the lattice dimensions below those for the pure iron-manganese compounds.

For the Fe_3O_4—Mn_3O_4 tie-line the figures given in Table 2 indicate a figure of 91% Mn_3O_4 (±2%) for the position of the bounding curve of the limited miscibility field on the manganese side of the diagram. The composition of naturally occurring hausmannites confirms this to some extent, in that the most iron-rich hausmannite so far recorded contains 6.91% Fe_3O_4, close to the bounding curve determined above. On the iron side of the diagram the position *C* of the bounding curve was determined from the specimen recorded as Långban 2 in Table 2. It is listed as a vredenburgite although the powder photographs did not show any lines corresponding to the tetragonal phase. Examination of polished sections of this specimen under the microscope showed however the presence of a few very narrow lamellae of the tetragonal phase, less than 5% in amount and evidently insufficient to give the characteristic lines on a powder photograph. An analysis of this specimen gave $Mn_3O_4 = 55.9\%$. The position *C* of the bounding curve is therefore put at 54% Mn_3O_4.

The use of minerals to establish the limits of the field of incomplete miscibility in the solid state rests on the assumption that these minerals are actually in a condition of chemical equilibrium. There are reasonable grounds for this assumption, in that the rate of changes in physical conditions, i.e., temperature and pressure, in nature is in general so extremely slow in comparison to that which can be attained in laboratory experiments that the chances for equilibrium to be continuously maintained are good. For the conditions of metamorphism under which these zinc-manganese-iron spinels have originated this must be particularly true. A further argument in favor of this concept can be adduced. From Table 2 it can be seen that the two phases in zinc-free vredenburgites, whether from different localities or different specimens from the same locality, show a marked constancy of lattice dimensions, especially when allowance is made for small quantities of magnesium in solid solution. This would indicate a constancy in chemical composition for these phases, suggesting that these specimens have reached a state of equilibrium which is the same in all.

The study of mineral specimens can thus contribute greatly to the knowledge of equilibrium conditions in chemical systems, since the time factor available for reactions under geological conditions is so vastly greater than that attainable in the laboratory. Although much has been done along these lines, the closer study of minerals will undoubtedly greatly advance our present knowledge of chemical equilibria.

Mineralogical Applications

In Fig. 7 analyses of minerals which fall within his system are plotted on the composition diagram. For this purpose the atom proportions of iron, manganese, and zinc were calculated from each analysis, converted to percentages, and plotted in the usual way. All the analyses were checked from the original publications, except for those of franklinite, which were taken from the table of collected analyses published in Palache's memoir on the minerals of Franklin and Sterling Hill (12).

On the basis of the phase relations within this system and this collection of mineral analyses an attempt has been made to define the valid mineral species within this system in terms of composition fields, as set out in Fig 7.

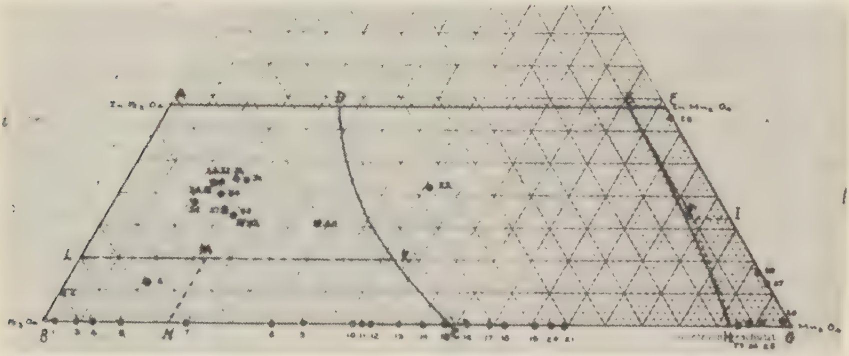

FIG. 7. Analyses of minerals falling within the system, and suggested composition limits for the different species. Magnetite *BNML;* jacobsite *NMKC;* franklinite *ADKL;* vredenburgite *DEHC;* hetaerolite *EFIJ;* hausmannite *GHIJ.*

Key to analyses for Fig. 7

1. Magnetite, Tongue, Scotland. *Mineral. Mag.*, **5**, 150 (1884).
2. ———, Franklin, New Jersey. *U. S. Geol. Survey, Prof. Paper* **180**, 44 (1935).
3. ———, Väster Silvberg, Sweden. *Mineral. petrog. Mitt.*, **7**, 110 (1886).
4. ———, Väster Silvberg, Sweden. *Mineral. petrog. Mitt.*, **7**, 110 (1886).
5. ———, St. Joseph du Lac, Quebec. *Mineral. Mag.*, **14**, 373 (1907).
6. ———, Franklin, New Jersey. *U. S. Geol. Survey, Prof. Paper* **180**, 47 [anal. 10] (1935).
7. Jacobsite, Siegen, Germany. *Rammelsberg, Mineral.-Chem.*, 132 (1875).
8. ———, Debarstica, Bulgaria. *Zeits. Kryst.*, **36**, 202 (1902).
9. ———, Nordmarken, Sweden. *Bull. soc. franç. minéral.*, **10**, 185 (1885).
10. ———, Långban, Sweden. *Geol. Fören. Förh.*, **3**, 384 (1876–77).
11. ———, Beldongri, India. *Trans. Nat. Inst. Sci. India*, **1**, 108 [779a] (1936).
12. ———, Sjögruvan, Sweden. *Bull. soc. franç. minéral.*, **10**, 172 (1887).
13. ———, Beldongri, India. *Trans. Nat. Inst. Sci. India*, **1**, 108 [779*b*] (1936).
14. ———, Beldongri, India. *Records Mysore Geol. Dept.*, **34**, 82 [no. 1] (1935).
15. ———, Sjögruvan, Sweden. *Bull. soc. franç. minéral.*, **10**, 173 (1887).
16. Vredenburgite, Långban, Sweden. *Nyt. Mag. for Naturvidenskaberne*, **29**, 304, 1885 (Manganomagnetite).
17. ———, Devada, India. *Records Mysore Geol. Dept.*, **34**, 82 [no. 2] (1935).
18. ———, Kodur, India. *Records Mysore Geol. Dept.*, **34**, 82 [no. 3] (1935).
19. ———, Långban, Sweden. *Geol. Fören. Förh.*, **65**, 266 (1943).
20. ———, Garividi, India. *Mem. Geol. Survey India*, **37**, 44 (1909).
21. ———, Jakobsberg, Sweden. *Zeits. Krist.*, **68**, 116 (1928).
22. ———, Franklin, New Jersey. *Geol. Fören. Förh.*, **68**, 55 (1946) (zincian vredenburgite).
23. Hausmannite, Långban, Sweden. *Geol. Fören. Förh.*, **65**, 159 [no. 27] (1943).

24. ———, Jakobsberg, Sweden. *Bull. soc. chim.* (3), **29,** 1110 (1903).
25. ———, Långban, Sweden. *Bull. soc. chim.* (3), **29,** 1110 (1903).
26. ———, Ilmenau, Germany. *Bull. soc. chim.* (3), **10,** 653 (1893).
27. ———, Ilmenau, Germany. *Bull. soc. chim.* (3), **10,** 653 (1893).
28. ———, Ilmenau, Germany. *Bull. soc. chim.* (3), **10,** 653 (1893).
29. Hetaerolite, Franklin, New Jersey. *Am. Mineral.*, **13,** 297 (1928).
30. Franklinite, Franklin, New Jersey. *U. S. Geol. Survey, Prof. Paper* **180,** 47 (1935), (anal. 6).
31. ———, Franklin, New Jersey. *U. S. Geol. Survey, Prof. Paper* **180,** 47 (1935), (anal. 9).
32. ———, Franklin, New Jersey. *U. S. Geol. Survey, Prof. Paper* **180,** 47 (1935), (anal. 8).
33. ———, Franklin, New Jersey. *U. S. Geol. Survey, Prof. Paper* **180,** 47 (1935), (anal. 7).
34. ———, Franklin, New Jersey. *U. S. Geol. Survey, Prof. Paper* **180,** 47 (1935), (anal. 16).
35. ———, Franklin, New Jersey. *U. S. Geol. Survey, Prof. Paper* **180,** 47 (1935), (anal. 14).
36. ———, Franklin, New Jersey. *U. S. Geol. Survey, Prof. Poper* **180,** 47 (1935), (anal. 3).
37. ———, Franklin, New Jersey. *U. S. Geol. Survey, Prof. Paper* **180,** 47 (1935), (anal. 2).
38. ———, Franklin, New Jersey. *U. S. Geol. Survey, Prof. Paper* **180,** 47 (1935), (anal. 1).
39. ———, Franklin, New Jersey. *U. S. Geol. Survey, Prof. Paper* **180,** 47 (1935), (anal. 13).
40. ———, Franklin, New Jersey. *U. S. Geol. Survey, Prof. Paper* **180,** 47 (1935), (anal. 12).

Physico-chemical considerations divide the diagram into three fields, by means of the two lines *CD* and *EH* limiting the field of incomplete miscibility in the solid state. Thus we have at the left of the diagram a field of cubic solid solutions, the magnetite-jacobsite-franklinite field, in the center the vredenburgite field, and on the right the field of tetragonal solid solutions, the hausmannite-hetaerolite field.

Only the field of vredenburgite is precisely determined in this way. Division of the field of magnetite-jacobsite-franklinite and that of hausmannite-hetaerolite into areas for the respective minerals cannot be made on the basis of clearly defined phase boundaries but must depend upon a more or less arbitrary procedure.

In an earlier paper (8) the writer suggested that the division between jacobsite and magnetite be drawn according to the dominance or otherwise of $MnFe_2O_4$, the formula usually ascribed to jacobsite, although it has not been shown that this formula represents more than a point in a mix-crystal field. If this procedure be followed then the point of division on the Fe_3O_4-Mn_3O_4 tie-line is at the point representing 16.7% Mn_3O_4. It is now suggested that a line—*NM* in Fig. 7—be drawn from this point parallel with the Fe_3O_4-$ZnFe_2O_4$ tie-line (i.e., keeping the percentage of manganese in the relative percentages of iron, manganese and zinc at 16.7) until it meets the boundary of the franklinite field, thereby separating the field of magnetite from that of jacobsite.

The field of franklinite might be defined in a similar way, by considering the boundary between franklinite and magnetite as being determined by the dominance or otherwise of $ZnFe_2O_4$ and drawing a line from the point thus determined parallel to the base of the diagram until it met the bounding curve of the vredenburgite field. This would, however, lead to a clustering of the points representing analyzed franklinites on either side of this line. In order to keep the compositions generally recognized as franklinite within one field it is therefore suggested that the boundary of the franklinite field be a line corresponding to 10% of zinc in the relative percentages of iron, manganese, and zinc shown by an analysis.

Thus the field of stable cubic solid solutions is divided into the following areas: *BLMN*, that of magnetite; *NMKC*, that of jacobsite; and *ADKL*, that of franklinite.

Turning now to the hausmannite-hetaerolite field the division here can well be made on the dominance or otherwise of $ZnMn_2O_4$. In the diagram this is indicated by a line *IJ* representing 16.7% zinc in the relative percentages of zinc, iron, and manganese. Thus *EFIJ* is the field of hetaerolite, and *GHJI* that of hausmannite.

Finer distinctions within these mineral species can be made by the use of the adjectival qualifiers suggested by Schaller (14), and adopted by the authors of the new (7th.) edition of Dana's *System of Mineralogy* (13).

In an earlier paper on the Fe_3O_4-Mn_3O_4 system (8), the writer devoted considerable space to the discussion of the nature and systematic position of vredenburgite, the essential points of which may be repeated here. Vredenburgite was originally described by Fermor (3), who gave it the formula $3Mn_3O_4 \cdot 2Fe_2O_3$ on the basis of analyses made at that time. Some years later the examination of polished sections of vredenburgite under the microscope, by Schneiderhöhn and Ramdohr (15), Orcel and Pavlovitch (11), and Dunn (1)—the latter on Fermor's original specimens showed that vredenburgite was an oriented intergrowth of jacobsite and hausmannite. Schneiderhöhn and Ramdohr pointed out that the structure was typical of exsolution on cooling of a mix-crystal formed at high temperatures, and showed that the excess oxygen over the simple $(Fe,Mn)_3O_4$ formula in the original analyses of vredenburgite was due to the selective replacement of the hausmannite lamellae by pyrolusite and psilomelane, probably the result of supergene processes.

Further analyses of the Indian vredenburgite were made by Iyer (5, 6). Iyer's analyses show an excess of oxygen over the simple $(Fe,Mn)_3O_4$ formula, but later microscopic examination (8, pp. 163–165) has shown that this is due to the presence of pyrolusite and psilomelane. However, Fermor (4) has extensively discussed Iyer's analyses and correlated them with those given in the original description of vredenburgite. On the basis of the variation in manganese and iron content of vredenburgites from different localities he has suggested two new names, devadite and garividite, for the originally homogeneous material from which vredenburgite was formed by unmixing. On account of the excess oxygen over the simple $(Fe,Mn)_3O_4$ formula shown by analyses of these Indian vredenburgites he also argues that this originally homogeneous material was not a spinellid, and that on unmixing it broke down not into jacobsite and hausmannite alone, but into jacobsite, hausmannite, and free MnO_2, the latter appearing as pyrolusite and psilomelane. Neither of Fermor's proposals are, however, valid; firstly microscopic examination of specimens of the Indian vredenburgite has shown that the MnO_2 is a secondary product, resulting from the selective replacement of the hausmannite lamellae; and secondly the variation in iron and manganese in vredenburgite is continuous, vredenburgites being members of a continuous mix crystal series, and therefore no real grounds exist for the division of vredenburgite into distinct species on the basis of relative content of iron and manganese.

From the nature of the equilibrium diagram it is evident that a homogeneous phase for any composition within the vredenburgite field can exist at ordinary temperatures and pressures only in a metastable condition. Arguments have been advanced above against the occurrence of such metastable phases as natural minerals. However, the writer has recently described (9) a homogeneous vredenburgite from Långban (anal. 19, Fig. 7). This material had however originated under rather special circumstances. It was pseudomorphous after bixbyite, $(Mn,Fe)_2O_3$, having been produced by a process of reduction probably at a comparatively low temperature. Evidently the first product of the reduction was this metastable homogeneous vredenburgite, and the temperature at which the reduction took place was so low that the rate of readjustment was effectively zero. As a result it has remained in this metastable condition. Primary vredenburgite, on the other hand, seems always to show the typical intergrowth of jacobsite and hausmannite produced by unmixing of the originally homogeneous solid solution.

Comparison of the positions of analyzed specimens of vredenburgite (Fig. 7) with the equilibrium diagram (Fig. 6) reveals an interesting grouping. All the analyses lies on the left side of the vredenburgite field. While this may be due partly to proportions between iron and manganese in the environment in which they originated, an important factor has probably been the temperature at which they formed; comparison with the equilibrium diagram shows that these analyses all fall below the 800° isotherm, and most of them are grouped about the 600° isotherm. The absence of analyzed vredenburgites lying within the higher isotherms suggests that the metamorphosed manganese ores from which vredenburgite has been recorded have never been subjected to these higher temperatures, and that recrystallization took place at temperatures below 800° and in some cases considerably lower. Vredenburgite can thus be used as a geologic thermometer for indicating minimum temperatures of formation, and detailed study of the variation in its composition in any ore-body may give useful evidence as to the thermal history of that ore-body.

REFERENCES

1. DUNN, J. A., A study of some microscopical aspects of Indian manganese-ores: *Trans. Nat. Inst. Sci. India,* **1,** 103–124 (1936).
2. VON ECKERMANN, H., Some remarks on the system Fe_3O_4–Mn_3O_4: *Geol. Fören. Förh.,* **65,** 258–262 (1943).
3. FERMOR, L. L., The manganese-ore deposits of India: *Mem. Geol. Survey India,* **37** (1909).
4. FERMOR, L. L., Notes on vredenburgite (with devadite) and on sitaparite: *Proc. Nat. Inst. Sci. India,* **4,** 253–286 (1938).
5. IYER, M. R. A., The formula proposed for the mineral vredenburgite: *Records Mysore Geol. Dept.,* **34,** 75–84 (1935).
6. IYER, M. R. A., A graphical representation of the composition of some manganese minerals including a discussion of the nature of the mineral vredenburgite: *Records Mysore Geol. Dept.,* **35,** 73–85 (1936).
7. JOHANSSON, K., Mineralogische Mitteilungen: *Zeits. Krist.,* **68,** 87–118 (1928).
8. MASON, B., Mineralogical aspects of the system FeO–Fe_2O_3–MnO–Mn_2O_3: *Geol. Fören. Förh.,* **65,** 97–180 (1943).
9. MASON, B., Alpha-vredenburgite: *Geol. Fören. Förh.,* **65,** 263–270 (1943).
10. MONTORO, V., Miscibilità fra gli ossidi salini di ferro e di manganese: *Gazz. chim. ital.,* **68,** 728–733 (1938).
11. ORCEL, J., AND PAVLOVITCH, S., Les caractères microscopiques des oxydes de manganèse et des manganites naturels: *Bull. soc. franç. minéral.,* **54,** 108–179 (1931).
12. PALACHE, C., The minerals of Franklin and Sterling Hill, Sussex County, New Jersey: *U. S. Geol. Survey, Prof. Paper* **180** (1935).
13. PALACHE, C., BERMAN, H., AND FRONDEL, C., *Dana's System of Mineralogy,* 7th ed., 43 (**1944**).
14. SCHALLER, W. T., Adjectival ending of chemical elements used as modifiers to mineral names: *Am. Mineral.,* **15,** 566–574 (1930).
15. SCHNEIDERHÖHN, H., AND RAMDOHR, P., *Lehrbuch der Erzmikroskopie,* Band 2 (**1931**).

THE STRUCTURE OF EUDIDYMITE ($HNaBeSi_3O_8$)

T. Ito, *The Mineralogical Institute, Imperial University of Tokyo, Tokyo, Japan.*

An intimate relationship has been supposed to exist between epididymite and eudidymite ever since these rare dimorphous minerals of the composition $HNaBeSi_3O_8$ were described by Brögger[1] and by Flink.[2] In 1929 Gossner[3] (with Kraus) and Zachariasen[4] determined the unit cell and space group of these minerals. More recently Palache,[5] basing his results on the work of Zachariasen, proposed a new set of axes for eudidymite.

The present writer examined epididymite by means of x-ray methods and obtained a structure which explains to a certain extent the experimental data, although minor adjustments of the positions of atoms were considered necessary to secure a better agreement between the theoretical and experimental F-values.[6,7]

The writer further, in discussing the structural relationship between them, pointed out that epididymite may be regarded as an *internal twin* of eudidymite, "twinning" being effected between groups of atoms within the unit cell.[8]

The purpose of the following investigation is two-fold. We intend to decide experimentally if the structural scheme proposed for epididymite will also apply to eudidymite, and to establish the phenomenon of internal twinning on a firmer basis, if such exists in minerals.

---

[1] Brögger, W. C., *Zeits. Krist.* **16,** 586 (1890).

[2] Flink, G., *Zeits. Krist.* **23,** 353 (1894).

[3] Gossner, B., and Kraus, W. O., *Centralbl. Miner.*, **A,** 257 (1927).

[4] Zachariasen, W. H., *Norsk. geol. Tidsskr.*, **10,** 449 (1929).

[5] Palache, C., *Zeits. Krist.* **85,** 425 (1933).

[6] Ito, T., *Zeits. Krist.*, **88,** 142 (1934).

[7] Wyckoff, R. W. G., *The Structure of Crystals*, Supplement 1930–1934 to the 2nd Ed., 108 (1935).

Wyckoff considered that the structure should be revised since some of its interatomic distances are impossible. He seems to stress minor points while the present writer's efforts were directed only to work out the structure in its main features but not all the details. It may be pointed out here, however, that there is actually a misprint concerning the coordinates of Be in Table 1 of the original paper, *viz.*

	x_a	y_b	y_c
Be	.035	.250	*.250* (instead of .052)

This correction, it is hoped, will clear up Wyckoff's remark.

[8] Ito, T., *Proc. Impl. Acad.*, **9,** 528 (1933).

MATERIAL

The crystal specimens used in the investigation came from Langesundfjord, Norway, and were purchased from Dr. F. Kranz, Bonn am Rhein. They are colorless, transparent crystals, tabular after (001), up to several mm. in thickness and up to 2 cm. in length; (331) and (111) together with (001) are well developed (Palache's notation). The platy crystals are often warped and overlap irregularly. Cleavage after (001) is very perfect, almost to the same extent as in mica. From these crystals cleavage pieces were obtained and ground for the spectrometer measurements, as oriented pieces were almost impossible to obtain owing to the high perfection of the cleavage.

UNIT CELL

The unit cell was found to be $a=12.62$ Å, $b=7.37$ Å, $c=13.99$ Å, $\beta=103°43'$. (Direct spectrometer measurement.) This gives for the axial ratio, $a:b:c:=1.712:1:1.898$, which agrees well with that obtained by Palache from the measurements published by Brögger in 1890.

There are eight molecules of $HNaBeSi_3O_8$ in the cell, giving for the theoretical density 2.561, compared with 2.553 as measured by Brögger.

SPACE GROUP

The results of our experimental work in which several Weissenberg-Buerger photographs (CoKα 1.788 Å) were taken show the following:

Reflections (hkl) are absent when $h+k$ is odd.
Reflections ($h0l$) are absent when h is odd, l is odd.
Reflections ($0k0$) are absent when k is odd.

From these data the space group for eudidymite is determined as C_{2h}^6—$C2/c$.

This is in accord with that given by Zachariasen and by Gossner and Kraus. Formerly the present writer considered C_{2h}^5 rather than C_{2h}^6 as the space group for eudidymite, for the reason that C_{2h}^5 is a subgroup of V_h^{16} which is the space group of epididymite. He considered that if epididymite were an internal twin of eudidymite, the space group of the latter would be reasonably a subgroup of the space group of the former. The experimental data, however, did not substantiate his opinion, but confirmed the work of Zachariasen and others.

Figure 1 shows the space group as found in eudidymite. There are two different sets of glide planes of two each, one set of four digonal rotation axes, one set of four digonal screw axes and two different sets of eight symmetry centers.

An atom in the general position has eight equivalent positions. These reduce to four if the atom is either on the reflection planes or on the centers of symmetry.

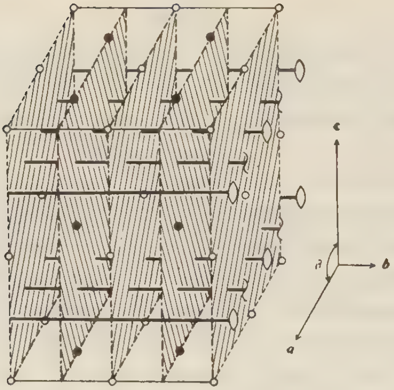

FIG. 1. Symmetry elements of the space group C_{2h}^6-C2/c. Small white and black circles represent centers of symmetry. Shaded planes represent glide planes.

We have to determine altogether the positions of seven oxygen atoms, three silicon atoms, one sodium atom, one beryllium atom and one (OH) group; the number of parameters to be determined amounting to thirty-nine as a maximum.

The intensity of reflection for the plane (*hkl*) is proportional to the square of

$$F = \Sigma 8f \cos^2 2\pi \frac{h+k}{4} \cos 2\pi\left(hx + lz + \frac{l}{4}\right) \cos 2\pi\left(ky - \frac{l}{4}\right),$$

where f is the atomic scattering factor appropriate to each atom and the summation is to be taken over all atoms in the cell.

ANALYSIS

We began the analysis by comparing x-ray and other data on eudidymite and epididymite (Tables 1 and 2).

TABLE 1. COMPARISON OF THE LATTICE CONSTANTS AND OTHER PHYSICAL CONSTANTS OF EUDIDYMITE AND EPIDIDYMITE

		Eudidymite	Epididymite
a		12.62 Å	12.63 Å
b		7.37 Å	7.32 Å
c		13.99 Å	13.58 Å
β		103°43′	
Specific gravity		2.553	2.548
Refractive indices	n_α	1.545	1.565
	n_β	1.546	1.569
	n_γ	1.551	1.569
2V		29°55′(+)	31°4′(−)
Hardness		6	6

We see that the two crystals have almost identical cell dimensions. The *a*- and *b*-lengths of both crystals are nearly equal, while $c \sin \beta$ of eudidymite is equal to the *c*-length of epididymite, with the result that the volume of the unit cell is, respectively, 1264.1 Å^3 (eudidymite) and 1255.5 Å^3 (epididymite), each containing eight molecules of $HNaBeSi_3O_8$.

The intensity of the reflections, on the other hand, shows a marked difference as well as certain similarities. We note that, whereas the (*h*00) and (00*l*) spectra indicate generally analogous trends, the (0*k*0) spectra are decidedly different in the two crystals.

TABLE 2. INTENSITY OF REFLECTIONS. MEASUREMENTS WITH THE IONIZATION SPECTROMETER

Indices	Eudidymite (Mo K_α radiation 0.71 Å)			Epididymite (Rh K_α radiation 0.61 Å)		
	Sin θ	$\rho\times10^6$	*F* obs.	Sin θ	$\rho\times10^6$	*F* obs.
200	.0582	32.4	68.8	.0487	90.0	92
400	.1165	152.0	246.0	.0973	120.0	154
600	.1746	3.7	43.0	.1459	5.5	41
800	.2327	3.9	50.7	.1946	12.0	69
10.0.0	.2910	1.6	37.2	.2433	23.6	111
12.0.0	.3495	—	—	.2919	27.3	135
14.0.0				.3405	—	—
020	.0972	72.7	139.0	.0839	30.3	68
040	.1945	—	—	.1678	242.0	289
060	.2918	—	—	.2518	20.2	109
080	.3891	—	—	.3357	2.7	46
0.10.0	.4864	—	—	.4197	5.6	79
004	.1043	50.3	104.5	.0905	198.0	191
006	.1565	7.2	47.5	.1359	64.0	136
008	.2087	12.6	74.1	.1807	56.0	143
0.0.10	.2610	14.6	90.5	.2262	58.0	168
0.0.12	.3132	2.0	37.0	.2714	6.1	62
0.0.14	.3653	3.2	53.5	.3167	23.0	128
0.0.16				.3618	21.8	135

Further, epididymite has feldspathoid cleavages, namely two nearly equal perfect cleavage faces (001) and (100) which are at right angles. The cleavages of eudidymite are rather mica-like, one after (001) being highly perfect, the other after (110) (Palache's notation) not so perfect.

These suggest at once that, though they are built up on the same general plan, the two structures may reveal certain differences especially with regard to the *b*-parameters of the atoms.

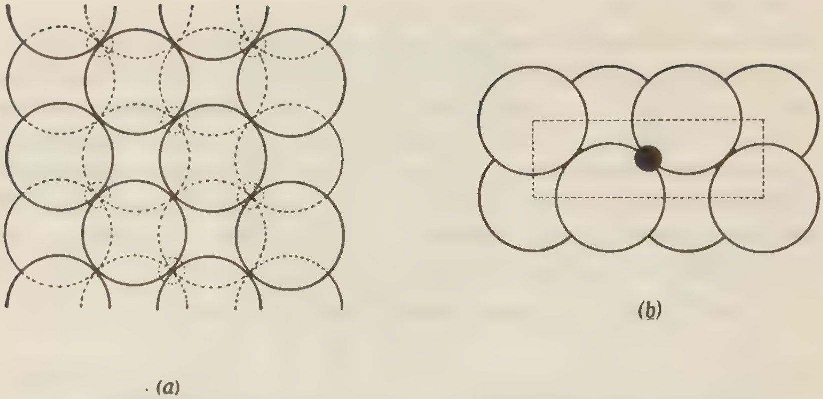

FIG. 2. Si_3O_8-chain. Large circles represent oxygen atoms and small circles silicon atoms (*a*) plan; (*b*) elevation (as viewed from the chain-direction).

We assume now that the same Si_3O_8 groups (Fig. 2) as found in epididymite play a main rôle in the structure of eudidymite. In epididymite the Si_3O_8 groups are joined to form a sheet of the composition $NaSi_3O_7$ by Na atoms lying on the centers of symmetry. In eudidymite this must be done by Na atoms lying on the two-fold rotation axes. The ways in which two different sheets of the same composition $NaSi_3O_7$ are built from the Si_3O_8 groups and Na atoms are illustrated in Fig. 3. The one fits well into the space group C_{2h}^6 and the other into the space group V_h^{16} as shown in Fig. 4.

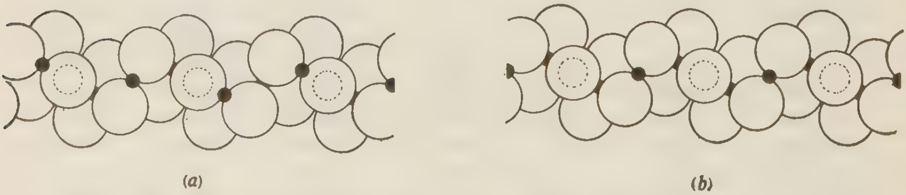

FIG. 3. Two different modes of forming a $NaSi_3O_7$ sheet. Large circles represent oxygen atoms, medium sized circles represent sodium atoms, and small circles represent silicon atoms. (*a*) epididymite; (*b*) eudidymite.

The fundamental framework thus obtained, it is now comparatively easy to adjust the positions of atoms within the groups and to place the remaining Be atoms and (OH) groups in appropriate positions until the experimental *F*-values are satisfactorily accounted for.

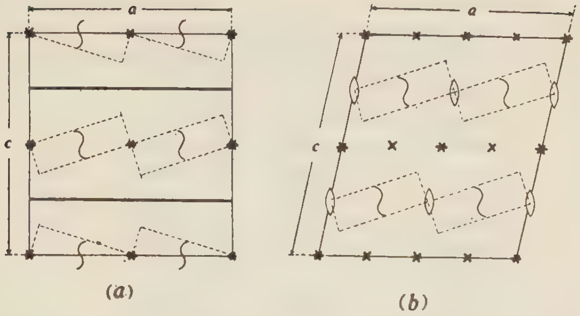

FIG. 4. The Si_3O_8 groups arranged in the space group V_h^{16} (epididymite) and in the space group C_{2h}^6 (eudidymite). Dotted rectangles represent the Si_3O_8 groups. Crosses and asterisks represent centers of symmetry. Heavy full lines represent the traces of reflection planes. Other symbols as in common use. Projections on (010). (*a*) epididymite; (*b*) eudidymite.

In Table 3 we give the coordinates of atoms in the structure. In Table 4 are given the F-values obtained with the ionization spectrometer compared with those calculated for the structure. In Table 5 are given the intensity of reflections observed on Weissenberg photographs compared with the calculated F-values. The agreement between the theoretical and experimental values is very satisfactory, in view of the number of parameters involved.

TABLE 3. COORDINATES OF ATOMS IN DECIMAL FRACTIONS OF THE AXIAL LENGTHS. THE ORIGIN IS PLACED AT A CENTER OF SYMMETRY

Kind of Atom	Number in the Cell	x/a	y/b	z/c
O_{I}	8	.052	.030	.396
O_{II}	8	.552	.030	.396
O_{III}	4	.000	.275	.250
O_{IV}	4	.500	.275	.250
O_{V}	8	.161	.030	.190
O_{VI}	8	.661	.030	.190
O_{VII}	8	.208	.315	.372
O_{VIII}	8	.708	.315	.372
Si_{I}	8	.063	.415	.312
Si_{II}	8	.563	.415	.312
Si_{III}	8	.241	.122	.243
Na_{I}	4	.000	.030	.250
Na_{II}	4	.500	.030	.250
Be	8	.427	.130	.320
(OH)	8	.303	.190	.494

TABLE 4. INTENSITY OF REFLECTIONS. MEASUREMENTS WITH THE IONIZATION SPECTROMETER (Mo Kα RADIATION 0.71 Å)

Indices	Sin θ	$\rho \times 10^6$	F obs.	F calc.
200	.0582	32.4	68.8	+ 99.6
400	.1165	152.0	246.0	+278.8
600	.1746	3.7	43.0	− 35.6
800	.2327	3.9	50.7	−117.7
10.0.0	.2910	1.6	37.2	− 84.0
12.0.0	.3495	—	—	+ 47.6
020	.0972	72.7	139.0	+197.2
040	.1945	—	—	+ 14.5
060	.2918	—	—	+ 2.9
080	.3891	—	—	− 16.8
0.10.0	.4864	—	—	+ 28.4
002	.0521	390.0	199.8	−391.0
004	.1043	50.3	104.5	+ 90.1
006	.1565	7.2	47.5	− 66.6
008	.2087	12.6	74.1	+ 78.0
0.0.10	.2610	14.6	90.5	+ 83.2
0.0.12	.3132	2.0	37.0	+ 32.3
0.0.14	.3653	3.2	53.5	+ 98.8

TABLE 5. INTENSITY OF REFLECTIONS. INTENSITY ESTIMATED ON THE WEISSENBERG PHOTOGRAPHS. (Co Kα RADIATION 1.788 Å)

Indices	*I* obs.	*F* calc.	Indices	*I* obs.	*F* calc.
110	—	+ 6.0	113	m	+ 45.5
130	w	+ 5.1	$11\bar{3}$	m	+ 52.0
220	s	+150.0	114	m	− 10.4
310	—	+ 11.2	$11\bar{4}$	w	− 2.0
330	—	− 16.3			
440	m	+ 59.0	131	—	− 1.8
510	—	− 7.4	$13\bar{1}$	w	− 34.3
710	w	+ 17.1	132	w	+ 6.6
			$13\bar{2}$	w	+ 8.2
204	w	+ 14.6	133	w	− 31.9
$20\bar{4}$	w	+ 14.0	$13\bar{3}$	w	− 23.0
404	w	− 48.0			
$40\bar{4}$	s	+236.0	221	m	+ 88.0
402	m	+ 65.5	$22\bar{1}$	s	−216.8
$40\bar{2}$	s	−267.9	222	m	+ 77.5
			$22\bar{2}$	s	+105.5
021	w	+ 35.0	223	w	− 15.3
022	s	−172.0	$22\bar{3}$	m	+ 70.5
023	w	+ 43.5	224	—	− 25.0
041	m	−120.0	$22\bar{4}$	m	−158.6
042	w	+ 40.0			
311	w	+ 26.5			
$31\bar{1}$	m	− 31.5			
312	w	+ 35.5			
$31\bar{2}$	—	+ 8.0			
331	w	+ 19.0			
$33\bar{1}$	w	+ 16.5			
332	w	− 25.9			
$33\bar{2}$	m	+ 30.3			

THE STRUCTURE DESCRIBED

The structure of eudidymite is shown in Fig. 5, which is a projection on (010). The structure, like that of epididymite, is built up of the complex chains Si_3O_8 stretched parallel to the *b*-axis. These Si_3O_8 groups are joined to each other holding in common oxygen atoms on the border and form with Na a sheet of the composition $NaSi_3O_7$ lying parallel to (001). In order to make the three-dimensional crystal the sheets are heaped one upon another in parallel position, beryllium atoms and the (OH) groups lying in between and linking them.

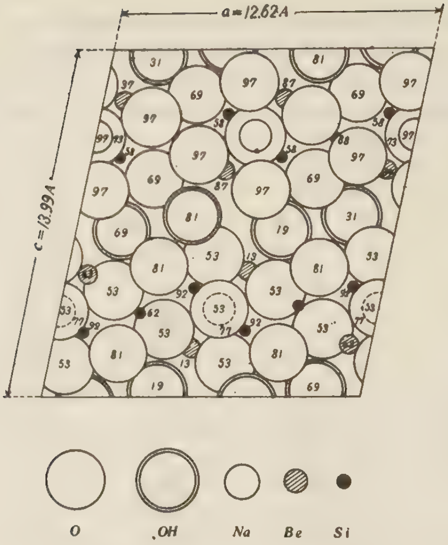

FIG. 5. The structure of eudidymite, projected on (010). Numbers given in decimal fractions of the *b*-length are the height of atoms.

In the structure thus built up Si atoms are surrounded by four oxygen atoms, Be atoms by three oxygen atoms and one (OH) group, both arranged nearly in tetrahedral fashion while Na atoms are at the center of more or less distorted octahedra formed of oxygen atoms. Each oxygen atom is shared either by two Si atoms or by one Si and two Na atoms, or by one Si, one Na and two Be atoms, while each (OH) group is linked to one Be atom. Ionic polyhedra, save Na octahedra which share faces with the adjoining Si tetrahedra, share only corners. Pauling's rule is obeyed completely. In Table 6 are given interatomic distances in the structure.

STRUCTURAL RELATION TO EPIDIDYMITE

In Fig. 6 the structure of epididymite is given contrasted to that of eudidymite. These are idealized projections on (001). We see here that the structural scheme is almost the same in both minerals. They have similar Si_3O_8 chains and $NaSi_3O_7$ sheets, the only apparent difference being that in epididymite one sheet lies on top of the other in a *symmetrical* position, while in eudidymite they lie in *parallel* position.[9]

---

[9] In eudidymite the atoms in one sheet have not the same *b*-parameters with the corresponding atoms in the next sheet, while in epididymite they have exactly the same *b*-parameters owing to the reflection planes. This explains the difference in the *b*-spectra of the two crystals.

TABLE 6. INTERATOMIC DISTANCES IN EUDIDYMITE

Atom	Neighbor	Distance in Å
Si_{I}	O_{I}	1.62
	O_{III}	1.45
	O_{V}	2.56
	O_{VII}	1.89
Si_{III}	O_{V}	1.44
	O_{VI}	1.44
	O_{VII}	2.06
	O_{VII}'	2.06
O_{I}	O_{III}	2.71
	O_{V}	3.50
	O_{VII}	2.65
O_{II}	O_{II}'	3.48
O_{III}	O_{V}	3.03
	O_{VII}	2.80
O_{IV}	O_{VII}	2.95
O_{V}	O_{VI}	2.48
	O_{VII}	3.24
	O_{VIII}	3.34
O_{VI}	O_{VII}	3.34
	O_{VIII}	3.24
O_{VII}	O_{VIII}	3.78
(OH)	O_{II}	3.33
	O_{III}	3.76
	O_{VI}	3.06
	O_{VII}	3.32
(OH)′	O_{VII}'	2.12
	O_{II}'	2.66
	O_{I}'	2.92
Na_{I}	O_{I}	2.04
	O_{III}	1.84
	O_{V}	2.36
Be	O_{I}	2.20
	O_{III}	1.98
	O_{VI}	1.36
	(OH)	2.14

Prime denotes atoms in the adjoining cell.

Epididymite, nevertheless, cannot be said in a strict sense to be an internal twin of eudidymite, since the $NaSi_3O_7$ group, which should be regarded as the constituent of "a twin," is different in the two structures.

It has been pointed out that in eudidymite the octahedral group of oxygen atoms around Na atom holds faces in common with adjoining tetrahedral groups around the Si atom. This is also the case with epididymite. The Na atom, however, in eudidymite, lies on the two-fold rotation axis and in epididymite on the center of symmetry. Faces commonly held by the octahedral and tetrahedral groups are *inclined* to each other in the former and *parallel* in the latter (Fig. 7). This point may be described thus: the arrangements of oxygen atoms are almost identical in both $NaSi_3O_7$ groups. There are, however, two different sets of positions for Si atoms, one being represented by Si atoms in eudidymite, the other by those in epididymite. Consequently epididymite should not be regarded as an internal twin of eudidymite, although very close to it.

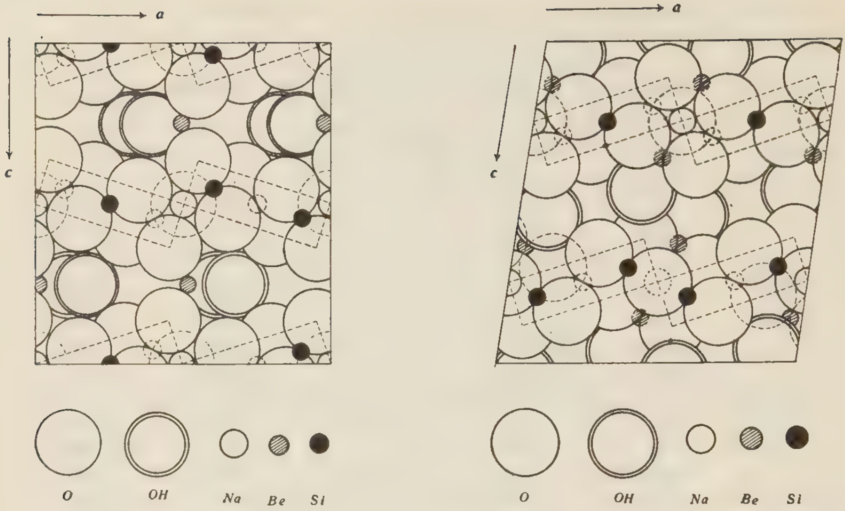

FIG. 6. The structure of epididymite (left) contrasted to that of eudidymite (right). The positions of atoms are displaced from their true positions to ideal positions to reveal the relationship of the two structures. Projections on (010).

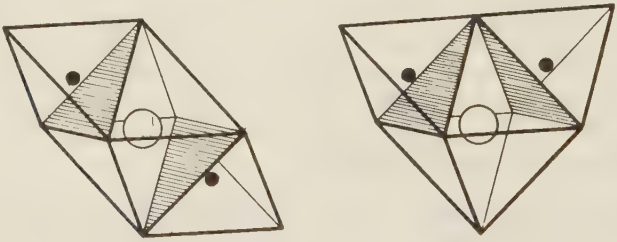

(a) (b)

FIG. 7. Tetrahedral groups adjoining an octahedral group of oxygen atoms in epididymite (*a*) and in eudidymite (*b*). Common faces are shaded. Large open circles represent sodium atoms. Small black circles represent silicon atoms. Oxygen atoms, lying on the octahedral and tetrahedral corners are omitted.

A further difference between the two structures is the role of BeOH which binds the sheets to form the three-dimensional crystal. In epididymite Be is in the center of a tetrahedron formed of two oxygen atoms and two (OH) groups, one of the oxygen atoms belonging to a $NaSi_3O_7$ sheet and the other to the next one. The tetrahedron holds commonly the (OH) groups with the adjoining similar tetrahedrons, forming a chain of the composition BeO_2OH stretched parallel to the direction of the *b*-axis and also to the direction of the Si_3O_8 chains. The structure is ionic in bond in every respect. In eudidymite, on the contrary, the Be atom is in the center of a tetrahedron formed by three oxygen atoms of a $NaSi_3O_7$ sheet and one (OH) group, forming a giant sheet $BeOHNaSi_3O_7$ parallel to (001). Such sheets are held together by a van der Waal force between them. The structure is molecular. The extremely perfect, mica-like cleavage after (001) in eudidymite is thus explained.

STEREOSCOPIC DRAWINGS OF CRYSTAL STRUCTURES

W. L. Bond, *Bell Telephone Laboratories, Murray Hill, New Jersey.*

Abstract

A method is presented for getting stereoscopic pairs of atomic structure views given the coordinates of the atoms and cell constants.

Stereoscopic pairs of pictures of crystal structures take much less space to store than do actual models. A box 4″×7″×8″ can hold 200 such views in individual envelopes, while 200 three dimensional models might require fifty square feet of shelf space.

One could produce the stereoscopic views by photographing an actual model or one can draw them directly, avoiding the work of construction of the three dimensional models. We turn then to the analysis of the simplest case, that of representing a point p in three dimensional space as two points on a plane, one point as seen by the right eye, the other as seen by the left eye.

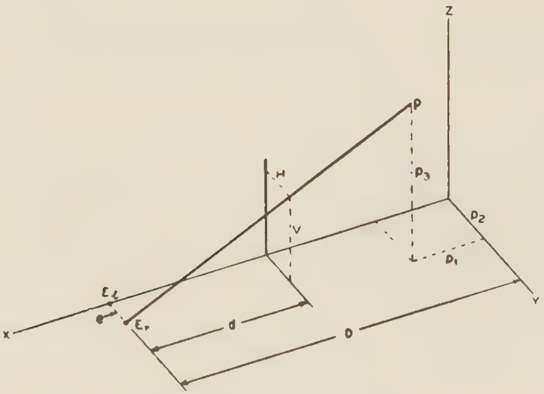

Fig. 1

Consider a rectangular coordinate system XYZ, Fig. 1. The two eyes are in the XYZ plane at a distance D from the Y axis, the left eye is on the axis at E_l, the right eye at a distance e from it at E_r. The plane of projection is parallel to the YZ plane and is at a distance d from the eyes. The right eye will see point p by looking along the line E_r–p, hence p can be represented by the point (x, y, z) where this line passes through the plane of projection. A similar line from E_l to p would give the point $(x'y'z')$ where this line passes through the projection plane, this point (x', y', z') represents p as seen by the left eye.

In solid analytical geometry it is shown that for any point (x, y, z) on the line joining points (x_1, y_1, z_1) and (x_2, y_2, z_2), the values of x, y, y

satisfy the equation:

$$\frac{x - x_1}{x_2 - x_1} = \frac{y - y_1}{y_2 - y_1} = \frac{z - z_1}{z_2 - z_1} = r,$$

For the right eye (see Fig. 1)

$$\begin{array}{lll} x = D - d, & x_1 = p_1, & x_2 = D \\ y = H, & y_1 = p_2, & y_2 = e \\ z = V, & z_1 = p_3, & z_2 = 0. \end{array}$$

For the left eye y_2 becomes zero and H becomes H'. If we substitute $1-s$ in place of r (for later convenience) we now find:

$$s = \frac{d}{D - p_1} \tag{1}$$

$$H' = sp_2 \tag{2}$$

$$H = H' + e(1 - s) \tag{3}$$

or

$$H = H' + f$$

$$V = sp_3 \tag{4}$$

although $f = e(1-s)$ it will be read from a chart, Fig. 3, instead of being computed. In this chart f has been arbitrarily increased by 2 cms. to allow for the prism deviation of the stereoscopic viewer. We will assume that $D = 125$ cms., $d = 25$ cms. and $e = 6$ cms. Also we assume that the object viewed is in the upper near quadrant and that the values of p_1, p_2 and p_3 are between 0 and 10 cms. but the assumptions of this sentence can be violated a little.

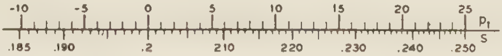

FIG. 2

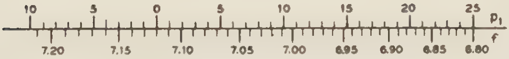

FIG. 3

If we consider the object being viewed as standing squarely in the corner at the origin the resulting projection will not be very pleasing. A very satisfactory result will follow, however, if the object is turned so that it is viewed at the clinographic angle. This "turning" can be accomplished if the coordinates p_1, p_2, p_3 are those computed for a clinographic projection.

Consider a rectangular coordinate system x, y, z associated with a crystal being drawn. Let z lie along the crystallographic c axis and x lie in the plane of a and c. If a vector R having components on the x, y, z axes of R_1, R_2, R_3, respectively, is written in matrix form as

$$(R)_x = \begin{bmatrix} R_1 \\ R_2 \\ R_3 \end{bmatrix}$$

then the components on a set of clinographic axes is given* by means of the matrix multiplication

$$(R)_c = K \begin{bmatrix} R_1 \\ R_2 \\ R_3 \end{bmatrix} \tag{5}$$

where

$$K = \begin{bmatrix} 18/\sqrt{370} & 6/\sqrt{370} & -1/\sqrt{37} \\ -1/\sqrt{10} & 3/\sqrt{10} & 0 \\ -3/\sqrt{370} & -1/\sqrt{370} & 6/\sqrt{37} \end{bmatrix} \tag{6}$$

or

$$K = \begin{bmatrix} .9358 & .3120 & .1644 \\ -.3162 & -.9487 & 0 \\ -.1560 & -.0520 & .9864 \end{bmatrix} \tag{6a}$$

The components of the vector R on the x, y, z system can be computed from its components on the a, b, c system by means of the matrix equation:

$$(R)_x = M(R)_a \tag{7}$$

where M is a matrix† peculiar to the crystal. Whence:

$$(R)_c = K(R)_x = KM(R)_a. \tag{8}$$

We now illustrate the foregoing by preparing a picture of cassiterite. For cassiterite $a:c = 1:0.6723$, hence the matrix M takes the value:

$$M' = \begin{bmatrix} 1 & 0 & 0 \\ 0 & 1 & 0 \\ 0 & 0 & .6723 \end{bmatrix}$$

---

* See Computation of Interfacial Angles, Interzonal Angles and Clinographic Projection by Matrix Methods: *Am. Mineral.*, **31,** 31–42 (1946).

† Computations of Interfacial Angles, etc., *Am. Mineral.*, **31,** 31–42 (1946).

tin atoms are at the points.**

$$\begin{bmatrix}0\\0\\0\end{bmatrix}_a, \begin{bmatrix}1\\0\\0\end{bmatrix}_a, \begin{bmatrix}0\\1\\0\end{bmatrix}_a, \begin{bmatrix}1\\1\\0\end{bmatrix}_a, \begin{bmatrix}0\\0\\1\end{bmatrix}_a, \begin{bmatrix}1\\0\\1\end{bmatrix}_a, \begin{bmatrix}0\\1\\1\end{bmatrix}_a, \begin{bmatrix}1\\1\\1\end{bmatrix}_a \text{ and } \begin{bmatrix}1/2\\1/2\\1/2\end{bmatrix}_a$$

while oxygen atoms are at the points

$$\begin{bmatrix}u\\u\\0\end{bmatrix}_a, \begin{bmatrix}1-u\\1-u\\0\end{bmatrix}_a, \begin{bmatrix}1/2-u\\1/2+u\\1/2\end{bmatrix}_a, \text{ and } \begin{bmatrix}1/2+u\\1/2-u\\1/2\end{bmatrix}_a$$

where $u=0.30$.

To compute the components of $(R)_c$ by equation (8a) we will need the product KM:

$$KM = \begin{bmatrix} .9358 & .3120 & .1644 \\ -.3162 & .9487 & 0 \\ -.1560 & -.0520 & .9864 \end{bmatrix} \begin{bmatrix} 1 & 0 & 0 \\ 0 & 1 & 0 \\ 0 & 0 & .6723 \end{bmatrix}$$

or

$$KM = \begin{bmatrix} .9358 & .3120 & .1105 \\ -.3162 & .9487 & 0 \\ -.1560 & -.0520 & .6632 \end{bmatrix}.$$

To avoid the further use of subscripts denoting the different axial systems we will henceforth refer to the vector from the origin to a point being represented as P if stated on the crystallographic axes a, b, c and p if stated on the clinographic axes. Hence the equation (8) becomes

$$p = KMP. \tag{8a}$$

If the cell is to be 10 cms. on a side we multiply all components on the a system by 10 so that, for the P corresponding to the point $\begin{pmatrix}1\\0\\0\end{pmatrix}_a$ we have

$$P = \begin{bmatrix}10\\0\\0\end{bmatrix}$$

whence

$$p = KMP = \begin{bmatrix}9.358\\-3.162\\-1.560\end{bmatrix}.$$

** Wyckoff, R. W. G., *The Structure of Crystals*, 2nd ed. p. 239, The Chemical Catalog Co.

Using $p_1 = 9.358$, reference to figures 2 and 3 give us:

$$\begin{aligned} s &= .2163 \\ f &= 7.015 \end{aligned}$$

Finally

$$\begin{aligned} H' &= sp_2 = -.684 \\ H &= H' + f = 6.331 \\ V &= sp_3 = -.337 \end{aligned}$$

The following tabular form is a considerable aid in keeping straight the mass of figures. It also helps in allowing all of one kind of computation to be finished before another kind is started. For instance all the p's were computed before any of the s's were determined, then all the s's were taken from Fig. 2, etc. Since hexagonal crystals are traditionally viewed differently than other crystals (i.e. 30° further around with respect to the a axis), we set up a special KM matrix for this case. We use

$$\begin{aligned} (KM)_h &= K \begin{pmatrix} 1/2\sqrt{3} & 0 & 0 \\ -1/2 & 1 & 0 \\ 0 & 0 & c \end{pmatrix} \\ &= \begin{pmatrix} .6544 & .3120 & .1644c \\ -.7482 & .9487 & 0 \\ -.10908 & -.0520 & .9864c \end{pmatrix} \end{aligned}$$

where c is the axial ratio. The procedure is the same as before and one will get values of H, H' and V as in the previous case.

If the points (H, V) and (H', V) are plotted on metric graph paper, the unit being a centimeter the resulting pictures are right for viewing in the old fashioned parlor stereoscope. Better results are achieved however, by one of two other methods. The easiest method is to plot the data on tracing paper on an enlarged scale, then photograph the drawings down to proper size, thus reducing the errors of drawing. The second method is to employ special methods of precision drawing.

PRECISION DRAWING METHOD

In the precision drawing method the data is plotted on a transparent plastic sheet laid over the graph paper. (Cellulose acetate 15 or 20 thousandths of an inch thick serves nicely.) The points (H, V) and (H', V) are plotted with a sharp pointed tool like a machinist's scriber, using a magnifying glass to reduce the errors. One should look at the scriber (which rests lightly on the plastic slide) studying its position from two different angles. When satisfied that the position is right the scriber is pressed into the plastic. We wish now to make a circle about the point, the size of the circle indicating the kind of atom the point represents. Ordinary dividers are not well suited to this purpose. They are too difficult to reset to the same size as before in case one has changed to another size. Also they are clumsy, if one wishes a circle of say 1/16″ diameter they slip and scar the sheet. A *circler* shown in Fig. 4 works well. It is a pin fitting nicely into a tube. The pin has an accurately centered conical point; the tube has a cutting lip. The tube is pushed up away from the point, the point is introduced into the hole, the pin forced firmly into the hole in an erect position, then with the other hand the tube is pushed down and rotated thus leaving a small ring engraved in the plastic. One needs several sizes of this tool.

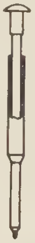

Fig. 4

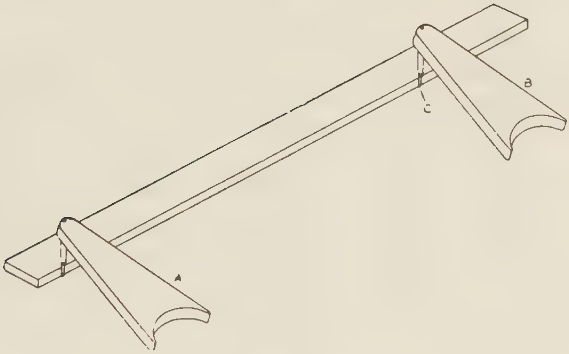

Fig. 5

Another difficulty is that of accurately joining points by lines. This difficulty is resolved by using two *joiners*, i.e. two special scribers with a support that holds them perpendicular to the table. These scribers, Fig. 5, have an accurately turned cylinder C near the point, the diameter of C is the same for both scribers of the pair, the conical point is true with the cylinder. A scriber is inserted in each of two holes that are to be joined, they are held down with a finger pressing at p on each, then a straight edge is pressed against both cylinders by pressure at the arrow, Fig. 5. When firm contact is made, the straight edge is held down, the near

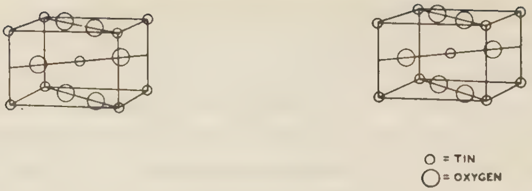

Fig. 6

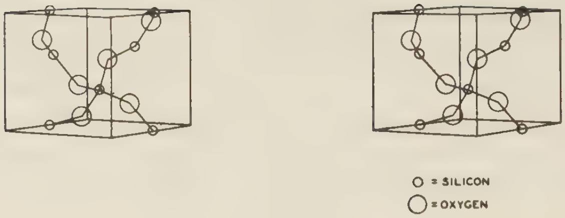

Fig. 7

S_n Atoms

P =	0	10	0	10	0	10	0	10	5
	0	0	10	10	0	0	10	10	5
	0	0	0	0	10	10	10	10	5
p =	0	9.358	3.120	12.478	1.105	10.465	4.225	13.583	6.791
	0	−3.162	9.487	6.325	0	−3.162	9.457	6.325	3.162
	0	−1.560	−.520	−2.080	6.632	5.072	6.112	4.552	2.276
s =	.200	.2163	.2051	.2222	.2018	.2183	.2071	.2242	.2114
f =	7.120	7.015	7.087	6.977	7.106	7.003	7.075	6.965	7.046
$H' = sp_2$	0	−.684	1.945	1.405	0	−.690	1.965	1.418	.668
$H = H' + f$	7.120	6.331	9.032	8.382	7.108	6.313	9.040	8.383	7.714
$V = sp_3$	0	−.337	−.107	−.462	1.337	1.107	1.265	1.022	.480

O Atoms

3	7	2	8	3	7
3	7	8	2	3	7
0	0	5	5	10	10
3.743	8.735	4.920	8.663	4.848	9.840
1.898	4.428	6.959	− .632	1.900	4.428
−.624	−1.456	2.588	+1.964	6.008	5.176
.2062	.2150	.2081	.2150	.208	.217
7.080	7.024	7.067	7.024	7.068	7.011
.392	.952	1.448	− .136	.395	.961
7.472	7.976	8.515	6.888	7.463	7.972
−.129	− .313	.539	.422	1.250	1.123

scriber is removed and the far one moved towards the operator, scratching as it goes, until it falls in the second hole.

With two of these devices one can draw the views quite accurately, locating each point to within 2 or 3 thousandths of an inch. In making stereo views a mistake may occur, such as misplotting a point. The best procedure is to finish the drawings, view the pair in the stereo viewer and mark all the points that seem to float in space or fail to blend. The slide is then replaced over the graph paper and the points in error are checked for correspondence with the entries in the data table. If the positions correspond with the tables, the data are of course recomputed. The correct data is conspicuously written on the slide and a new piece of plastic is fastened over the old slide. Using the magnifier a new slide is copied from the old making the corrections. Before unclamping the new slide slip a piece of white paper between the two slides and view by reflected light to make sure that there are no omissions.

Figures (6) and (7) show cassiterite and quartz drawn by the precision method.

GRAVITY-SEPARATION IN POWDER MOUNTS AS AN AID TO THE PETROGRAPHER

Wilfrid R. Foster, *Champion Spark Plug Company, Ceramic Division, Detroit, Michigan.*

Abstract

Attention is called to the tendency on the part of refractive index liquids to cause gravity-separation in immersion mounts of mineral mixtures. By the proper choice of liquids, this tendency can be accentuated and used to advantage in the routine petrographic examination of a number of raw and processed minerals. A satisfactory procedure for this purpose is outlined, and suitable media are described. The value of the method is illustrated by a number of a typical examples of its application.

Introduction

The use of refractive index liquids for the determination of the specific gravities of minerals under the microscope has been advocated by Rogers (7), Meen (5) and Jahns (2). The phenomenon of gravity settling in index oils can also be used with considerable profit in the microscopic analysis of mineral mixtures. Many petrographers probably do not realize the tendency of index oils to effect segregations in mounts of polymineralic powders, and, therefore, sometimes fail to detect certain constituents present in small amounts. Once recognized, however, this behavior proves to be an advantage rather than a disadvantage. There are numerous instances in which a pair of minerals that are practically indistinguishable through their principal optical properties can thus be differentiated on the basis of specific gravity differences.

Procedure

The technique involved need be no more elaborate than the preparation of an ordinary powder mount. The use of a naked mount without benefit of cover-slip, as practiced by Rogers (7), is not recommended. Meen (5) employed a covered mount and observed the behavior of the smallest of the particles. This method is quite satisfactory. It may be found preferable, however, to insure that the depth of the film of immersion oil be several times greater than the diameter of even the larger grains. This may be accomplished by adding to the fine-grained powder a few coarser sand grains in order to prop up the cover-slip. Satisfactory results may also be obtained by the use of "hanging-drop" or "deep-well" slides, but the depressions in these are unnecessarily large and deep and require rather large amounts of liquid.

A method which has been found very convenient involves the use of a simple and easily constructed slide. Two strips about three-eighths inches in width are cut from the ends of a 26×46 millimeter slide. These are cemented along the sides of the upper surface of a second slide by means of "water-glass." They are then ground down to about one-fourth or one-fifth of their original thickness. This provides a shallow trough down the center of the slide about one inch in length, one-quarter inch in width, and about 200 to 250 microns in depth. Cover-slips obtained by quartering five-eighths inch square cover-glasses will just bridge the trough (Fig. 1).

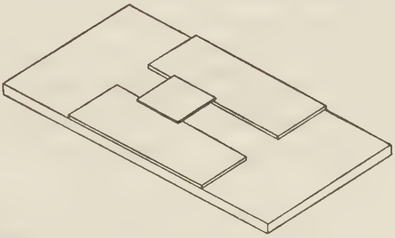

Fig. 1

A drop of the desired immersion liquid is placed in the trough, a pinch of the mineral powder added and stirred, a cover-slip dropped on, and, if necessary, a second drop of liquid placed so as to creep under the cover-slip and expel the remaining air. By a mere change of focus of the microscope objective, one can readily differentiate between grains which lie on the bottom of the trough and those which float just beneath the cover-slip. If the "floats" should be found to mask the underlying "sinks" too completely, the slide should be slightly tilted on end and the cover-slip carefully moved a short distance towards the raised end of the trough. The lighter minerals will tend to follow this movement, whereas the heavier constituents will lag behind.

Suitable Media

In general, liquids of low indices of refraction also have low specific gravities, and liquids of high indices have high specific gravities. Consequently, any blended series of index media covering a considerable range of indices will serve also as a ready-made series of specific gravity standards. The more satisfactory liquids for this purpose exhibit a small change of specific gravity for the smallest measurable increment of refractive index. This feature permits close calibration of specific gravity through measurement of the refractive index, as practiced by Jahns (2), Meen (5) and Merwin (6). Curves showing the relationship between refractive indices and specific gravities for a number of commonly used liquid series are presented in Fig. 2. It will be seen that mixtures of the halogenated naphthalenes and methylene iodide are less suitable than Clerici, Klein, Thoulet, or Rohrbach solutions. The former, however, are available in many petrographic laboratories and can be used to effect many desired segregations in mounts of powdered mineral mixtures.

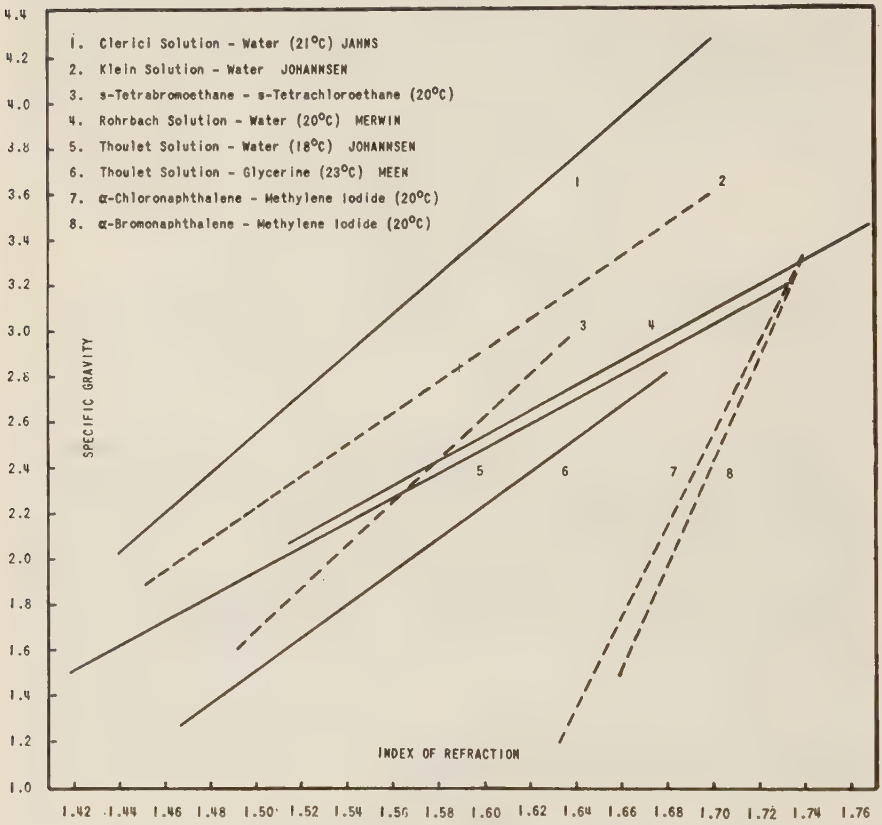

FIG. 2. Relation between specific gravity and refractive indices for various liquid-mixtures. Solid Lines: Plotted from data of previous workers as indicated. Broken Lines: Plotted by interpolation of data for pure end-members, taken largely from Lange (4).

There are instances in which it is profitable to employ a liquid combining a certain specific gravity with a certain refractive index. Thus, in complex mineral mixtures it may be desirable approximately to match the indices of a particular constituent while at the same time bringing about gravity separation. It has been found possible by judicious choice of liquids, either singly or in appropriate mixtures, to obtain almost any desired combination of refractive index and specific gravity. For such purposes, the extensive data given by Lange (4) will prove helpful.

Typical Applications

In the routine examination of refractories by the immersion method, alpha-alumina (corundum) in small amounts can easily be overlooked if one fails to take cognizance of the gravity-separating action of methylene iodide-rich immersion liquids. Even in the shallow depth of the usual microscope mount the tiny alumina grains, resting directly on the slide, will be out of focus with the bulk of the powder and thus escape detection. Careful focussing on the lowermost level of the mount in effect screens out the predominant lighter constituents so that the alumina can be readily recognized. The presence of small quantities of corundum in rock-powders is also more readily confirmed by the use of this procedure.

In special porcelains containing beryllia (bromellite) and magnesia (periclase) or magnesium aluminate (spinel) small amounts of the latter two constituents are difficult to detect. The refractive indices of all three of these crystalline phases are quite close and in aggregate-grains the trace of magnesia or spinel may go unnoticed. However, in a liquid (S.G. = 3.2) which approximately matches the indices, any free grains of magnesia (S.G. = 3.6) or spinel (S.G. = 3.6) will assume a lower level in the mount than will the beryllia (S.G. = 3.0). Careful search of the bottom level of the immersion mount will reveal the isotropic magnesia or spinel. In like manner the presence of chrysoberyl (S.G. = 3.7) in beryllia bodies can be established, notwithstanding the fact that the two compounds are very similar in refractive indices and birefringence.

During an investigation of the impurities in a grab sample of brucite from Luning, Nevada, powder from a supposed crust of hydromagnesite (S.G. = 2.18) was being checked microscopically in a certain index liquid (S.G. = 2.15). As was anticipated, the irregular fragments of hydromagnesite rested on the bottom of the mount. Unexpectedly, however, there also appeared some floating laths and needles, suggesting a different and lighter mineral. Further work led to its identification as the rare mineral artinite (S.G. = 2.03), hitherto unreported from any American locality except Hoboken, New Jersey. It is interesting to note that the mean indices of hydromagnesite and artinite are very close. Had there been no gravity separation, the artinite needles would undoubtedly have been dismissed as fibrous grains of hydromagnesite. It had been intended to report this occurrence in a separate paper until inquiries revealed that the recent paper of Hurlbut (1) was already in press.

The advantages of this technique in more successfully studying certain of the impurities in commercial brucite have been suggested in the preceding paragraph. Thus hydromagnesite (S.G. = 2.18), artinite (S.G. = 2.03), and hydrotalcite (S.G. = 2.06) have decidedly lower specific gravities that brucite (S.G. = 2.4). Similar benefit may be derived in the examination of samples of some of the common hydrated magnesium silicates. The presence of brucite in chlorite (S.G. = 2.7), talc (S.G. = 2.7) or serpentine (S.G. = 2.6) might be easily overlooked because of the nearness of its indices to those of these three common associates. But the use of methylene bromide (S.G. = 2.5) as an immersion liquid will cause the lighter brucite to segregate in the upper level of the mount.

An andalusite-diaspore "ore" employed in the manufacture of spark plug insulators is checked petrographically to insure uniformity in the composition of successive shipments. A preliminary estimate of the subordinate pyrophyllite and muscovite is obtained from an ordinary powder mount. If these lighter constituents are then floated by using s-tetrabromoethane (S.G. = 2.96) as the immersion medium, the determination of the relative proportions of the two heavier and predominant constituents, andalusite and diaspore, is considerably facilitated. It so happens that the immersion oil almost matches the andalusite grains, but is distinctly lower in indices than the diaspore.

The minerals andalusite (S.G. = 3.15) and barite (S.G. = 4.5) are particularly difficult to distinguish optically when both are present in the same mixture. Examples of natural occurrences in which these two minerals occur together are an andalusite-corundum "ore" from Mono County, California, and a dumortierite-andalusite "ore" from Oreana, Nevada. The usual microscopic examination of these materials invariably failed to reveal the presence of the less abundant barite, although subsequent chemical analyses indicated an appreciable barium oxide content. The use of methylene iodide (S.G. = 3.3) solved the difficulty by floating the andalusite and leaving the heavier barite at the bottom of the mount. Low-fluorine topaz (S.G. = 3.5) is another mineral that is very easily confused optically with andalusite. Topaz is a fairly common associate of the sillimanite minerals and thus may accompany andalusite, yet stand little chance of detection in the mixture. Gravity separation in methylene iodide will aid in its recognition.

The presence of black opaque flakes in a rock-powder often poses the problem as to whether these represent carbonaceous material or a metallic mineral. A simple gravity-settling test will indicate whether it is the relatively light carbonaceous matter or a heavy metallic compound. Disseminated graphite may be distinguished from molybdenite in this manner. The special slide, previously described, is also suitable for testing the possible magnetism of black opaque grains. A strong horse-shoe magnet lying flat on the stage of the microscope is moved to and fro alongside the slide. Any magnetic grains are free to rotate, unhampered by the overlying cover-slip, as the magnet is moved.

That the specific gravity of a mineral can be accurately determined on the stage of the microscope by the use of index liquids has been ably demonstrated by Jahns (2) and Meen (5). It should be pointed out, however, that prior isolation of the mineral is not at all necessary. The specific gravity of a mineral can be just as accurately measured in a mixture, providing that its optical properties are sufficiently characteristic to distinguish it from its associates. Should the sample at hand be that of a pure mineral, it may be found helpful to add a tiny bit of fine-grained corundum (S.G. = 4.0) or other heavy mineral to the powder mount during the preparation of the latter. It is then an easy matter to determine whether the mineral under investigation is at the same level as the corundum or at the higher level just beneath the cover-slip.

No attempt has been made to consider all of the possible applications of gravity settling in the microscopic examination of powdered mineral mixtures. Only those cases encountered in the routine analysis of certain ceramic raw materials and products have been discussed. If one may fairly judge from the data given in the mineralogical literature, the following pairs of minerals having closely similar optical properties should also lend themselves readily to differentiation by this procedure: crestmoreite (S.G. = 2.2) and riversideite (S.G. = 2.64); fluorite (S.G. = 3.18) and yttrocerite (S.G. = 3.36); dolomite (S.G. = 2.87) and aragonite (S.G. = 2.94); colemanite (S.G. = 2.42) and howlite (S.G. = 2.58); ulexite (S.G. = 1.65) and inyoite (S.G. = 1.87); kurnakovite (S.G. = 1.85) and inderborite (S.G. = 1.93). Doubtless many other instances could be found among both minerals and inorganic chemicals.

REFERENCES

(1) HURLBUT, C. S. (1946), Artinite from Luning, Nevada: *Am. Mineral.*, **31**, 365–369.

(2) JAHNS, R. H. (1939), Clerici solution for the specific gravity determination of small mineral grains: *Am. Mineral.*, **24**, 116–122.

(3) JOHANNSEN, A. (1918), *Manual of Petrographic Methods* (McGraw-Hill Book Co., Inc. New York, N. Y.), pp. 250, 255.

(4) LANGE, N. A. (1944), Index or refraction-liquids: *Handbook of Chemistry*, 5th Edition (Handbook Publishers, Inc., Sandusky, Ohio), pp. 932–1026.

(5) MEEN, V. B. (1933), Determination of specific gravity of minerals by use of index liquids: *Univ. Toronto Stud.*, Geol. Series, No. **35**, 47–50.

(6) MERWIN, H. E. (1911), A method of determining the density of minerals by means of Rohrbach's solution having a standard refractive index: *Am. Jour. Sci.*, 4th ser., **32**, 425–428.

(7) ROGERS, A. F. (1906), The determination of minerals in crushed fragments by means of the polarizing microscope: *School of Mines Quarterly*, **25**, 340–359.

NOTES AND NEWS

SULFIDE REPLACEMENTS OF A TRIGONOCARPUS FOSSIL FERN FRUIT

W. D. Keller, *University of Missouri, Columbia, Missouri.*

An uncommon replacement, practically complete, of fossil fern fruit by galena, sphalerite, and pyrite, with dickite and kaolinite in the cracks, is here described. The occurrence of the Trigonocarpus fossils from another of the few localities in Missouri is likewise placed on record.[1]

The fossil fruits, which have been popularly called "petrified pecan nuts" because of their superficial resemblance to modern pecans, were given to the writer about 10 years ago by Mr. James Myers, of near Eldon, Missouri. They were collected from the old McClure's coal bank,[2] S.E. $\frac{1}{4}$, Sec. 12, T. 41 N., R. 16 W. which was temporarily reopened during the depression following World War I. Nothing is known of their occurrence except that they were recovered during the mining operation.

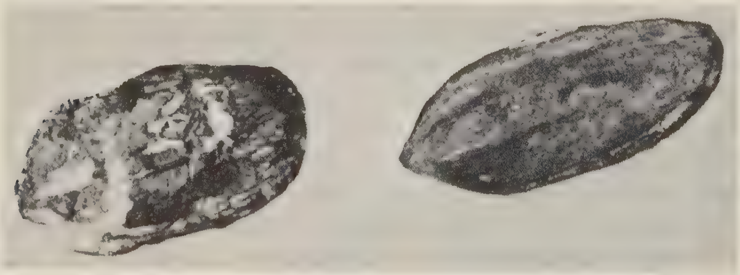

Fig. 1. Trigonocarpus fern fruit replaced by sulfides, with dickite and kaolinite along the cracks. Approximately natural size.

Two of the fruits are shown in Fig. 1. They are 3.5 to 4 cm. long, about 2 cm. wide, and about 1.5 cm. thick, but their slightly flattened shape may be due to squeezing after deposition.

Three nearly equal divisions or partitions which run lengthwise in the fruit are joined along depressed contacts which end in little ridges at the fruit ends. Faint longitudinal lines run along the shells parallel to the partitions.

---

[1] Previously mentioned in, A preliminary catalogue of the fossils occurring in Missouri, G. Hambach: *Bull.* **1**, *Missouri Geological Survey*, 85 (1890).

Fossil flora of the lower coal measures of Missouri, David White: *U. S. Geological Survey*, Monograph No. **37**, 280 (1899).

[2] Geology of Miller County, Sydney H. Ball and A. F. Smith: *Missouri Bureau of Geology and Mines*, vol. **1**, 2nd sec., 153 (1903).

Little or no carbon, or other organic material remains. Perhaps as much as 95 per cent of the fruit specimen has been replaced by galena which shows its characteristic luster and cleavage in the one specimen that is broken at the end. Covering the galena, apparently as a more or less continuous shell or peeling about ½ mm. in thickness, lies resinous sphalerite. This is coated irregularly with a very thin film of brassy pyrite.[3]

Cracks which were opened along divisions in the fruit, or along cleavages in the galena are filled with glistening white clay flakes. The clay flakes have indices of refraction falling within the kaolin group, and most of them, but not all, are euhedral and hexagonal in outline, which suggests they are dickite rather than kaolinite. Some books showed across the cleavages a biaxial positive interference figure which is also characteristic of dickite, but none was found which showed an extinction angle more than 5°—negative evidence for dickite. An x-ray diffraction pattern of the clay was generously run by Professor O. R. Grawe[3] who reported:

> In some respects our diffraction pattern closely resembles that of dickite, in others that of kaolinite. The results would suggest that both minerals are present.

Subsequently, an electron diffraction photograph made of the Trigonocarpus clay was compared with those of known dickite and kaolinite and found to substantiate Grawe's report that a mixture of dickite and kaolinite was present. The association of dickite with sulfides is interesting in view of other Missouri occurrences.

Tarr[4] found dickite in southeastern Missouri associated with galena in the Ordovician Bonneterre dolomite, and Tarr and Keller[5] found dickite associated with chalcopyrite, galena, pyrite, and millerite in chert in Mississippian Burlington limestone in Missouri. Allen[6] reported dickite in a chert geode from St. Louis County. Grohskopf[7] and Hundhausen found dickite in nine Cambrian and Ordovician formations in Perry County, where it (dickite) was intergrown with pyrite, and associated with sphalerite and galena.

Tarr interpreted the occurrence of dickite as indicative of hydrothermal solutions which brought in the sulfides, and Allen accepted a hydrothermal origin for it, thus affording "evidence . . . that hydrothermal solutions reached east central Missouri during post-Mississippian time." Because the Trigonocarpus fossils are Pennsylvanian in age, the sulfides and dickite of Miller County must be Pennsylvanian or later in age, which is in accord with Allen's dating. The rather widespread association of dickite and sulfides across Missouri implies some interesting academic and possibly economic geological possibilities.

---

[3] Determination by x-ray diffraction, O. R. Grawe: personal communication (December, 1946).

[4] Origin of the southeastern Missouri lead deposits, W. A. Tarr: *Econ. Geol.*, **7**, 749 (1936).

[5] Dickite in Missouri: *Am. Mineral.*, **21**, 109–114 (1936).

[6] Dickite from St. Louis County, Missouri, Victor T. Allen: *Am. Mineral.*, **21**, 457–459 (1936).

[7] Occurrence of dickite and fluorite in the Cambrian and Ordovician of Perry County, Missouri, J. G. Grohskopf and Mary Hundhausen: Appendix III, 59th Annual Report, *Missouri Geological Survey and Water Resources*, 3–13 (1937).

Kaolinite which resembles superficially the clean, white Trigonocarpus clay has been reported[8] as a deposit from solution in several Missouri localities, but the temperature of its origin is not certain. The writer would like to raise this question about a hydrothermal interpretation of the origin of dickite occurring in otherwise unaltered sediments: is it reasonable that sedimentary rocks which are fairly deeply buried may be heated high enough by conduction in establishing a normal geothermal gradient so that dickite is deposited in them instead of, or along with kaolinite? Water in them might be warm (hydrothermal?) over a wide area without necessarily emanating from a magma which otherwise would have to be postulated as being disturbingly widespread.

The writer is indebted to Professor Ralph W. Chaney for identification of the fossil fern fruit and comments on it. He wrote (July 16, 1945):

> The specimens represent fruits of the Pennsylvanian genus Trigonocarpus. This is a seed fern whose stem equivalent is Medullosa and whose equivalent foliage genus is Alethopteris. These fruits are of fairly common occurrence in Pennsylvanian rocks throughout the northern hemisphere. I have never before seen any partly replaced with metals.

Only one other fossil was reported from the McClure coal bank: (zinc) "blende was found, upon the exterior of which is a perfect imprint of a fern."[9]

---

[8] Some occurrences of kaolinite deposited from solution, W. A. Tarr and W. D. Keller: *Am. Mineral.*, **22**, 933 (1937).

[9] Ref. No. 2, p. 180.

CHLORITOID AT KALGOORLIE

Rex T. Prider, *Department of Geology, University of Western Australia, Nedlands, Western Australia.*

Introduction

Gustafson (1) has recently noted the occurrence of chloritoid at Porcupine and Kalgoorlie. He considers the chloritoid at these two localities to be of hydrothermal origin and therefore that it is necessary to revise the general opinion that chloritoid is a stress mineral. My studies of the chloritoid-bearing rocks of Kalgoorlie indicate, however, that the development of chloritoid, although due to hydrothermal alteration of the greenstones, is only an indirect product of this alteration, viz. that hydrothermal changes in these basic igneous rocks has produced a suitable environment in which chloritoid has subsequently developed under conditions of stress metamorphism. Moreover since Gustafson does not give any details regarding the Kalgoorlie occurrence, some of my observations of the areal extent of the chloritoid-bearing greenstones may be of interest.

Occurrence

Simpson and Gibson (3, pp. 142–143) first noted the occurrence of chloritoid at Kalgoorlie and Simpson (2, pp. 27–30) subsequently published a detailed description with chemical analyses both of the chloritoid and the enclosing rock. Stillwell (4) has contributed nothing further regarding the occurrence of the chloritoid but indicates the locality where it had been found on his geological map. Up to this time (1929) the only known locality was a shaft at the north-east corner of the Lake View townsite (Fig. 1). In 1932–33 five boreholes were drilled in the area to the south of the Trafalgar railway station (Fig. 1) by the South Kalgurli Consolidated, Ltd., by whom I was, at that time, employed. These boreholes disclosed a wide belt of quartz doleriate greenstone containing abundant chloritoid. The chloritoid-bearing zone is at least 800 feet wide and extends at least 50 chains along the strike. Summarized logs of these boreholes, the locations of which are shown in Fig. 1, are as follows:

Bore No. 1. Depression 45°; depth 600 feet.

The only rock type encountered was slightly bleached quartz dolerite greenstone* containing chloritoid throughout. The presence of chloritoid in these rocks is not very evident in the hand specimen but the microscope reveals its presence throughout the whole borehole.

---

* Nomenclature of the greenstones is that used by F. L. Stillwell: *Geol. Surv. West. Aust., Bull.* **94.**

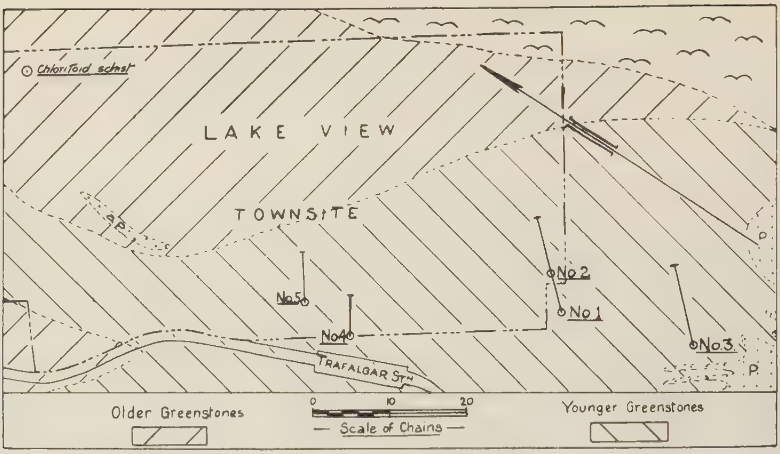

FIG. 1. Geological map of the vicinity of Lake View townsite, Kalgoorlie (taken from F. L. Stillwell's map published with *Geol. Surv. West. Aust., Bull.* **94**) showing location of boreholes. Dotted areas are the porphyrites (P = porphyrite; aP = albite porphyry) and flying birds sign is superficial alluvium.

Bore No. 2. Depression 45°; depth 500 feet.

The only rock type represented is a highly bleached (ankeritized) and sheared quartz dolerite greenstone with abundant chloritoid giving the rock a spotted appearance. Between depths of 374 and 448 feet, and also 488 and 500 feet, the rock was a fine-grained silky-lustred schist (? calc schist of the Older Greenstone Series) with spotted appearance due to the development of abundant chloritoid porphyroblasts averaging 1 mm. diameter.

Bore No. 3.† Depression 45°; depth 905 feet.

The three specimens (from 190′, 746′ and 905′) available from this borehole are all somewhat sheared and ankeritized quartz dolerite greenstones containing chloritoid. In the first two specimens the chloritoid is rather sparsely developed while in that from 905′ it is abundant.

Bore No. 4. Depression 45°.

The three specimens (from 181′, 363′ and 400′) available from this bore are all highly ankeritized quartz dolerite greenstones. The first two contain no chloritoid and that from 400′ very rare chloritoid.

Bore No. 5. Depression 45°; depth 620 feet.

To a depth of 210 feet the rock was a bleached and sheared quartz dolerite greenstone without chloritoid; from 210 to 290 feet it was quartz dolerite greenstone with rare chloritoid; from 290 to 440 feet it was a silky lustred schist (? calc schist of Older Greenstone Series) with abundant chloritoid; from 440 to 570 feet it was albite porphyry (?) with occasional chloritoid and fairly abundant microscopic needles of tourmaline; from 570 to 620 feet a schist similar to that between 290 and 440 feet was encountered.

These bore-logs indicate therefore that chloritoid is developed in the various metasomatized rocks of the Kalgoorlie Series—in the Older Greenstones (calc schists which are ankeritized basic lavas), in the intrusive Younger Greenstones (quartz dolerite greenstones), and in the still younger albite porphyries—over a band at least 800 feet wide (the eastern margin of this chloritoid-bearing band was not encountered in any borehole). Simpson (2, p. 28) considers that all the chloritoid-bearing rocks which he examined from the shaft at the north-east corner of the Lake View townsite were variants of the intrusive quartz dolerite (Younger Greenstones). By courtesy of the Government Geologist of Western Australia (Mr. H. A. Ellis) and the Government Mineralogist (Mr. H. Bowley) I have been able to re-examine Simpson's specimens and find that they are all calc schists of the Older Greenstone Series. The occurrences disclosed by the five bores described above are, therefore, the first record of chloritoid in the intrusive quartz dolerite group of rocks. That these rocks undoubtedly belong to the quartz dolerite greenstones will be evident from Fig. 2 in which, in spite of the extensive metasomatism, the original ophitic texture can be readily discerned, as can the large skeletal plates of leucoxenized ilmenite which are such a characteristic feature of the quartz dolerite greenstones.

---

† Boreholes 3, 4, and 5 were drilled subsequently to my departure from Kalgoorlie. I am indebted to Mr. H. B. Newman, Underground Manager of South Kalgurli Cons. Ltd., for specimens from these bores.

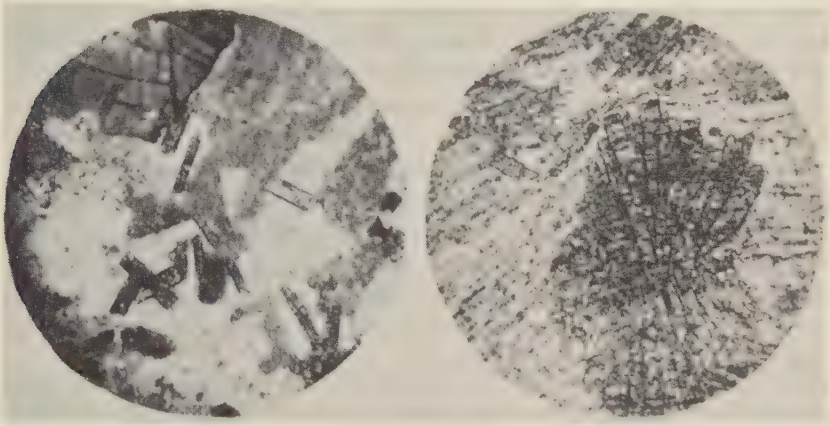

2 3

FIG. 2. Photomicrograph of bleached quartz dolerite greenstone showing chloritoid (high relief) confined to sericitic areas (colorless) after feldspar. The greyish cloudy material is an aggregate of chlorite and ankerite after original ferromagnesian minerals. A large plate of leucoxenized ilmenite is visible. Photo taken in transmitted light with some reflected light to show up the skeletal ilmenite. ×30. (*Photo. by H. J. Smith*).

FIG. 3. Photomicrograph of sheaf-like bundles of chloritoid prisms in highly sheared quartz dolerite greenstone, showing schistosity passing through the chloritoid and slight distortion of the schistosity by growing chloritoid. ×40. (*Photo by H. J. Smith*).

The manner in which the chloritoid occurs in these quartz dolerite greenstones is shown in Figs. 2 and 3. Figure 2 shows the occurrence of isolated porphyroblasts of chloritoid in an unsheared but highly metasomatized quartz dolerite greenstone. A significant feature of this rock is that the chloritoid is confined to the sericitic aggregates which are pseudomorphous after the original feldspar and do not occur in the darker-colored chlorite-ankerite aggregates which represent the original ferromagnesian minerals. The sericitic environment in which the chloritoid is here developed does not differ much from a sericitic phyllite, the normal rock in which chloritoid is commonly developed (5). Figure 3 illustrates the manner in which the chloritoid is developed in the more highly schistose rocks. Here it occurs in sheaf-like bundles scattered uniformly throughout the rock which is a carbonate sericite schist. The schistosity passes through the later developed chloritoid porphyroblasts and is somewhat distorted by the growing chloritoid prisms—the late development of the chloritoid is here very evident.

In both of the rocks illustrated the chloritoid has developed in a sericitic environment similar in character to a sericite phyllite. The analyses of the chloritoid-bearing calc schists given by Simpson (2, p. 28) show that these rocks are rich in alumina and ferrous oxide and comparatively poor in lime and magnesia, most of which, in any case, is in the form of ankerite. This alumina-rich and lime-poor environment is the one in which chloritoid normally develops (5, p. 317).

Conclusions

Chloritoid is developed at Kalgoorlie in both the Older and Younger Greenstone Series over a considerable area. Its development is the result of metasomatism of basic igneous rocks yielding a favorable alumina-rich and lime-poor environment in which it has been developed by low-grade dynamothermal metamorphism subsequent to the main shearing movements and hydrothermal alteration to which the rocks of the Golden Mile have been subjected. Its development is due to stress and the part that hydrothermal changes have played is not in the introduction of the chloritoid but rather in producing a suitable medium in which it could develop.

References

1. Gustafson, J. K. (1946), Two occurrences of chloritoid as a hydrothermal mineral in igneous rocks: *Am. Mineral.*, **31,** 313–316.
2. Simpson, E. S. (1930), Contributions to the Mineralogy of Western Australia, Series V: *Jour. Roy. Soc. West. Aust.*, **16,** 25–40.
3. Simpson, E. S., and Gibson, C. G. (1912), The geology and ore deposits of Kalgoorlie, Part I: *Geol. Surv. West. Aust., Bull.* **42.**
4. Stillwell, F. L. (1929), Geology and ore deposits of the Boulder Belt, Kalgoorlie: *Geol. Surv. West. Aust., Bull.* **94.**
5. Tilley, C. E. (1925), Petrographical notes on some chloritoid rocks: *Geol. Mag.*, **62,** 309–319.

THE USE OF THOULET'S SOLUTION FOR HEAVY MINERAL SEPARATION

Judith Weiss, *Bryn Mawr College, Bryn Mawr, Pennsylvania.*

Preparation and Separation

(a) Preparation of the Rock Specimen.

The rock was broken into bits about $\frac{1}{4}'' \times \frac{1}{4}'' \times \frac{1}{4}''$ in size, and crushed in a porcelain mortar. The grains were run though a series of sieves so that the final grain size was between .125 and .250 mm. This size was chosen because it was about that of the smaller grains in the thin sections of the same rocks.

(b) Preparation of the Solution.

The solution was prepared by adding distilled water to mercuric iodide powder and potassium iodide crystals in a porcelain evaporating dish in the following proportions:

mercuric iodide	seven parts
potassium iodide	six parts
water	two parts

Eighty-seven grams of mercuric iodide, seventy-five grams of potassium iodide and twenty-seven ml. of water made about fifty ml. of solution. The resulting solution was evaporated over a steam bath until a thin crystalline film began to form over the surface of the liquid, or until a small fragment of pure fluorite (specific gravity = 3.18) just began to rise from the bottom of the evaporating dish. The solution was filtered and its specific gravity checked with a pycknometer. If the specific gravity was too low, a little more mercuric iodide was added to the solution, together with a little hot water, and a re-evaporation was carried out as described above. About two ml. of mercury were kept in the evaporating dish during the process, in order to prevent the separation of free iodine. The maximum specific gravity for the solution (and this should be checked on cold solution, because the specific gravity of the warm solution is somewhat lower) is 3.19, but it was found desirable to use the solution a little below its saturation point, with the specific gravity about 3.15 or 3.16. The solution is a clear, light yellow color.

(c) Technique in Separation

About thirty-five ml. of solution were placed in a separatory funnel and a one gram sample of ground rock was added. The mixture was stirred three or four times, at one minute intervals. When the separation was distinctly clean the heavy portion was drawn off into a funnel containing rapid filtering paper. The filtered solution was caught in a beaker and returned to the bottle of fresh solution. (The solution must be kept in a brown glass bottle with a glass stopper and a few ml. of mercury should be kept in the bottle to prevent the separation of free iodine.) The mineral grains in the filter paper were washed with hot ten per cent potassium iodide solution, these washings being saved for later recovery of the solution. The mineral grains were then washed with hot, distilled water until no yellow color was left on the filter paper. A final washing was made with acetone to aid in drying the grains. The light fraction was drawn off into a funnel large enough to receive all of the solution. This eliminated the necessity for opening and closing the stop-cock of the separatory funnel several times, and thus prevented the scratching or clogging of the stop-cock by the mineral grains. The filtering of this second fraction took about ten to fifteen minutes and it was found helpful to use a hot-water funnel. This inhibited somewhat the crystallization of the solution on the filter paper. The separatory funnel was washed down with hot potassium iodide solution, and the grains were collected with the rest of the light fraction. Further washing and drying were carried out as described above.

Advantages of the Solution

The specific gravity of from 3.12 to 3.16 will keep biotite in mica-rich rocks in the light fraction of the separation. The fairly low viscosity of the fresh solution and its lack of convection currents make a rapid and clean separation possible. It is not volatile and, therefore, gives off no unpleasant fumes. If the rocks are crushed and ready for sampling before the preparation of the solution, about twenty to twenty-five separations may be run through with fifty ml. of solution. Only about one-half to one ml. of solution is lost, but collected in the washings, with each separation.

Disadvantages of the Solution

After continued use the solution becomes more viscous and crystallizes on the filter paper during filtering, thus slowing up the process considerably and causing greater loss of fresh solution with each separation. The use of a hot-water funnel will help some, but after several weeks of use, or even after standing in the bottle for several weeks, the solution begins to deteriorate. The apparatus must be all glass or porcelain since the solution is very corrosive and will attack rubber or metal. It causes bad burns if it touches the skin. Considering the solution expendable, a separation costs about five or six cents. A pound of mercuric iodide plus a pound of potassium iodide costs about $7.50 and yields about three hundred ml. of solution, from which one hundred and twenty-five to one hundred and fifty separations can be made.

Method of Recovery*

The cost of separation may be reduced somewhat by partial recovery of the solution. The following method was tried and found to recover about one-half of the solution.

The used solution is added to the washings. An excess of potassium iodide is thus introduced from the washings. This is desirable since the mercuric iodide will crystallize first out of solution unless the potassium iodide is present in slight excess of the stoichiometric proportions of the double salt. With evaporation, this double salt will be the first to crystallize out. When the solution is evaporated about half-way to dryness and permitted to cool, these crystals may be collected, the liquid being drawn off by suction. The dry crystals are re-dissolved with hot distilled water and the liquid is evaporated as in the original preparation. The resulting solution will have the correct specific gravity since it is made of the pure double salt. The purpose for evaporating only half-way to dryness is to keep the excess potassium iodide in solution. If this should crystallize out and be dissolved along wih the double salt, then the resulting solution will have too low a specific gravity.

* Procedure suggested by A. Rosenzweig, Department of Geology, Bryn Mawr College, Bryn Mawr, Pennsylvania.

THE SUPERABUNDANT INDEX IN THE HEXAGONAL BRAVAIS SYMBOL

J. D. H. Donnay, *The Johns Hopkins University, Baltimore 18, Maryland.*

Every crystallographer knows that, in the hexagonal four-index symbol referred to the Bravais axes, the sum of the first three indices is zero. This is why one of these indices, usually the third one, is often omitted altogether and replaced by a period. The general form is then symbolized $\{hk.l\}$. The period stands for $-(h+k)$.

Example: $\{21.4\}=\{21\bar{3}4\}$.

The purpose of the four-index symbol, however, is to bring out the symmetry of the form, by the permutations of the first three indices. Leaving out one of the three defeats the very purpose of the notation. The third index should, therefore, be explicitly written. Some authors represent it by the letter i, others by the same letter i surmounted by a negative sign ($\bar{i}$). This has been a source of misunderstanding.[1]

---

[1] Pabst, A., *Am. Mineral.*, **32,** 16–30 (1947). Professor Pabst now states (priv. comm.) that he would like to amend his text by deleting lines 15–16 and footnote 5, on page 21. His criteria are written for the general form $\{hkil\}$.

If the symbol is written $\{hkil\}$, then obviously $i=-(h+k)$. If, however, the symbol $\{hk\bar{i}l\}$ is used, then $i=h+k$. In the example given above, $\{21\bar{3}4\}$, authors of the first school will say that $i=\bar{3}$, the others will take $i=3$.

There is an advantage in using the minus sign over the i in the symbol $\{hk\bar{i}l\}$ because the form is symbolized by a face that has its first two indices positive, so that the third index is always negative. (The symbol of the form is, of course, spoken thus: "h, k, minus i, l.") This procedure has been adopted by A. F. Rogers in his first edition.[2] The same principle was followed by Kraus,[3] who used $\{hi\bar{k}l\}$, with $k=h+i$. This notation has been retained in Kraus, Hunt and Ramsdell.[4]

Lately (and here is where the trouble comes from), printers have omitted the dot over the i wherever the i is surmounted by the minus sign. This, I understand, is being done for the sake of typographical elegance! Examples of this kind of type setting are found in Rogers' third edition, in the new Dana,[5] and in my recent paper on hexagonal symbols.[6] The reader is urged to realize that $(hk\bar{\imath}l)$ stands for $(hk\bar{i}l)$, so that $i=h+k$ is still true. Likewise, in a zone symbol $[uv\bar{\jmath}w]$, the dot over the j is omitted, but $j=u+v$.

---

[2] Rogees, A. F., *Introduction to the Study of Minerals*, McGraw-Hill, New York. First ed. 1912 (see page 44). Third ed. 1937 (see page 76).

[3] Kraus, E. H., *Essentials of Crystallography*. Wahr, Ann Arbor, Mich., 1906. (see page 48).

[4] Kraus, E. H., Hunt, W. F., and Ramsdell, L. S., *Mineralogy*. McGraw-Hill, New York. First ed., 1920. Second ed., 1928. Third edition 1936.

[5] Palache, C., Berman, H., and Frondel, C., *Dana's System of Mineralogy*, 7th edition, vol. 1. Wiley, New York, 1944. On page 25, line 8 up, some copies show $\bar{\imath}=(h+k)$, others show $i=(h+k)$; the latter is correct.

[6] Donnay, J. D. H., *Am. Mineral.*, **32**, 52–58 (1947).

INTERNATIONAL GEOLOGICAL CONGRESS
XVIII SESSION, LONDON, 1948

The XVIII Session of the International Geological Congress, originally planned for 1940 and postponed on the outbreak of war, is to be held in Great Britain in 1948, on the invitation of the Geological Society of London.

A Third Circular containing preliminary arrangements for the Session has been issued. Sessional Meetings will take place in London from August 25 to September 1, 1948, and the following subjects have been provisionally listed for discussion:

1. Problems of Geochemistry.
2. Metasomatic Processes in Metamorphism.
3. Rhythm in Sedimentation.
4. The Geological Results of Applied Geophysics.
5. The Geology of Iron-Ore Deposits.
6. The Geology of Petroleum.
7. The Geology, Paragenesis and Reserves of the Ores of Lead and Zinc.
8. The Geology of Sea and Ocean Floors.
9. The Pliocene-Pleistocene Boundary.
10. Faunal and Floral Facies and Zonal Correlation.
11. The Correlation of Continental Vertebrate-bearing Rocks.
12. Earth Movements and Organic Evolution.

The Circular gives details of geological excursions covering most of the British Isles which are planned to take place between August 7 and September 18, 1948, as part of the Congress program. They include 16 long excursions (7–16 days) before the meetings in London, and 16 of similar length after the meetings. There will also be daily excursions, centered on London, between August 22 and September 3.

The General Organizing Committee is anxious that the plans for the Session, which will be the first major international assembly of geologists for 11 years, shall be as widely known as possible. About 1500 geologists, including some 800 from countries overseas, would have attended in 1940 if the arrangements for that year had not been disrupted by war; it is hoped that the attendance in 1948 will be of the same order, and that it will include representatives of universities, geological surveys, geological and mining societies, and other interested institutions from most countries of the world.

Sir Thomas Holland, K.C.S.I., F.R.S., is President of the General Organizing Committee and President-Designate of the Congress. The General Secretaries are Mr. A. J. Butler and Dr. L. Hawkes, and the Treasurer is Mr. F. N. Ashcroft. All communications should be addressed to the General Secretaries, XVIII Session International Geological Congress, Geological Survey and Museum, Exhibition Road, London, S.W. 7.

The international journal *Spectrochimica Acta* was first published by Julius Springer in Berlin in 1939. Two completed volumes (15 numbers) were issued when publication was interrupted by the war.

It has been decided to re-establish this journal for spectroscopists and spectrochemists. It will be published in the Vatican under the editorship of Dr. Alois Gatterer, assisted by the following who will serve as associate editors:

Dr. R. Breckport of Belgium
Dr. H. Kaiser of Germany

Dr. E. Van Someren of England
Dr. Lester W. Strock of the United States

It is expected that the first number of the revived journal (no. 1 of vol. 3) will be ready for the press by August 1, and that from 6 to 8 numbers will appear annually thereafter.

Papers in English from America should be submitted to Dr. Lester W. Strock, 21 Madison Ave., Saratoga Springs, New York. Other editors will take care of papers in other languages from other countries. The official languages of *Spectrochimica Acta* are English, French and German, although papers will also be accepted in Italian and Spanish.

NEW YORK MINERALOGICAL CLUB, INC.

American Museum of Natural History

Abstracts of Minutes of meeting for March 19, 1947

The speaker of the evening was Mr. A. N. Holden who spoke on "Growing Crystals from Solution." The crystals grown were ammonium dihydrogen phosphate, a piezoelectric material, which is used by the Bell Telephone Co. for voice frequency filters. These filters will pass certain frequencies and cut out others thereby enabling several messages to be sent over the same wire, at the same time, at different frequencies without interference. The material selected had to have the necessary piezoelectric property and had to be suitable for growing large crystals rapidly in the laboratory.

If a seed crystal is suspended in a solution, growth does not take place uniformly over the entire surface but a current is set up which moves up around the crystal and the bottom of the crystal grows faster than the top, giving a stepped back effect. This can be eliminated by stirring the solution but this develops turbulence so it must be stirred very slowly.

The effect of even very small amounts of impurities such as chromium and tin have a marked and harmful effect on the crystals.

At the Bell Laboratories the crystals are grown by fixing a seed plate on an arm which rotates slowly in a solution of uniform temperature and then reversing the direction of rotation periodically so that growth is uniform. Material is added to the seed plate as pyramids at the four corners of each side of the plate and these pyramids get larger until they grow together forming one pyramid. In the solution used these crystals grow only on the pyramids so that on continued growth the crystals become elongated in the direction of the pyramids while the prism does not get any thicker.

The talk was illustrated with lantern slides and specimens.

Parfield Kent, *Secretary*

Dr. George Tunell of the Geophysical Laboratory, Washington, D. C., has accepted the appointment of Associate Professor of Mineralogy at the University of California at Los Angeles.

Dr. E. Wm. Heinrich of the Department of Geology, Montana School of Mines, has been appointed Assistant Professor of Mineralogy at the University of Michigan.

Dr. Gordon A. Macdonald, District Geologist, U. S. Geological Survey, has been granted a leave from the Survey and can be addressed at Dept. of Geology, University of Southern California, University Park, Los Angeles 7, California.

William H. Broadwell, well known mineral collector in the New Jersey-New York area and one of the founders of the Newark Mineralogical Society, died on April 2 at the age of 71 years.

BOOK REVIEW

PHYSIKALISCHE CHEMIE DER SILIKATE by WILHELM EITEL. (Originally published by J. A. Barth, Leipzig, 1941.) Lithoprinted by Edwards Brothers, Inc., Ann Arbor, Michigan, 1944. Second completely revised edition. iv+826 pages (1944). Price $21.00.

This book by Eitel treats of the physical chemistry of silica and the silicates in a very comprehensive manner, as is shown by the world-wide coverage of the literature and an author's index of approximately 2325 entries. The contributions from laboratories in the United States form an important part of this book. Foremost in Eitel's treatment is the work of the Geophysical Laboratory of the Carnegie Institution of Washington. Other laboratories which have furnished much data for this book are the Kaiser-Wilhelm-Institut für Silikatsforschung, Berlin-Dahlem, where Eitel was the director; the U. S. Bureau of Standards; and the Portland Cement Fellowship, also at the Bureau of Standards.

A brief chapter on the geochemistry of silica and the silicates introduces the book and this is followed by a fourfold division of its contents.

Part I is concerned with the states of aggregation of silicates and this is based on the results of crystal structure studies. The crystalline nature and the related properties of the clay minerals are reviewed. Thereafter, various properties of silicate melts are discussed including viscosity, diffusion, surface tension, electrochemical properties, and density. Some of the experimental data were obtained on fused rocks. The constitution of silicate melts and glasses is examined in terms of the modern theory developed by Zernike and Prins, Zachariasen, and Warren. The physical properties of silicates in the colloidal state are considered next and such topics as grain size, dialysis, charge relations of silicic acid sols, optical properties of sols, x-ray and electron diffraction studies on colloids, silica gels, adsorption, base exchange, and diffusion in gels are discussed and illustrated.

Part II, on the thermochemistry of the silicates, is treated more briefly, owing largely to the lack of reliable data. Various calorimetric devices, for the measurement of specific heat, heats of formation, and heats of reaction are described. The methods of applying the Nermst Heat Theorem to silicates are outlined and illustrated with the A-U-diagrams for cristobalite-quartz; silica glass-quartz; kyanite-sillimanite, and $\alpha CaSiO_3$—$\beta CaSiO_3$.

Part III presents the techniques for investigating the phase relationships in dry silicate systems. The quenching method and the heating and cooling curve methods for examining silicate melts are described and illustrated. Various supplementary techniques for fixing inversion temperatures by optical, x-ray, dilatometric and specific heat measurements are given. This is followed by brief descriptions with phase diagrams and literature references for equilibrium in systems involving silica (or a silicate) as one component.

Part IV covers systems of silicates and a volatile constituent i.e., water, carbon dioxide or fluorine. A description of the methods of hydrothermal synthesis and the apparatus is given. Syntheses discussed include clay minerals, micas, the spilite reaction, hydrous magnesium silicates, and hydrous calcium silicates. Other topics reviewed are solubility of water in silicate melts, dehydration studies, the zeolite group of minerals and base exchange. Part IV is concluded by a brief treatment of reactions in the solid state.

Part V is devoted to silicate systems of technical importance. Fundamental data obtained on technical products composed of silicates have been summarized. Thus the study of glasses has yielded fundamental data on the devitrification characteristics of silicate melts, the escape of gases from glasses, the melting reactions in glass mixtures, viscosity relations of commercial glasses, opacity in glasses, and the chemical resistance of glass.

The study of slags by J. H. L. Vogt was of the utmost importance in orienting the program of experimental petrology. Eitel gives brief reviews of sulfide-silicate immiscibility, the quaternary system SiO_2-Al_2O_3-CaO-MgO, and Tammann's idealized diagram Fe_2SiO_4-Fe-FeS with its implication in the theory of the earth's interior.

A general summary of the system: clay-water is given and includes such physical properties as thixotropy, viscosity, and dehydration studies. A short review is presented of the minerals formed by the firing of clays and aluminosilicates, also of ceramic products in the systems MgO-SiO_2; MgO-Al_2O_3-SiO_2; MgO-TiO_2; MgO-TiO_2-ZrO_2, and the refractories of the silica group.

This book is concluded by a section on cements which gives the description of the results of microscopic and x-ray studies on clinker constituents, the relation of clinker formation to phase rule studies; the modifications introduced by the presence of iron oxides, alkalies, fluorides, etc., in cements; the hydration of cements.

This compilation by Eitel is notable for the selection of so many reliable data. A minimum of work of poorer quality is included to round out the picture of those systems or compositions not otherwise treated. The reviewer thinks that Eitel has treated his subject successfully.

The petrologist will find this book of much value to him as a reference work for it supplies a background of the available physico-chemical data of the silicates. The data and summaries given will help to increase his knowledge of the character and nature of a magmatic liquid, its crystallization and of the influence of the physical properties of silicate melts on the manner of intrusion of a magma.

This book is a lithoprinted edition of the original book printed by Barth of Leipzig. The text is very satisfactorily reproduced as are also most of the figures. Certain figures, however, are not complete—for example on p. 247, figure 223, the letter "r" at the end of the diagonal line from "s" is missing. Likewise on p. 252, in figure 226, the number 1 is missing at the terminus of the lower curve.

The reviewer recommends this book to petrologists and to mineralogists interested in silica and the silicates.

George T. Faust

NEW MINERAL NAMES

Lembergite

Tosio Sudo, On some low temperature hydrous silicates found in Japan. *Bull. Chem. Soc. Japan*, **18,** 281–329 (1943).

This name, for J. Lemberg, who described similar material in 1877, is given to a dark green to brownish-green mineral found in several Japanese deposits of iron-bearing sandstones. These ores contain magnetite, augite, feldspar, quartz, altered volcanic rocks, etc., cemented by the fine-grained green mineral (grains 0.02 mm. or less). The indices of refraction recorded are somewhat variable, 1.56–1.58; double refraction 0.015–0.030. Material was purified by suspension in water and by magnetic separation. The mineral is readily decomposed by hot dilute HCl, and 9 analyses are given (only in the form of molecular ratios) of the soluble portion. These analyses gave the ratios:

	Al_2O_3	FeO*	MgO	CaO	H_2O+	$\begin{cases}Fe_2O_3\\FeO\end{cases}$
Average analysis	0.40	0.92	1.00	0.34	1.86	—
Extremes of analyses	0.36	0.67	1.00	0.15	1.70	0.76
	to	to	to	to	to	to
	0.47	1.43	1.00	0.70	2.12	3.40

* All iron calculated as FeO.

X-ray powder photographs of the green mineral showed a very close similarity to those of nontronite and montmorillonite, and some similarity to those of garnierite and genthite. It is concluded that the mineral belongs to the montmorillonite group.

Discussion: The data do not seem to justify a new name for what appears to be an intermediate member of the montmorillonite group. Furthermore, the name lembergite has already been used, having been given in 1895 to a synthetic hydrated sodium aluminum silicate, see *Dana's System*, 6th Edition, Appendix I, p. 42.

Michael Fleischer

Aluminocopiapite

L. G. Berry, Composition and optics of copiapite. *Univ. Toronto Studies*, Geol. Ser., No. **51,** 21–34 (1947).

The general structural formula of copiapite is shown to be $X\ (OH)_2\ R_4'''(SO_4)_6 \cdot nH_2O$, where X is one oxygen equivalent of one or more of the following elements: Na, K, Cu, Fe″, Mn, Mg, Zn, Ca, Al, Fe‴, and n equals 20. R‴ is ferric iron and sometimes in part aluminum. The name aluminocopiapite is proposed for the variety in which X is predominantly aluminum. The names ferricopiapite, magnesiocopiapite, ferrocopiapite, and cuprocopiapite had been proposed previously.

M.F.

Frohbergite

R. M. Thompson, Frohbergite, $FeTe_2$: a new member of the marcasite group. *Univ. Toronto Studies*, Geol. Ser., No. **51,** 35–40 (1947).

See abstract in *Am. Mineral.*, **32,** 210 (1947).

M.F.

Monteponite

Ernest E. Fairbanks, The punched card identification of ore minerals. *Econ. Geol.*, **41,** 761–768 (1946). The name monteponite is suggested for the mineral cadmium oxide (CdO), reported by Wittich and Neumann in 1901 from near Monte Ponti, Sardinia. (See *Dana's System*, 7th Ed., pp. 502–503.)

M.F.

NEW DATA

Heazlewoodite

M. A. Peacock, On heazlewoodite and the artificial compound Ni_3S_2. *Univ. Toronto Studies*, Geol. Ser., No. **51,** 59–69 (1947).

Heazlewoodite was described in 1896 by Petterd as a nickel sulfide from Heazlewood, Tasmania. The description was sketchy, and the mineral has been regarded as being probably a variety of pentlandite. Restudy now shows it to be a valid species.

Chemical Properties: Composition Ni_3S_2. Analysis by I. H. Milne on 0.1 g. gave: Ni 72.13, S 25.96, Fe 0.55, insol. 0.59; sum 99.23%. Etch tests are given.

Crystallographic and *X*-Ray Data: *X*-ray powder photographs of the natural material were identical with those of the material synthesized by fusing Ni and S in the proportions 3:2 in an evacuated silica glass tube. The spacings agreed closely with those of Westgren (1938) on artificial Ni_3S_2. The mineral is rhombohedral with a 5.730, c 7.125 kX; r 4.072 kX, α 89°25′. The space group is $D_3^7-R\,32$ and the rhombohedral unit cell contains Ni_3S_2. *X*-ray powder data are given.

Physical Properties: Luster metallic, color pale bronze, streak light bronze. The mineral is non-magnetic.

Hardness 4, Talmage hardness C+, G. (pycnometer) 5.82 on natural material, 5.87 on synthetic material, 5.87 calculated from x-ray data. In polished section, the mineral is yellowish cream-colored, with strong anisotropism and polarization colors brown to bluish gray, or even lilac to green. A mosaic structure was present (twinning?)

Occurrence: Occurs intergrown with magnetite in a band in serpentine. A very small amount of pentlandite was present. The surface was coated with zaratite.

M.F.

Sjögrenite

P. Quensel, Om sjögrenite som mineralnamn. *Geol. För. Förh.*, **68,** 110–111 (1945).

Quensel points out that the name sjögrenite, proposed by Frondel (*Am. Mineral.*, **26,** 309 (1941)) for the hexagonal dimorph of pyroaurite, had previously been given by Krenner (*Proc. Geol. Congress Stockholm*, Vol. **1,** 129 (1910)) to a basic ferric phosphate. This mineral, with the formula $5Fe_2O_3 \cdot 3P_2O_5 \cdot 8H_2O$, was first described, without a name, by Kinch and Butler (*Mineralog. Mag.*, **7,** 65 (1886)). The phosphate has priority.

Discussion: The phosphate should be re-studied. If it is a valid species, the dimorph of pyroaurite will have to be renamed.

M.F.

Wiserite

W. Epprecht, Die Eisen- und Manganerze des Gonzen. *Beitr. Geol. Schweiz, Geotechn. Ser. Lief.* **24,** 128 pp. (1946).

Wiserite, first described from Gonzen, Switzerland, in 1842, and considered since 1868 to be altered pyrochroite, was re-examined. The mineral occurs as fibrous, asbestiform masses in fissures on hausmannite, pyrochroite or rhodochrosite. The luster is silky, color white to brownish or reddish. Optically uniaxial, negative, *n*E 1.66–1.67, *n*O about 1.74, weakly pleochroic, with E bright yellow-orange, O colorless. Fresh pyrochroite had *n* E 1.681, *n*O 1.723.

X-ray powder photographs were distinct from those of pyrochroite, manganite, and synthetic α—MnOOH and β—MnOOH. (Also seem to be distinct from that of groutite—Abstractor.) Dehydration study showed that most of the water is lost at 200–300°, hausmannite and β—Mn_2O_3 being among the products formed. Pyrochroite gave a very similar dehydration curve.

Analysis by J. Jakob gave: Mn_2O_3 64.23, Al_2O_3 none, Fe_2O_3 0.13, MnO 9.38, MgO 3.09, CaO, K_2O, Na_2O none, H_2O+ (120°) 16.17, H_2O- 1.10, CO_2 5.26, Cl, SO_3 none; sum 100.00%. The active oxygen content was not determined, but Mn_2O_3 was calculated after assigning the analytical deficiency to active O. This gives roughly $4Mn_2O_3 \cdot (Mn, Mg)_2(CO_3)(OH)_2 \cdot 8H_2O$.

M.F.

DISCREDITED MINERALS

Stiepelmannite = Florencite

Erik R. Ygberg, Svanbergite from Horrsjöberg. *Arkiv Kemi, Mineral. Geol.*, **20A,** No. 4, 17 pp. (1945).

The mineral stiepelmannite was first described by Ramdohr and Thilo (see *Am. Mineral.*, **25,** 626 (1940)) as a member of the alunite group analogous to the cerium mineral florencite, but with yttrium and ytterbium predominant. Ygberg states (p. 13), "According to a personal communication from Professor Ramdohr, it has later been found that stiepelmannite is a variety of florencite containing Ce, La, and Pr."

M.F.

Berthonite = Bournonite

R. M. Thompson, Berthonite identical with bournonite. *Univ. Toronto Studies*, Geol. Ser. No. **51,** 81–83 (1947).

X-ray powder photographs of berthonite from the type locality Slata Mine, Tunisia, are identical with that of bournonite. This agrees with the work of Harcourt, *Am. Mineral.*, **27,** 109 (1942).

M.F.

NOMINATIONS FOR OFFICERS OF THE MINERALOGICAL SOCIETY OF AMERICA FOR 1948

The Council has nominated the following as officers of The Mineralogical Society of America for the year 1948 to be voted on by the membership at the December election:

PRESIDENT: M. A. Peacock, University of Toronto, Toronto, Canada.
VICE-PRESIDENT: Adolph Pabst, University of California, Berkeley, California.
SECRETARY: C. S. Hurlbut, Jr., Harvard University, Cambridge, Massachusetts.
TREASURER: Earl Ingerson, U. S. Geological Survey, Washington, D. C.
EDITOR: Walter F. Hunt, University of Michigan, Ann Arbor, Michigan.
COUNCILOR (1948–51): Clifford Frondel, Harvard University, Cambridge, Massachusetts.

ANNOUNCEMENT OF THE TWENTY-EIGHTH ANNUAL MEETING

The twenty-eighth annual meeting of the Society will be held in Ottawa, Canada, December 29–31, 1947, in connection with the fifty-ninth annual meeting of the Geological Society of America.

Members of the Society who are planning to present papers at the scientific sessions of the annual meeting should notify the Secretary as soon as possible in order to receive the proper blanks for their abstracts. All abstracts should be in the Secretary's office by *October 15.*

Advance announcement of the annual meeting will be distributed to members of the Society, with the ballot for officers, in the middle of October. The final program of the meeting, including the schedule of papers, abstracts, and other information will be sent to each member in December. Further specific information regarding the annual meeting may be obtained from the Secretary's office.

C. S. HURLBUT, JR., *Secretary*